PROTEIN STRUCTURE AND INTERACTIONS STUDIED BY
ELECTROSPRAY MASS SPECTROMETRY

(Spine title: Protein Structure and Interactions Studied by ESI-MS)

(Thesis format: Integrated Article)

by

Jiangjiang Liu

Graduate Program in Chemistry

A thesis submitted in partial fulfillment
of the requirements for the degree of
Doctor of Philosophy

The School of Graduate and Postdoctoral Studies
The University of Western Ontario
London, Ontario, Canada

© Jiangjiang Liu 2013

THE UNIVERSITY OF WESTERN ONTARIO
School of Graduate and Postdoctoral Studies

CERTIFICATE OF EXAMINATION

Supervisor

_____
Dr. Lars Konermann

Examiners

_____
Dr. David W. Shoesmith

_____
Dr. Silvia Mittler

_____
Dr. Gilles Lajoie

_____
Dr. Sarah Trimpin

The thesis by

Jiangjiang Liu

entitled:

Protein Structures and Interactions Studied by Electrospray Mass Spectrometry

is accepted in partial fulfillment of the
requirements for the degree of
Doctor of Philosophy

_____
Date

_____
Chair of the Thesis Examination Board

ii

Abstract

Since the emergence of electrospray ionization (ESI) mass spectrometry (MS) as a tool for protein structural studies, this area has experienced tremendous growth. ESI-MS is highly sensitive, and it allows the analysis of biological systems ranging in size from a few atoms to large multi-protein complexes. This work aims to solve questions in protein structural biology by using ESI-MS in conjunction with other techniques.

We initially apply ESI-MS for studying the monomeric protein cytochrome *c* (Chapter 2). The physical reasons underlying the irreversible thermal denaturation of this protein remain controversial. By utilizing deconvoluted charge state distributions, oxidative modifications were found to be the major reason underlying the observed behavior. The positions of individual oxidation sites were identified by LC-MS/MS-based tryptic peptide mapping.

Chapter 3 and 4 focus on noncovalent protein complexes. ESI allows the transfer of multi-protein complexes into the gas phase, thereby providing a simple approach for monitoring the stoichiometry of these assemblies by MS. It remains somewhat unclear, however, in how far this approach is suitable for measuring binding affinities. We demonstrate that the settings used for rf-only quadrupoles in the ion path are a key factor for ensuring uniform transmission behavior, which is a prerequisite for meaningful K_d measurements. Overall, our data support the viability of the direct ESI-MS approach for determining binding affinities of protein–protein complexes in solution.

Having established suitable conditions for the analysis of noncovalent protein complexes, ESI-MS is applied for monitoring the folding and assembly of hemoglobin (Hb). The native structure of this protein comprises four heme-bound subunits. Hb represents an important model system for exploring coupled folding/binding reactions, an area that remains difficult to tackle experimentally. We demonstrate that efficient Hb refolding depends on the heme ligation status. Only under properly optimized conditions is it possible to return denatured Hb to its tetrameric native state with high yield. ESI-MS allows the observation of on-pathway and off-pathway intermediates that become populated during this highly complex self-assembly process. In summary, this work demonstrates that ESI-MS is a highly versatile tool for addressing questions at the interface of chemistry and structural biology.

Keywords: electrospray ionization mass spectrometry, thermal denaturation, noncovalent complexes, protein folding and assembly, cytochrome *c*, beta lactoglobulin, hemoglobin.

Statement of Co-Authorship

The work in Chapters 2 and 3 were published in the following articles, respectively:

Jiangjiang Liu and Lars Konermann (2009). Irreversible Thermal Denaturation of Cytochrome C Studied by Electrospray Mass Spectrometry. *J Am Soc Mass Spectrom* **20**, 819-828. Reproduced with permission. © 2009, Elsevier

Jiangjiang Liu and Lars Konermann (2011). Protein Binding Affinities in Solution Determined by Electrospray Mass Spectrometry. *J Am Soc Mass Spectrom* **22**, 408-417. Reproduced with permission. © 2011, American Society for Mass Spectrometry

The work in Chapter 4 has been incorporated into the following article:

Jiangjiang Liu and Lars Konermann (2012). Assembly of Hemoglobin from Denatured Monomeric Subunits: Effects of Heme Ligation and Off-pathway Intermediates Studied by Electrospray Mass Spectrometry. *In preparation.*

The first draft of each above article was prepared by the author (J.L.). Subsequent revisions were done by the author and Dr. Lars Konermann together. All experimental work was done by the author. Peak shape simulation analysis in Chapter 2 was developed and done by Dr. Lars Konermann.

If Winter comes, can Spring be far behind?

                        - Percy Bysshe Shelley

Dedication

To my parents, my husband and Ben for their love and support

Acknowledgements

First of all I would like to express my deepest gratitude to my supervisor Dr. Lars Konermann. He has used his excellent expertise to guide me and open doors for myself in this field of research. There have been a lot of challenges during my PhD study, and I could never go through all these without the strong support and warm encouragement from Lars. His generosity and input have made the past five years an invaluable experience for me.

Thank you to Lee-Ann Briere and Dr. Stanley D. Dunn from biochemistry department for their help in my second project. Thank you to Paula Pittock and Dr. Gilles Lajoie for loaning a nanoESI source.

Thank you to my Supervisory Committee: Dr. John F. Corrigan, Dr. Gillies Elizabeth, and Dr. Leo Lau. Thank you to my thesis examiners: Dr. David W. Shoesmith, Dr. Silvia Mittler, Dr. Gilles Lajoie, and Dr. Sarah Trimpin.

Thank you to all the past and present group members for their help: Jingxi Pan, Yuhong Liu, Xin Tong, Brian Boys, Peter Ferguson, Elias Ahadi, Yan Pan, Brad Stocks, Siavash Vahidi, Stephen Sciuto, Amanda Comeau, Antony Rodriguez, Anil Khanal, Modupela Sowole, Yalda Liaghati, Mahasilu Amunugama, Tomasz Czarny, Mohammad Halim, Jason Hedges, Edurado Jorge Pilau, Xuan-feng Yue.

I would like to provide my heartfelt thanks to my parents and my husband. Their love, understanding, and support have helped me move forward all the time.

Table of Contents

List of Tables

List of Figures

Chapter 1

Chapter 2

Chapter 3

Chapter 4

List of Appendices

List of Symbols and Abbrevations

A – Absorbance

AHSP – α-hemoglobin stabilizing protein

α^h – holo-α globin

α^a – apo-α globin

BLG – β-pactoglobulin

β^h – holo-β globin

β^a – apo-β globin

CD – circular dichroism

CEM – chain ejection model

CID – collision induced dissociation

CRM – charged residue model

CSD – charge state distributions

c – sample concentration

cyt c – cytochrome c

D – homodimer

D – Gaussion distribution function

ESI – electrospray ionization

E – FRET efficiency

ε – the molar absorption coefficient

ε_0 – permittivity of vacuum

ε – dielectric constant of the medium

FRET – Förster resonance energy transfer

f – protein shifted mass profile

f_{sol} – the fraction bound

ΔG^o – difference in Gibb's free energy

$\Delta G^{\ddagger}$ – Gibb's free energy of activation

H_{closed} – amide hydrogens in non-exchangeable states

H_{open} – amide hydrogens in unprotected states

ΔH – enthalpy change

Hb – Hemoglobin

$h(CN)_2$ – hemin dicyanide

HOMO – the highest occupied molecular orbital

HDX – hydrogen deuterium exchange

h – Plank's constant

I_o – incoming light intensity

IEM –ion evaporation model

I – transmitted light intensity

K_{eq} – equilibrium constant

K_d – solution-phase binding affinities

k_B –Boltzmann's constant

k_{ch} – chemical HDX rate constant at unprotected site

k_{cl} –rate constant of protein closing motion

k_f – *reaction rate of protein folding*

k_{op} – rate constant of protein opening motion

LC – liquid chromatography

l – light path length

LUMO – lowest unoccupied molecular orbital

λ –wavelength of light

MALDI – matrix-assisted laser desorption/ionization

metHb – met-hemoglobin (heme iron in the 3+ oxidation state)

M – monomer from homodimer

MS – mass spectrometry

N – native conformation

p – mass distribution of a broadened peak

Q-TOF – quadrupole-time-of-flight

R – distance between donor and acceptor

R_{ESI-MS} – ion abundance ratio of monomer and dimer from ESI-MS measuremntes

R_0 – the förster radius at E=0.5

R_{sol} – concentration ration of dimer and monomer at equilibrium

ΔS – entropy change

S_0 – the ground state

S_1 – the singlet state

TOF – time of flight

TS – the transition state

Trp – tryptophan

U – unfolded conformation

UV-Vis – Ultraviolet Visible

z_R – the charge at Ryleigh limit

Chapter 1-Introduction

In all organisms, there are several types of polymeric macromolecules that perform almost all essential activities. The genetic information of each organism is stored in DNA molecules. Through the transcription process this genetic information is transferred to messenger RNA. Both DNA and RNA are poly-nucleotides. Messenger RNA directs the ribosome-mediated synthesis of polypeptides, which are long chains of amino acids. These polypeptide chains represent the "proteins" that fold into unique structures and constitute much of the cellular machinery. Proteins are responsible for structural support, transport, signaling, catalysis, host defense and many other functions. When proteins misfold, or when they fail to remain in appropriate conformations due to mutations or other defects, various types of diseases can ensue. A wide range of biophysical methods is available to probe aspects of protein behavior *in vivo* and *in vitro*. These methods provide a unified description of biological processes, thereby facilitating the development of novel therapeutic strategies.

1.1 Hierarchical Structures of Proteins

Protein structures can be divided into four levels, termed primary, secondary, tertiary and quanternary structures (**Figure 1-1**). Primary structure refers to the atomic compositions of the polypeptide chain, i.e., the amino acid sequence. Twenty naturally occurring L-amino acids represent the building blocks used during protein biosynthesis [1]. All amino acids are connected into a polypeptide chain via amide bonds. In **Figure 1-1a**, three adjacent amino acids in a peptide chain are shown, depicting the special structural

a.

Primary structure

b.

Secondary structure

c.

Tertiary structure

d.

**Quaternary structure
-biologically active form**
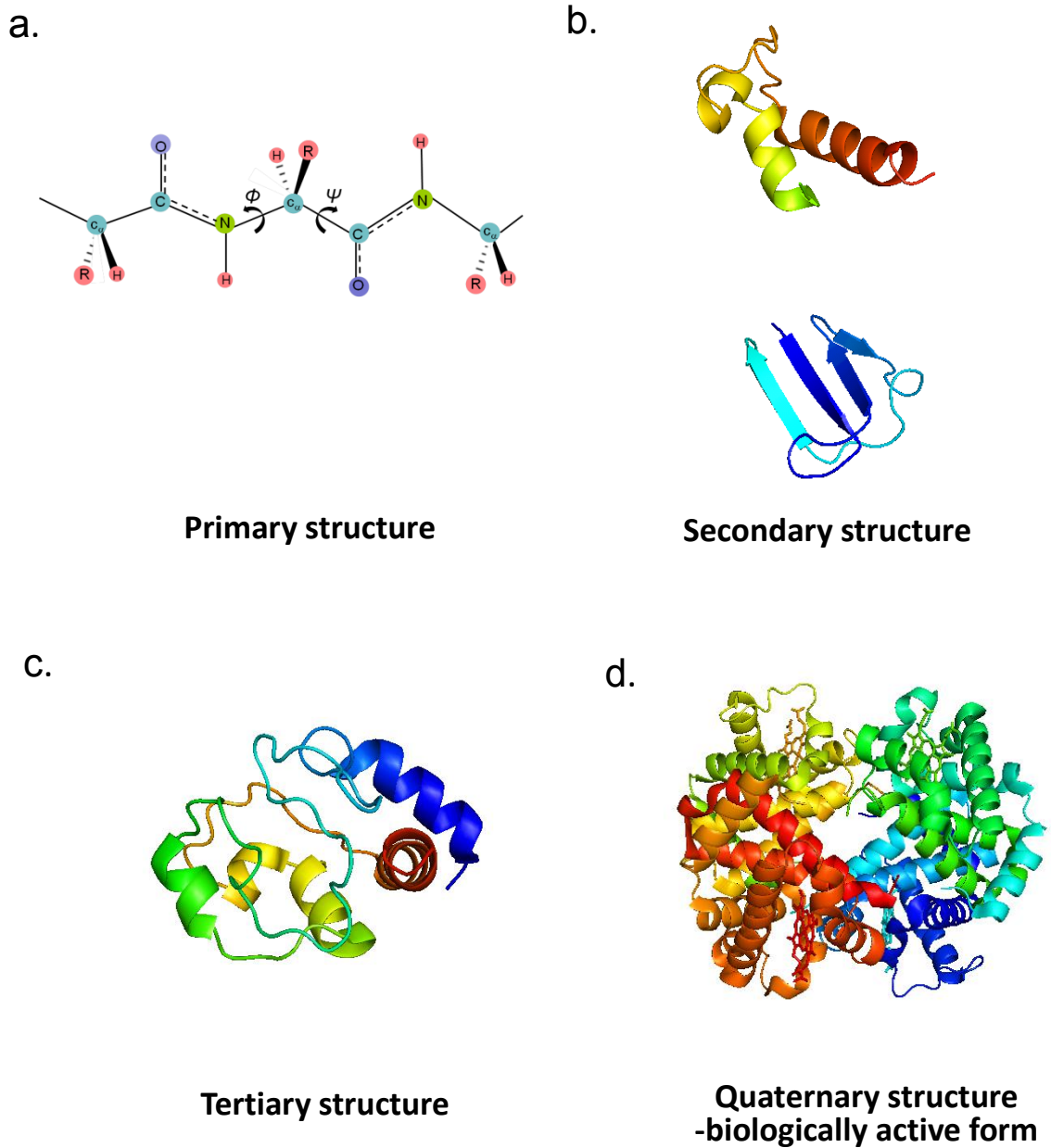
Figure 1-1. Schematic representation of four hierarchical levels of protein structure. a. Primary sequence. b. Secondary structural elements: α helix and β sheet. c. Tertiary structure of bovine cyt c (pdb 2b4z). d. Quanternary structure of bovine hemoglobin (pdb 2qss).

features around an α-carbon, which is the chiral center of each amino acid (except for glycine). "R" is the amino acid side chain. The R groups provide unique chemical properties to each amino acid, such as acidic, basic, polar, or hydrophobic. Conformations of polypeptide main chains are defined by the dihedral Ψ and Φ angles on both sides of each α carbon (**Figure 1-1a**). Due to steric restrictions, only a limited range of backbone conformations are allowed. The spatial arrangement of the protein sequence in terms of allowed main chain conformations gives rise to the secondary structure (**Figure 1-1b**). Linus Pauling first recognized the formation of α-helical conformations for the polypeptide chain via intra-chain hydrogen bonds [2]. For this contribution he was awarded the 1954 Chemistry Nobel Prize. In addition to α-helices, β-sheets represent a common type of secondary structure. These are formed by extended chain segmeents via intramolecular hydrogen bonds, in either parallel or anti-parallel fashion. The spatial arrangement of secondary motifs is called tertiary structure, representing highest structural level for monomeric proteins. Quaternary structure is formed via intermolecular interactions of two or more proteins.

1.2 Factors that Stabilize Native Protein Structures

Electrostatic Interactions

If two charges q_1 and q_2 are separated by a distance r, the potential between them can be described as:

$$U(r) = \frac{q_1 q_2}{4\pi\varepsilon_o \varepsilon r} \qquad (1)$$

where ε_o is the permittivity of vacuum (8.85×10^{-12} C^2/N•m) and ε is dielectric constant of the medium. The dielectric constant is a measure of electrostatic interaction screening of the medium. Nonpolar liquid hydrocarbons have a dielectric constant around 2; ε of liquid water is about 80 [3]. Inside the hydrophobic core of a protein, the dielectric constant is around 2 to 4 [4]. The interaction of a positively and a negatively charged residue inside a protein molecule gives rise to a salt bridges. Acidic and basic residues, as well as the two chain termini can participate in salt bridge formation.

Because of their 1/r dependence, electrostatics give rise to long range interactions. Once electrostatics were thought to be the main driving force for protein folding. Today it is known that electrostatic interactions provide an enthalpic contribution of about 10kJ mol^{-1} per ion pair to the stability of folded protein structures [5].

Van der Waals Interactions

In addition to salt bridges (see above), electrostatic attraction can also originate from permanent dipoles and induced dipoles. The later kind of interaction, which is due to local fluctuations in electron distribution, gives rise to attractive London dispersion forces. Van der Waals interactions are relatively weak. They act at short range and are proportional to $1/r^6$ [3]. Based on Pauli's exclusion principle, when the distance between two atoms is close to their Van der Waal's radii, a strong repulsion arises. The combination of attractive and repulsive components yields a so-called Lennard-Jones potential:

$$U(r) = 4\varepsilon\left(\left(\frac{\sigma}{r}\right)^{12} - \left(\frac{\sigma}{r}\right)^6\right) \qquad (2)$$

where σ and ε are constants depend on the interacting atoms [6]. Inside the protein hydrophobic core, these Lennard-Jones interactions are important for native protein stabilization [7].

Hydrogen Bonds

When hydrogen donor groups (e.g., OH, NH_3) and hydrogen acceptor atoms with lone electron pairs are in close proximity, hydrogen bonds can be formed, as two electron negative atom compete for the same hydrogen (e.g., $R=O•••H-NR_2$). As mentioned in section **1.1**, hydrogen bonds are a major stabilizing factor for α-helices and β-sheets. Hydrogen bonds can also be formed between protein and water, and among solvent molecules.

Hydrophobic Effect

The hydrophobic effect refers to the tendency of non-polar solutes to cluster together in an aqueous enviornment. For native protein structures, the hydrophobic effect is reflected in the spatial arrangement of side chains. Nonpolar residues are usually buried in the interior, sequestered from water by hydrophilic residues on the exterior of the protein. This phenomenon may be explained on the basis of thermodynamic arguments. Enthalpically, exterior hydrophilic residues can be solvated by forming hydrogen bonds with water. Usually, hydrophobic residues are neither good hydrogen bond donors nor acceptors. Collapsing hydrophobic residues into protein core also avoids high entropic

penalties, as envisioned by the "iceberg model" [8]. In bulk water, there is a dynamic hydrogen bonded network, characterized by a relative high entropy. Placing hydrophobic molecules in water causes the formation of a partially immobilized "iceberg" shell around them. Iceberg formation decreases the entropy of the solvent in the vicinity of the exposed nonpolar site, which is unfavorable. Isolation of hydrophobic residues from water avoids this high entropic price. It is widely accepted that the hydrophobic effect plays a major role during protein folding [9-11].

1.3 Thermodynamic Aspects of Protein Stability

For many applications it is convenient to consider the two-state equilibrium between the native conformation (N) and the unfolded state (U) of a protein

$$N \rightleftarrows U \qquad (3)$$

The difference in Gibb's free energy ($\Delta G°$) controls this equilibrium according to

$$\Delta G°_{N \rightarrow U} = -RT ln K_{eq} = -RT ln \frac{[U]_{eq}}{[N]_{eq}} \qquad (4)$$

When N is stable, $K_{eq} \ll 1$, and $\Delta G°$ is a large positive number. Based on the Second Law of Thermodynamics, $\Delta G^o{}_{N \rightarrow U}$ can also be expressed as:

$$\Delta G°_{N \rightarrow U} = \Delta H° - T\Delta S° \qquad (5)$$

Both enthalpy (ΔH) and entropy (ΔS) of the protein itself and the surrounding solvent contribute to $\Delta G°$. Factors that have to be considered include the entropy of solvent and

polypeptide chain, interactions between protein and solvent, and interactions within the protein. N is only marginally stable, slightly lower in free energy than U.

1.4 Protein Folding

1.4.1 Why is Protein Folding Important?

Protein folding refers to a process, which includes a series of structural changes leading from random coil state *U* to the native conformation *N*. This unique behavior distinguishes proteins from synthetic polymers. Synthetic polymers are usually composed of repeated monomeric units, and they do not fold into a specific three-dimensional structure. Most proteins can fold spontaneously *in vitro* in the absence of the cellular machinery. This suggests that protein folding is directed by the primary structure. Deciphering the protein folding code will provide us with the key to understand biological processes, such as metabolism, host defense and signaling. Understanding protein folding also facilitates the development of novel therapeutic approach and the treatment of diseases.

Only by understanding the protein folding process, scientists will be able to engineer proteins with desired functions. For example, a binding site can be optimized computationally, and this is the start of protein therapeutic drug production. Subsequently, this designed binding site has to be engineered into a protein sequence. Without knowing the role of each individual residue during folding, formation of the designed binding site cannot be achieved. Also, many enzymes catalyze biological

reactions with extreme specificity and efficiency. Metabolic reactions in our body have lower energy barriers in the presence of enzymes. One example is catalase, which catalyzes the decomposition of hydrogen peroxide and lowers the activation energy from 76 kJ mol^{-1} to 30 kJ mol^{-1} [12]. The protein sequence, which directs folding and hence biological function, has been evolutionary optimized over millions of years. Designing proteins with novel catalytic capabilities requires deciphering the evolutionary mysteries of folding.

Protein misfolding can happen due to cellular defects triggered by oxidative stress or aging [13]. Several diseases including Alzheimer's, Parkinson's and Huhtington's are related to protein misfolding and aggregation [14-18]. Typically, if monomeric proteins misfold, cytotoxic quaternary structures can be formed by self-aggregation of the misfolded monomers. As amyloid plaques are formed within the cell by these misfolded proteins, diseases can arise.

Another goal of protein folding research is to predict native structures based on sequence information. Fundamental knowledge of protein folding provides the foundation of computer-based structure predictions. There is a competition known as Critical Assessment of Techniques for protein Structure Prediction (CASP), where computational scientists predict protein structures based on known but unpublished sequences. The performance of structure prediction algorithms has improved in each round of the competition [19]. Generally, smaller proteins are easier to predict than larger ones due to the greater structural complexity of the latter.

1.4.2 Brief History of Protein Folding

After Linus Pauling and his colleagues predicted the existence of α helices in 1954 [2], the existence of secondary structure type was confirmed by the resolved X-ray crystal structures of myoglobin and hemoglobin in 1960's [20]. Anfinsen's work on the folding of ribonuclease *in vitro* provided further insights, and this work brought him the 1972 Chemistry Nobel prize [21]. Anfinsen's work consists of two major contributions: (1) For the first time, he showed that the native protein structure is thermodynamically stable, and that it is determined by intramolecular interactions of amino acids and solvent-solute interactions. (2) In the absence of ribosomes and chaperones, it is still possible for a protein to refold from its denatured state by restoring physiological conditions *in vitro*. From then on, the research field of protein folding has been expanding steadily until today.

Based on Anfinsen's findings, it is clear that protein folding must be directed by a 'folding code' embedded in the amino acid sequence. However, there is an apparent mismatch between possible conformations of protein chains and actual protein folding time scale, as pointed out by Levinthal [22]. Let's consider a hypothetical protein chain with 95 amino acid residues. The conformation of each amino acid is controlled by its Φ and Ψ angles. If each of these two angles can adapt only three conformations, there are 3^{190} possible conformations in total. The time required for a conformational search that leads to the native structure can be estimated using the Eyring equation

$$k = \frac{k_\text{B}T}{h} e^{\left(\frac{-\Delta G^\ddagger}{RT}\right)} \qquad (6)$$

where k is the rate constant, k_B is Boltzmann's constant, h is Planck's constant, T is the absolute temperature, $\Delta G^{\ddagger}$ is the Gibb's energy of activation, and R is the gas constant. The fastest possible rate of any conformational switch is around 10^{12} s^{-1} for $\Delta G^{\ddagger} = 0$. Thus, if the number of possible conformations is 3^{190}, the total time for an unbiased conformational search would be ~10^{71} years. Strikingly, experiments reveal that protein folding typically only requires seconds to go to completion. This mismatch of several tens of orders of magnitude is known as "Levinthal's paradox". It indicates that protein folding cannot possibly be achieved by an unbiased conformational search [23].

1.4.3 Folding Energy Landscape: The "New View" of Protein Folding

To resolve Levinthal's paradox it must be concluded that folding is not a pure random process but a biased conformational search [24]. In the "hydrophobic collapse" model, nonpolar residues initially interact nonspecifically to avoid unfavorable solvent exposure, and the native structure is formed by subsequent rearrangement. Another folding model called "nucleation" proposes that native structure is formed through condensation on a template of some transient secondary structures from short sequence regions. There is no clear-cut evidence that protein folding has to follow either one or the other mechanism. In fact, folding might contain elements of both theories.

Because folding of many small single-domain proteins can be described as an apparent two-state process [25-27], we will first discuss these reactions using transition state theory. In this classical chemical reaction theory, protein folding is a process
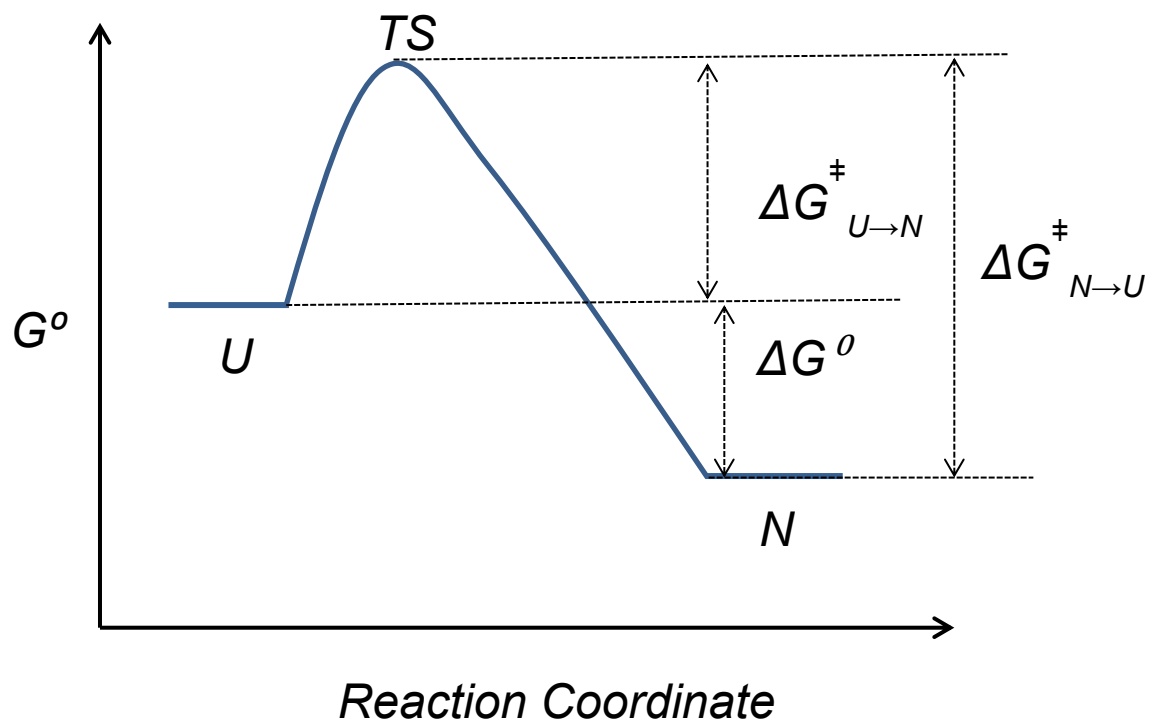
Figure 1-2. One-dimensional free-energy diagram for two-state protein folding ($U{\rightarrow}N$) via a *TS* barrier. The standard Gibb's free energies (G^{0}) are plotted against reaction coordinates. The change of standaed Gibb's free energy (ΔG^{0}) of protein folding reaction is indicated. The differences in Gibb's free energy of folding ($U{\rightarrow}N$) and unfolding ($N{\rightarrow}U$) through *TS* barrier are also labeled.

between unfolded and folded protein populations in a macroscopic sense. If the reaction rate of folding is k_f, the rate of native protein formation is given by

$$\frac{dP_N}{dt} = k_f P_U \quad \text{with} \quad P_N + P_U = 1 \quad (7)$$

where P_N and P_U are native protein and unfolded protein fractions, and where k_f can be expressed using eq. 6. This whole process can be depicted in an Arrhenius diagram (**Figure 1-2**). In this diagram, unfolded proteins fold into native protein structure through an unfavored transition state (TS) structure. An empirical estimate of this energy barrier yields values larger than $3k_BT$ [28]. Even though this theory explains the two state processes, it omits any detailed conformational aspects of proteins. For small molecules, entropic contributions to the TS barrier are not very significant. In contrast, entropic factors even small proteins experience significant entropic changes during folding [29].

Based on advances in both experiments and theory a "new view" of protein folding theory has been developed. This framework envisions protein folding using a funnel-like concept that allows parallel folding trajectories. Cartoon representations of protein folding energy landscape are shown in **Figure 1-3**. These diagrams plot the intrinsic free energy of the protein as a function of two conformational dimensions [23]. The intrinsic free energy includes everything except the conformational entropy of the protein. The latter is represented by the width of the funnel. The unfolded state is highly heterogeous and populates the funnel "rim". As protein chains approach the native structure from these unfolded states, the conformational freedom decreases. In **Figure 1-3a**, a flat folding funnel represents the random conformational search envisioned by Levinthal, which would result in unreasonably slow folding. In **Figure 1-3b**, a rugged protein
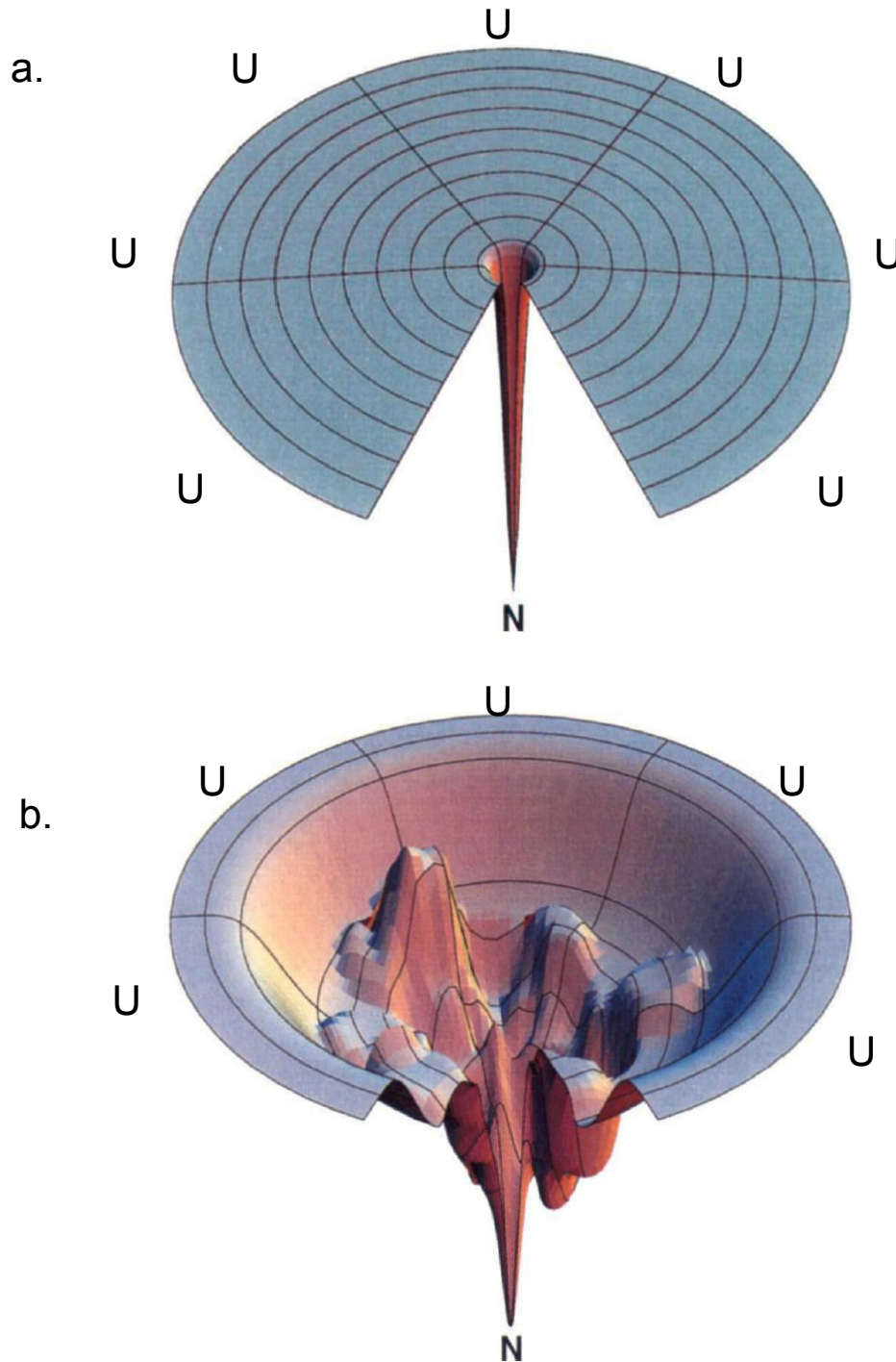
Figure 1-3. a. Levinthal energy landscape and **b.** Rugged energy landscape representing multi-pathways of protein folding. Different protein conformations could have same intrinsic free energy, and different protein folding routes could be evolved from these different conformations [23]. **N** stands for the native conformation. **U** represents the structurally heterogeneous unfolded state.

folding landscape is shown. This later picture more resembles a real protein folding process. Upon restoration of folding conditions, proteins at different positions of funnel edge will take different routes to fold to the native state. Due to the steep slopes of the funnel side, proteins undergo rapid collapse to form compact structures. Another important result of the funnel ruggedness is the existence of local minima that can give rise to the accumulation of transient intermediates or misfolded conformers. To escape from such local energy traps, misfolded proteins have to undergo thermally activated uphill steps by reconfiguring nonnative contacts into native interactions such that successful folding can commence.

1.4.4 Equilibrium and Kinetic Experiments

Protein folding can be studied using two types of experiments, i.e., equilibrium and kinetic studies. In equilibrium experiments, protein conformation is studied as a function of denaturant concentrations, typically in the unfolding direction. The concentration of denaturants is gradually increased in small steps, and after each step equilibration proceeds until the newly formed protein conformers adapt to the altered environment. Such experiments do not require a fast detection technique. High resolution with slow detection speed, such as NMR spectroscopy and optical methods are suitable for such experiments [30,31].

In kinetic experiments, protein conformational changes are studied as a function of time, following a rapid trigger event. Initiation of folding can be achieved by change in temperature, pH, or denaturant concentration [32,33]. Both unfolding and folding can be

studied in kinetic experiments. Because experimental data are acquired as a function of time, fast detection methods are needed. In section 1.6, some commonly used techniques for protein structural studies are reviewed in terms of mechanism and current development.

1.5 Protein Conformational Dynamics

To execute function, rigid tertiary and quaternary structures are not sufficient. The ability to undergo conformational changes or having flexibility is an important prerequisite that allows proteins to accomplish their tasks. Proteins in solution are highly dynamic with motions that take place on time scales that range from picoseconds to seconds [34-37]. These motions include ring-flipping [38] and thermal fluctuations of side chains and of the backbone, and large scale fluctuations involving distinct domains ("foldons") also take place [39-43].

Another important type of protein motions are conformational transitions between two equilibrium structures, typically induced by ligand binding or other external stimuli. Both types of protein motions are important for function [44-48]. Random thermal motions may represent a "molecular lubricant", allowing proteins to switch rapidly between different conformations. Large conformational changes induced by substrate binding or covalent modifications are required for many biological tasks. Examples include ATP synthase [49], signal transduction across cellular membrane [50] and enzyme catalysis [51].

1.6 Methods for Studying Protein Structure

1.6.1 Optical Spectroscopy

Optical techniques are widely used for examining protein conformations. Due to their high sensitivity and ease of use, they are quite popular in bio-analytical labs. Examples include UV-Visible (UV-Vis) absorption spectroscopy, circular dichroism (CD) and fluorescence spectroscopy. Signals obtained from these techniques report on the average properties of a protein sample. One advantage of these techniques is that proteins can be studied directly under physiological conditions without any chemical modifications.

In UV-Visible absorption spectroscopy, an electron in the highest occupied molecular orbital (HOMO) is excited into the lowest unoccupied molecular orbital (LUMO). Allowed HOMO LUMO transitions include $\sigma \rightarrow \sigma^*$, $\pi \rightarrow \pi^*$, $n \rightarrow \sigma^*$ and $n \rightarrow \pi^*$. In proteins, the constituent amino acids and binding cofactors usually have conjugated π systems that can absorb light. Absorbance (A) is defined as

$$A = \log \frac{I_o}{I} \qquad (8)$$

where A is absorbance, I_o is the incoming light intensity, and I is the transmitted light intensity [52]. Protein concentrations can be calculated based on the Beer-Lambert Law

$$A = \varepsilon(\lambda) lc \qquad (9)$$

where $\varepsilon(\lambda)$ is the molar absorption coefficient as a function of wavelength lambda, l is the light path length, and c is concentration. In addition to concentration measurements, this

technique can be applied to probe conformational aspects of proteins, especially where prosthetic group are present. Heme-bound proteins represent a particularly important case. The heme has strong electronic absorbance bands that depend on its metal oxidation state, ligation, and chromphore environment [53]. Subtle conformational changes can be reflected in the UV-Vis spectra as absorption band shifts. The main disadvantage of UV-Vis spectroscopy is that conformational changes of proteins without suitable chromophores cannot be detected with this method.

Circular Dichroism (CD) spectroscopy is an absorption-based technique for probing secondary and tertiary structure. CD is a phenomenon that is caused by the fact that chiral molecules absorb left and right circular polarized light differently. A CD spectrum is basically a plot of $(\varepsilon_L - \varepsilon_R)$ versus λ. Different secondary structures give rise to distinct CD signals in the *far-UV* (190-250 nm) region. In an α-helical environment, $n - \pi^*$ transitions of amide groups are associated with CD bands around 222nm, and $\pi - \pi^*$ transitions of amide groups are associated with CD bands around 208 nm for positive values and around 190 nm for negative values. The CD signal at 222nm is roughly proportional to the percentage of amino acids in an α-helical environment. In CD spectra of β-sheets there is a broad negative band around 215 nm, and random coil-like elements of proteins have their minimum at 202 nm [54]. Tertiary structure analysis can be made by *near UV CD* measurements in the range of 250-350 nm [55,56]. In this wavelength region protein absorption spectra are dominated by side chains of aromatic residues (Phe, Tyr and Trp). Within the protein structures unique three dimensional arrangements of these CD chromophores give rise to CD signals, and the intensity of such signals depends on the number of aromatic residues. Because of poor signal to noise ratio of typical CD

measurements, long integration time is often required. Consequently, CD is usually used under equilibrium conditions to monitor conformational changes.

Fluorescence is the emission of light when molecules return from the electronically excited singlet state (S_1) to the ground state (S_0). Among the natural amino acids tryptophan (Trp) is by far the most intense fluorophore [52]. Trp absorbs around 280 nm, and it emits around 350 nm. Fluorescence is highly sensitive to the environment; its efficiency depends on temperature, solvent ionic strength, and on the presence of quenchers. Generally, the fluorescence efficiency is higher in non-polar solvents because a hydrophobic environment can cause much less thermal deactivation of the excited state. By utilizing this characteristic, rapid hydrophobic core formation during protein folding can be monitored [57,58]. Another useful fluorescence technique is based on Förster resonance energy transfer (FRET). FRET was first demonstrated by Theodor Förster in the 1940s. He showed that excitation energy can transfer from one molecule to another. The FRET efficiency is defined as

$$ E = \frac{R_0{}^6}{R_0{}^6 + R^6} \qquad (10) $$

where R is distance between donor and acceptor, and R_0 is the Förster radius where E = 0.5. FRET represents a "molecular ruler" in both kinetic and equilibrium experiments. Sometimes covalent modification of proteins are required to perform such FRET experiments [59,60]. FRET can also lead to fluorescence quenching [61,62]. For example, proteins with heme groups can be studied using this phenomenon because heme acts as Trp quencher [63,64].

1.6.2 X-ray Crystallography

Protein molecules cannot be directly viewed by optical microscopy due to the long wavelength of visible light. X-ray crystallography, however, provides a way to locate the exact positions of individual atoms, since the X-ray wavelength is comparable to chemical bond lengths (~ 1 Å). Within an ordered protein crystal, unit cells, which are the smallest structural entity representing the entire crystal, are repeatedly arranged in a few ways along defined axes. Crystal planes of atoms are formed within such arrangements, and diffraction patterns can be obtained by X-ray radiation [65]. Protein crystal structure can be obtained from these diffraction patterns using Fourier transform methods.

 Ferdinard and Kendrew solved the first protein crystal structures (hemoglobin and myoglobin) in the 1950's [66] and won the 1962 Nobel Prize for this contribution. Today there are roughly 70,000 protein crystal structures deposited in the Protein Data Bank (www.pdb.org). X-ray crystallography provides time-averaged static protein conformations, and has greatly enhanced our understanding of protein structures and functions. However, dynamic aspects of protein structure can usually not be captured using crystallographic methods. Also, the growth of protein crystals can be a challenging task.

Protein crystals contain a significant amount of water. These solvent molecules allow diffusion and binding of small substrates to take place. In recent years, researchers also developed X-ray crystallography-based techniques to study small-scale protein dynamic events, e.g., transient intermediates on enzymatic pathways. Such transient

species can be studied by either low temperature trapping or by time resolved methods [42,67].

1.6.3 NMR

Nuclear Magnetic Resonance (NMR) spectroscopy represents another standard technique to characterize protein structure. There are roughly 8000 NMR structures in the PDB (corresponding to 11% of all entries). NMR monitors how magnetic nuclei absorb energy at particular resonance frequencies within an external magnetic field. This resonanance frequency depends on the type of element and on its chemical environment. Only nuclei with an odd number of protons and/or neutrons have a non-zero spin, and their chemical environment can be probed by NMR. For proteins, this includes ^{1}H, ^{13}C and ^{15}N. Heteronuclear NMR can be used to trace backbone assignment for better biomolecule structural refinement.

Unlike X-ray crystallography, NMR spectroscopy can be readily used for both the structural and dynamic characterization of proteins, because the relaxation of nuclei following an rf pulse is also affected by intramolecular motions [68]. ^{15}N and ^{13}C in the amide bonds of proteins can be probed in relaxation experiments for dynamic studies. Such studies can provide dynamic information on the ps-ns time scale [40].

NMR spectroscopy can also be combined with hydrogen deuterium exchange (HDX) (see section 1.6.4) to study protein dynamics in the millisecond range. If NH→ND exchange events happen in heavy water (D_2O), the disappearance of the corresponding proton signals can be monitored as a function of time. In this way residue-

specific dynamic information is obtained [69,70]. The free energy of unfolding can also be measured upon varying temperatures and pH [71,72]. During protein folding some amides form stable structures that are protected against deuterium labeling earlier than others. By probing the protection sequence of amides along protein sequences by HDX NMR, protein folding can be monitored in time-resolved experiments [73,74]. The upper size limit for protein structure determination by NMR is around 40 kDa, due to resonance overlap and relaxation time issues [75]. NMR spectroscopy requires mM protein concentration. Aggregation phenomena are often encountered in this concentration range.

1.6.4 Hydrogen Deuterium Exchange (HDX)

HDX was pioneered by Linderstrom-Lang and coworkers at the Carlsberg Laboratories in Copenhagen in the 1950s [76]. Linderstrom-Lang exposed proteins to D_2O labeling solution and measured deuteration using density gradient tubes. In the early 1990s the first protein conformational studies using HDX MS was published by Chait et al. [77].

As proteins are incubated in D_2O, labile hydrogens those in -NH, -SH and –OH bonds can exchange with deuterium. Typically only the HDX behavior of backbone amides are of interest for three major reasons: (1) Hydrogens involved in stable H-bonds (e.g. in α-helices or β-sheets) are largely protected from exchange. (2) Amide hydrogens are present along entire protein sequence. Except for proline residues HDX data can accurately reflect protein properties in terms of flexibity and solvent accessibility.   (3) Deuterated side chain hydrogens undergo rapid back-exchange (e.g., during HPLC) [78].

a.

b.
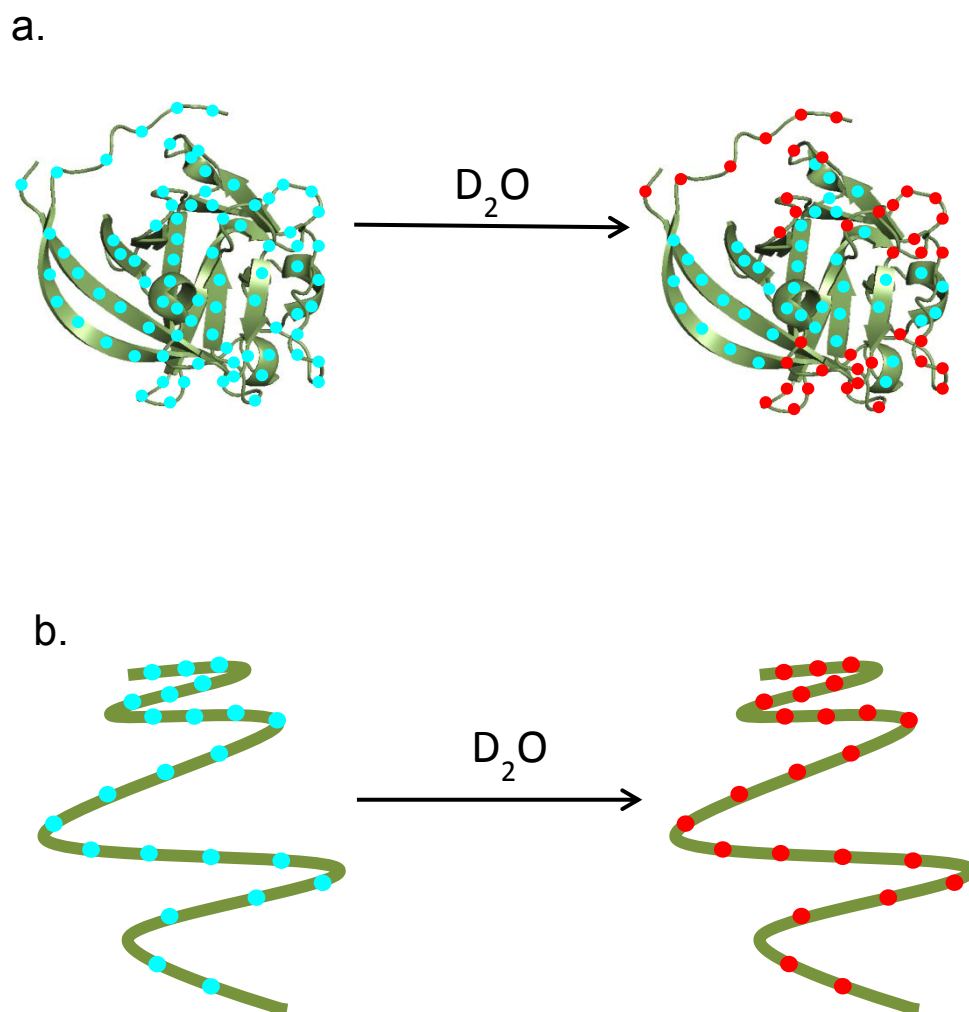
Figure 1-4. Schematic representation of HDX of (a) native protein and (b) denatured protein resulting in different labeling extents. Hydrogen (dots in cyan) Deuterium (dots in red)

 As proteins undergo thermal motions, hydrogen bonds can be disrupted and buried amide hydrogens can transiently become exposed, such that slow HDX can take place. Amide hydrogens in disordered structures undergo much faster HDX than those in folded regions. As a result, HDX provides information on protein structure and dynamics. For example, native proteins are readily labeled only in flexible loops (**Figure 1-4a**). Denatured proteins are labeled by deuteriums to much higher extent due to their random coil structures (**Figure 1-4 b**).

   HDX experiments are typically used to study conformational dynamics of proteins at equilibrium. Amide hydrogens are either in protected non-exchangeable states (H_{closed}) or transient unprotected states (H_{open}) due to protein motions. HDX reaction can be expressed as in equation 11

$$N-H_{closed} \underset{k_{cl}}{\overset{k_{op}}{\rightleftarrows}} N-H_{open} \xrightarrow[D_2O]{k_{ch}} N-D_{exchanged} \quad (11)$$
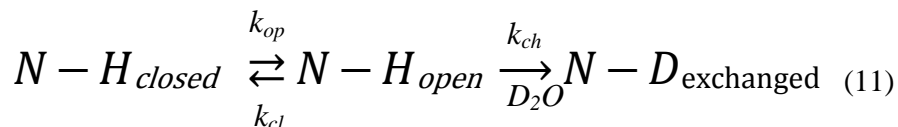
where k_{op}, k_{cl} and k_{ch} are rate constants of opening, closing and chemical exchange at unprotected sites respectively. This chemical reaction equation indicates that HDX can be divided into two regimes referred to as "EX1" and "EX2" [79,80]. Under EX1 conditions, $k_{ch} \gg k_{cl}$, HDX of amide hydrogens happen immediately once the protein opens up, and the HDX rate constant is equal to k_{op}. In the EX2 case, $k_{cl} \gg k_{ch}$, the HDX rate constant depends on both protein motions and chemical exchange rate according to

$$k_{HDX} = K_{op}k_{ch} \quad (12)$$

where $K_{op} = (k_{op}/k_{cl})$ [80,81].

1.7 Mass Spectrometry

Although MS has been a well-known analytical tool for quite some time, intact biomolecular analysis by MS only become possible in the late 1980s due to the invention of two soft ionization techniques, namely Matrix-Assisted Laser Desorption/Ionization (MALDI) and Electrospray Ionization (ESI). In 2002 the Chemistry Nobel Prize was shared by Tanaka [82] and Fenn [83] for their contributions in these areas. With ESI and MALDI fragile macromolecules such as proteins can be transferred into the gas-phase without fragmentation. Because ESI is exclusively used throughout this work, the following sections will discuss the mechanisms of this process. MALDI will only be discussed very briefly. MALDI was developed by Karas and Hillenkamp in 1985 [84]. For MALDI, proteins are initially embedded in a crystalline matrix consisting of small ultraviolet–absorbing molecules. This matrix is then irradiated with a short laser pulse to induce desorption of proteins together with matrix molecules. One or more protons can be attached or removed from a protein thus generating gas-phase ions that can be detected by MS. MALDI is highly sensitive, and it is tolerant to salts and impurities [85]. The charges of proteins ionized by MALDI are generally low, and a high m/z range detector (such as a TOF analyzer) is necessary to observe protein ions.

1.7.1 Ionization of Proteins by ESI

Electrospray has been used as a painting method in the automobile industry for many years. Fenn used this idea to develop an MS ionization technique [83]. ESI is a versatile and soft ionization technique allowing proteins to be transferred into the gas phase as

intact ions (**Figure 1-5).** The analyte solution is pumped through a metal capillary, to which a positive high voltage (3-5 kV) applied (negative voltages are less commonly used). Positive ions are enriched at the tip of the capillary, causing the solution to form a Taylor cone. Charge-balancing redox processes at the metal/liquid interface of the ESI capillary include the following:

Solvent oxidation $\quad\quad\quad$ $H_2O \rightarrow 2H^+ + 2e^- + 1/2\ O_2$

Metal Oxidation $\quad\quad\quad$ $Fe \rightarrow Fe^{n+} + ne^-$

Analytes Oxidation $\quad\quad$ $M \rightarrow M\bullet+ + e-$

Positively charged droplets are emitted from the Taylor cone. Solvent continuously evaporates from these droplets. At the Rayleigh limit where charge repulsion is equal to surface tension forces [86], fission of the original droplet occurs, and droplets with much smaller sizes are produced via jet fission. After this process repeats itself several times, the radius of the droplets is close to the size of a single protein molecule. Multiply charged protein ions are produced from nanodroplets. The mechanism of this last ion production step is still not clear. Two general models have been proposed for this step, the Charged Residue Model (CRM) and the Ion Evaporation Model (IEM). In the IEM model, analytes are ejected out of the droplet due to high electric field at the droplet surface for droplet radii less than 100 Å [87-89]. Natively folded proteins are believed to follow the charge residue model (CRM), where protein ions are formed as the droplet evaporates to dryness, while all leftover charge is absorbed by the protein [87].
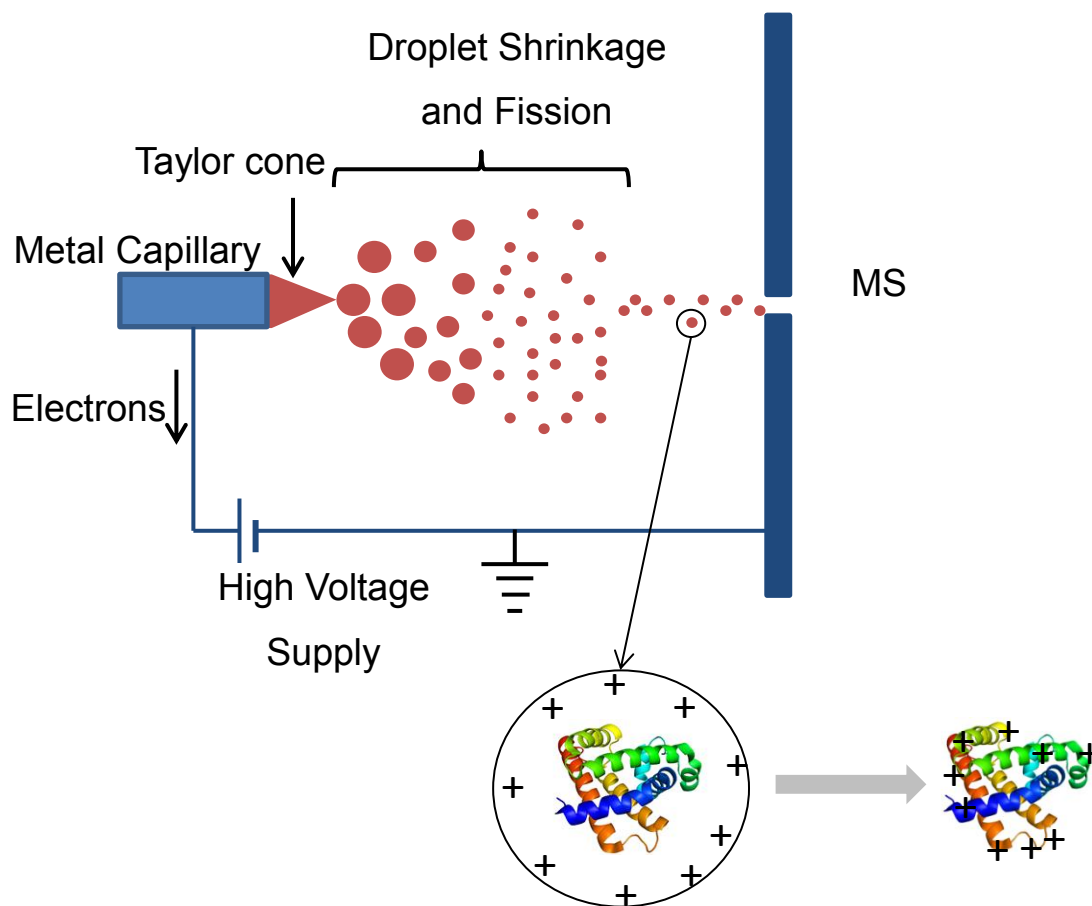
Figure 1-5. Schematic depiction of the positive ion mode ESI process. Protein solution (red) is sprayed from a metal capillary (blue), and a Taylor cone is formed as a result of the applied high voltage. Multiply charged protein ions are formed via multiple droplet shrinkage and fission processes.

Protein ions produced by ESI are not all carrying the same charge, instead these ions appear in charge state distributions (CSD). Individual peaks appear at m/z values that are given by

$$R = \frac{M+zm}{z} = \frac{M}{z} + m \qquad (13)$$

where R is observed mass-to-charge ratio, M is mass of analyte, z is number of charges and m is the mass of the adduct ion, typically H^+. The charge states of native proteins are close to $[M+z_RH]^{z_R+}$, where z_R is the number of charges at the Rayleigh limit

$$z_R = \frac{8\pi \ (\varepsilon_0 \ \gamma \ r_{droplet}{}^3)^{1/2}}{e} \qquad (14)$$

where ε_o is the vacuum permittivity, γ is the surface tension, and $r_{droplet}$ represents the droplet radius. Formation of protein ions close to Z_R provides strong support for the notion that native protein ionization follows the CRM. Protein unfolding can be induced by adding volatile acids or organic solvents to the solution. The resulting mass spectra show very wide CSDs at values much higher than Z_R. The CRM does not apply to the ESI process of unfolded proteins. Recent simulation studies have shown that unfolded proteins ionize via ejection from nanodroplets, which is a type of IEM mechanism [90]. For a nanodroplet containing an unfolded protein ion, unfavorable charge repulsion on droplet surface can be minimized through ejection of the unfolded protein. Due to this different ionization mechanism, CSDs can be used to probe protein solution phase structures. Even though some other factors may affect protein CSDs, it is clear that solution phase conformation is the major determinant [91]. High charge states are seen for

proteins after denaturation in acid, base, heat, disulfide bond cleavage, and for intrinsically disordered proteins [92-95]. During protein folding and unfolding there can be numerous intermediates that can be studied by ESI-MS through analysis of their CSDs. A more detailed discussion of protein ESI mechanisms is provided in section 1.8.

1.7.2 Mass Analyzers

Following ESI, gaseous protein ions follow a trajectory along "downhill" electric potential gradients, and finally they reach a suitable detector. Gas phase ions can be separated according to *m*/*z* while they transverse the mass spectrometer. Such separation can be achieved by application of electric or magnetic fields [96,97]. Quadrupole and Time of Flight (TOF) analyzers are most commonly used for research, and they provide the basis for this thesis.

1.7.2.1 Quadrupole Mass Analyzer

A quadrupole is composed of two pairs of cylindrical rods. DC and RF voltages with opposite polarity are applied to each pair of rods (**Figure 1-6a**). With fixed ratio, DC and RF voltage amplitudes are scanned at constant frequency from several volts to ~ 1 kV. At each DC/RF ratio only ions with one specific m/z value have a stable trajectory and can be transmitted through the quadrupole, while other ions all collide with the rods (**Figure 1-6b**). Ion trajectories can be predicted using Newton's Laws [98]. The ion behavior can be explained using a stability diagram in a,q Cartesian coordinates (**Figure 1-7**). The area under blue curve represents the stabe region. Ions with a and q values within the stable

a.

$$U - V_0 \cos \omega t$$

$$r_0$$

$$-(U - V_0 \cos \omega t)$$
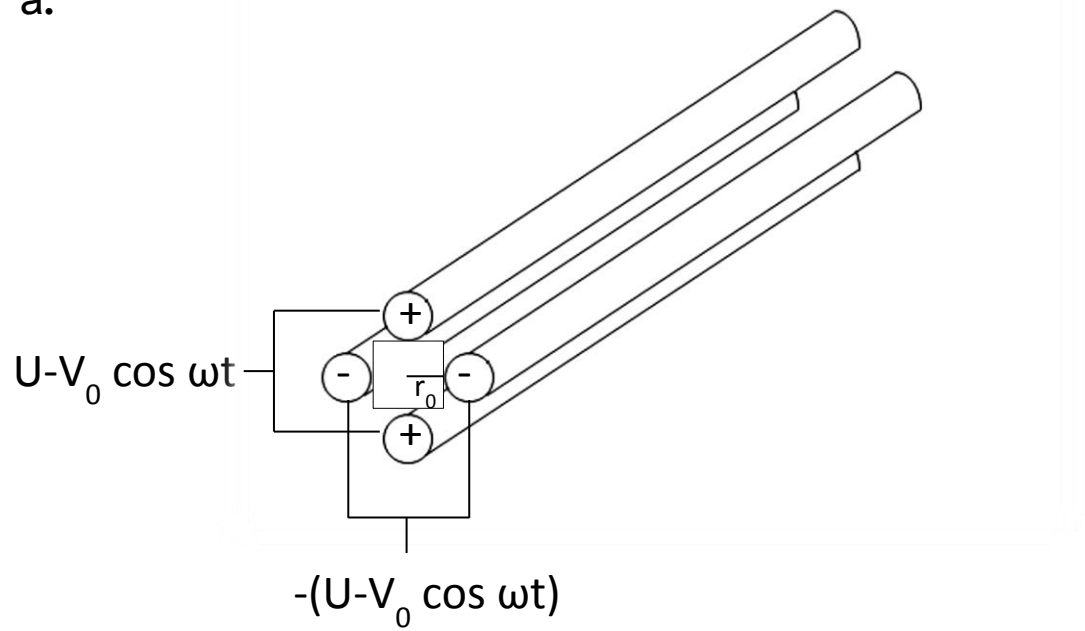
Figure 1-6a. Schematic representation of a quadrupole mass analyzer.

b.
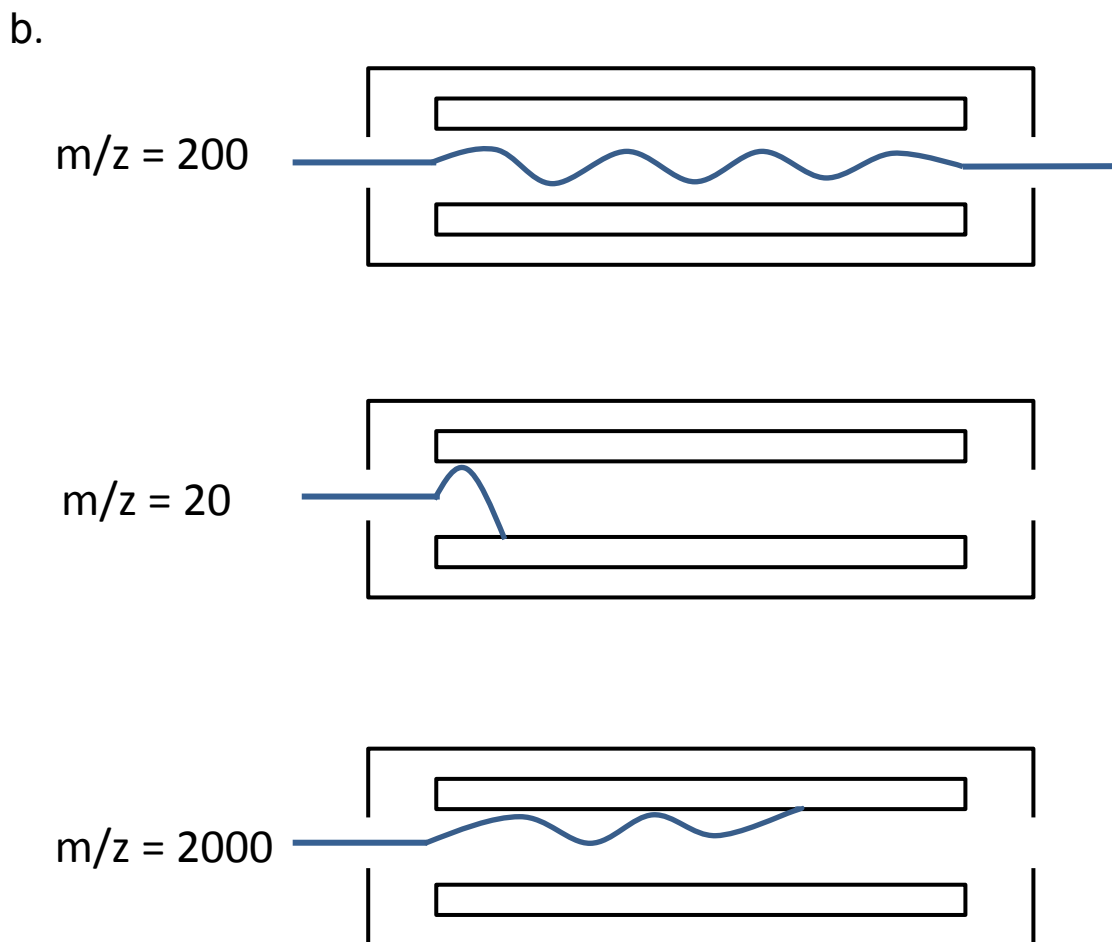
m/z = 200

m/z = 20

m/z = 2000

Figure 1-6b. Examples of stable and unstable ion trajectories at certain DC/RF voltages which allow ions with *m/z* 200 transmitted through the quadrupole. Lower and higher mass ions collide with the rods because they have unstable trajectories.
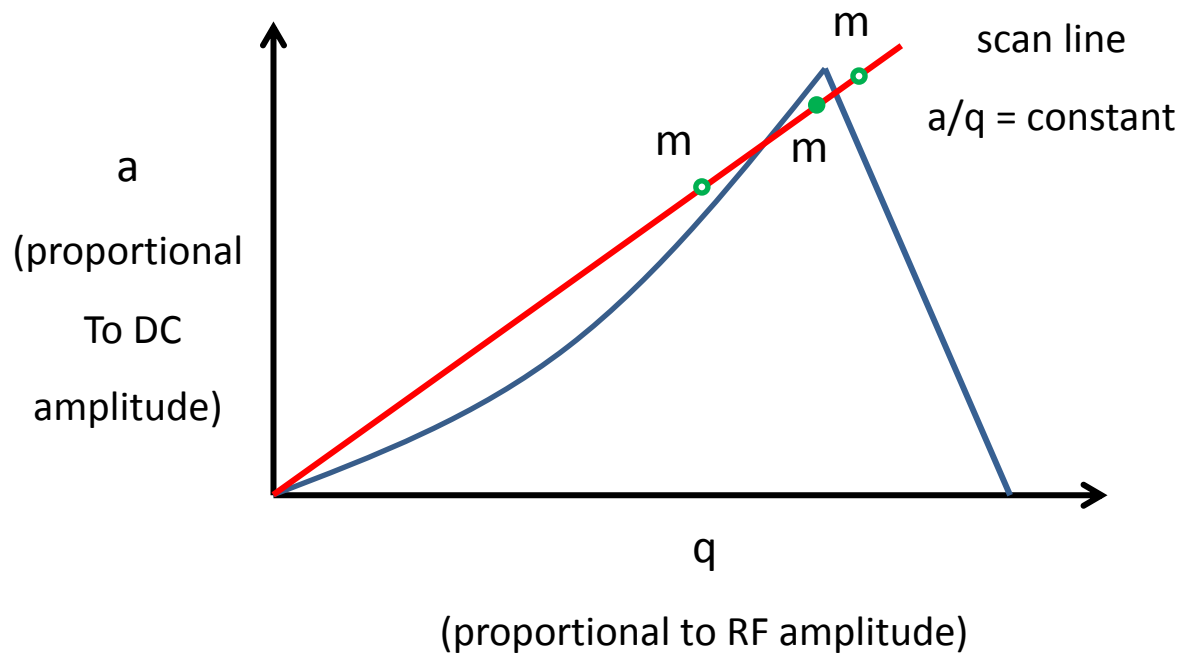
Figure 1-7. Schematic depiction of a quadrupole stability diagram, together with the scan line (red line), and ions with stable (m_2) and unstable (m_1 and m_3) trajectories.

region are transmitted (top picture in **Figure 1-6b**). Ions in unstable regions will hit the cylindrical rods and be neutralized (middle and bottom, in **Figure 1-6b**).

A quadrupole can be used as "mass filter" by choosing a combination of DC/RF values to selectively transfer certain ions. To obtain mass spectra for certain mass range, the DC/RF voltages are changed along the scan line (red curve in **Figure 1-7**) with fixed ratio of DC/RF voltages. At each DC/RF value, ions with a specific *m/z* value are located at the tip of the stability diagram (solid green dot, **Figure 1-7**), and detected after transmission. Ions with *m/z* values outside the stability region (open green circles, **Figure 1-7**) will collide with the quadrupole. By changing the slope of the scan line, the resolution can be optimized. The transmission decreases as resolution increases.

1.7.2.2 Time of Flight (TOF) Mass Analyzer

For TOF mass analysis the injected ions are accelerated towards the detector by a suitable voltage pulse. Potential energy is converted to kinetic energy, and the time required for ions taken to reach the detector can be calculated as follows:

$$E_{pot} = E_{kin}$$

$$ze\Delta U = 1/2 mv^2 \text{ and } v = \frac{l}{t} \quad (15)$$

$$t = l\sqrt{\frac{m}{z}\frac{1}{2e\Delta u}} \quad (16)$$

where ΔU is the acceleration voltage and l is the length of time of flight tube. Based on equation 16, ions with different m/z can be separated by their different flight time. Ions with the same *m/z* might result in slightly different velocities due to imperfictions in the pusher region, resulting in peak broadening [99]. To compensate for this effect, a reflectron is coupled to the TOF mass analyzer (**Figure 1-8**). Using a reflectron, the TOF resolution can be increased from 4000 to 20,000. Again with increased resolution, lower sensitivity is a sacrifice due to lower ion transmission. Based on these considerations a resolution of 10,000 is usually optimal for TOF instruments. Quadrupole-time-of-flight (Q-TOF) mass spectrometers (**Figure 1-8**) are hybrid instruments that work analogously to a triple quadrupole mass spectrometer, except that the third quadrupole has been replaced with a TOF.

1.7.2.3 Other Mass Analyzers

There are also several other types of mass analyzers, some of which are briefly described in this section. Fourier Transform Ion Cyclotron Resonance (FT-ICR) MS has evolved to be the highest resolution mass analysis method [100,101] since it is invented by Melvin B. Comisarow and Alan G. Marshall in 1974 [102]. In FT-ICR ions are forced into periodic motions in a magnetic field generated by a large superconducting magnet. The ion cyclotron frequency depends on *m/z* according to

$$\omega_c = \frac{zeB}{m} \qquad (17)$$

For the entire generated ions, time domain signals are transferred into corresponding peaks in frequency domain through a Fourier Transform (FT) process, and in turn mass spectra are obtained through equation 17 by calculating m/z values for peaks in frequency domain. Mass resolution of FT-ICR MS is actually frequency resolution and can be improved by longer acquisition time or larger magnetic strength [103]. Typically the resolution is larger than 10^6. Ion motions induce image current and are detected in a pair of receiver plates. Unlike other mass analyzers, FT-ICR is non-destructive and the same bunch of ions can be measured repeatedly.

The orbitrap mass analyzer was developed around 2000 [104]. Many aspects of orbitrap operation resemble FT-ICR. As ions are pulsed into orbitrap mass analyzer these ions are circulating around a central electrode and oscillate with distinct axial frequencies. Axial oscillations are harmonic and generate an image current on the two outer electrodes where the signal is measured. Frequency of this harmonic motion is also m/z dependent, and mass spectrum is obtained via FT [105]. The resolution of orbitrap mass analyzer is usually around 10^5.

Ion mobility spectrometry (IMS) is an analytical technique which separates ions in a buffer gas as they are exposed to a weak electric field. IMS coupled with MS is a powerful technique to study gas phase ion structures. One widely used commercial IMS MS system is the Synapt HDMS, which is a hybrid quadrupole/travelling wave IMS/oa-ToF instrument [106]. By applying a travelling voltage to a stacked-lens RF ion guide, gas phase ions can be separated based on their mobilities. With proper gas pressure high mobility ions can keep up with the travelling voltage waves, and low mobility ions gradually fall behind. By employing proper calibration it is possible to obtain collision

cross sections (CCSs) of the ions [107]. Computer algorithms have been developed to calculate CCSs [108]. These approaches have been successfully applied to gain insights into structural features of gas phase protein ion complexes [109-111].

1.8 ESI Process for Native and Unfolded Proteins

Since ESI-MS can be used as a tool to distinguished solution-phase protein conformations, it is important to understand the ionization mechanism for different protein conformers. Even though CRM and IEM are classically considered to be the major ionization mechanisms, recent studies have found another ionization mechanism called Chain Ejection Model (CEM) which applies to unfolded proteins [90,112].

Native proteins typically have compact folded globular structures with numerous polar and charged residues, which surround the hydrophobic core. For example, horse myoglobin pocesses numerous charged residues, including 2 Arg, 19 Lys, 13 Glu, 2 Asp, 2 heme propionates, and the carboxyl terminus. X-ray data show that these 46 charged
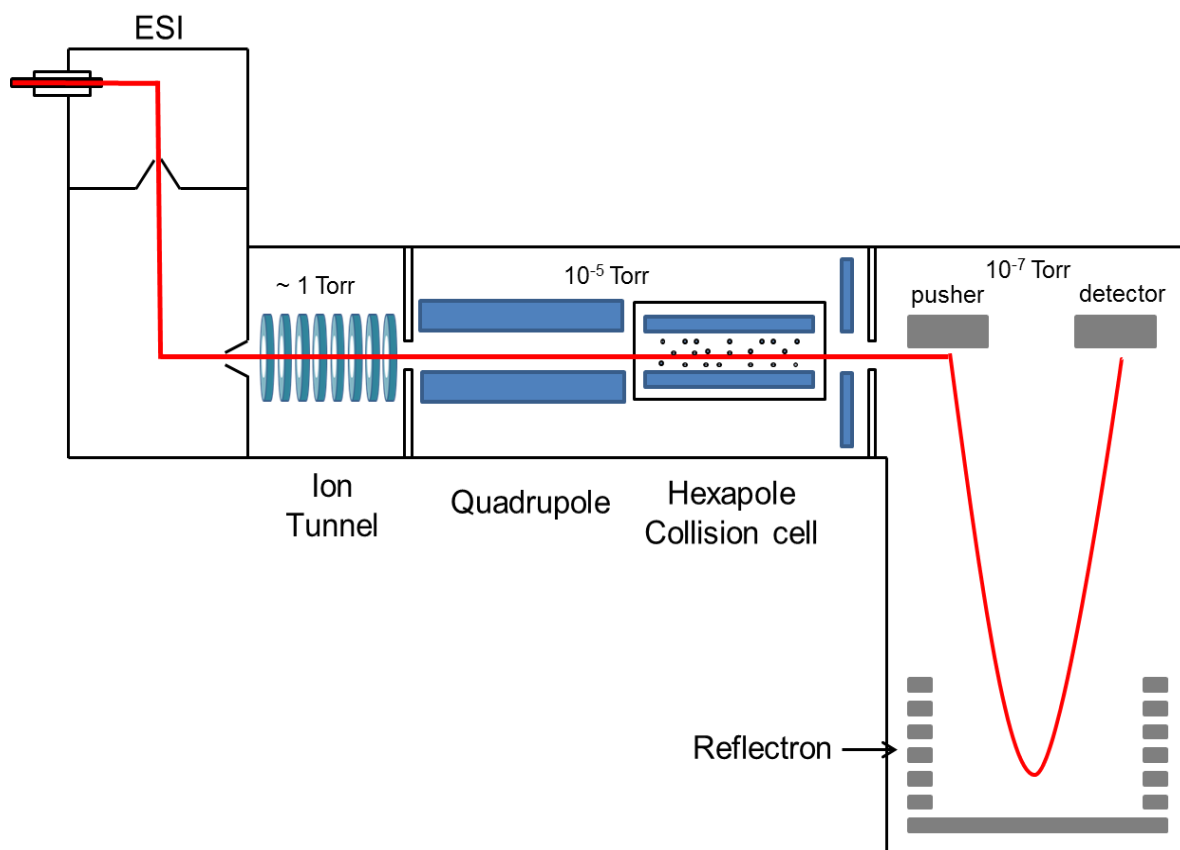
Figure 1-8. Schematic depiction of a Q-TOF mass spectrometer equipped with hexapole collision cell for collision induced dissociation (CID). The red line indicates the ion trajectory.

moieties are all exposed to the solvent, where as a large number of hydrophobic residues are buried [113]. Thus, the native protein is hydrophilic and can be nicely solvated in water. MD simulations revealed that such hydrophilic structures will remain inside the nanometer sized charged water droplets [112]. Mass spectra of native proteins show experimental charge states that match the charges calculated by the Rayleigh equation [87,114] (eq.14). Therefore, ESI process of native folded proteins proceeds via the CRM.

In contrast, ESI mass spectra of unfolded protein show much wider charge state distributions centered at higher protonation states. MD simulations indicate that these unfolded proteins are gradually ejected from charged nanometer-sized water droplet during ESI [112]. However, this Chain Ejection Model (CEM) mechanism is different from the classical small ion IEM scenario. Small ions are ejected from the droplet surface via field emission in a single step [87,115-118]. In contrast, unfolded proteins are ejected in a sequential manner, one residue at a time. Such ejection is driven by Coulomb repulsion between positively charged side chains and charges on the droplet. Because unfolded proteins expose non-polar residues in the hydrophobic core, the CEM is also facilitated by unfavorable interactions between water and hydrophobic residues. Charge partitioning during ESI of unfolded proteins resembles the dissociation of gaseous multi-subunit proteins [90].

1.9 Studying Noncovalent Protein Complexes by ESI-MS

In a cell most proteins do not exist as single entities. Instead, many proteins noncovalently interact with various binding partners to carry out biological activities [119]. Such noncovalent interactions can occur with proteins, nucleic acids, metal ions and cofactors. ESI-MS allows the transfer of intact noncovalent protein complexes into the gas phase within a reasonable *m/z* range [120-122]. ESI-MS data can reflect solution phase structural information by providing m/z ratios of protein complexes. Additionally, coupled with gas phase or solution phase dissociation methods, the constituent masses and binding stoichiometry can also be determined. As a result, ESI-MS is now well established as a tool for studying structural aspects of noncovalent protein complexes [123-125]. Nonetheless, analysis of noncovalent complexes by ESI MS is challenging due to several reasons: (1) interactions between protein subunits are easily disrupted under typical analysis condition; (2) analyzer capable of detecting high m/z ions are required during data acquisition; (3) peaks in the mass spectra can be extensively broadened due to adduct formation.

1.10 Scope of Thesis

In this thesis, ESI-MS is used in conjuction with optical spectroscopy to explore protein structure and interactions.

In **chapter 2**, the physical reasons underlying irreversible thermal denaturation of *cytochrome c (cyt c)* was investigated. Covalent oxidative modifications induced by heating are shown to be responsible for the observed behavior. By using optical tools and HDX together with ESI-MS, differences in conformational dynamics of *cyt c* between acid denaturation and thermal denaturation have been confirmed. LC-MS/MS was used to locate oxidative modification sites after tryptic digestion.

In **chapter 3**, solution phase binding affinities of noncovalent complexes are studied ESI-MS. We established experimental procedures to ensure that ESI-MS data properly reflect solution-phase binding addinities. Different ESI sources and various experimental conditions are tested and compared.

In **chapter 4**, formation of a noncovalent protein complexes, hemoglobin, was studied by using ESI-MS together with optical spectroscopy. We examine the effects of off-pathway intermediates and protein aggregation. Refolding intermediates were assigned based on their *m/z* values. In this way it is demonstrated that ESI-MS can be used for studying a highly complex biomolecular self-assembly process.

1.11 References

1. Voet, D. V., J. G., and Pratt, C.W. *Fundamentals of Biochemistry, 2nd Edition*; John Wiley & Sons, 2004.

2. Pauling, L.; Corey, R. B.; Branson, H. R. The structure of proteins: two hydrogen-bonded helical configurations of the polypeptide chain. *Proc. Natl. Acad. Sci.* **1951,** *37*, 205-211.

3. Tinoco, I.; Sauer, K.; Wang, J. C. *Physical Chemistry: Principles and Applications in Biological Sciences*3rd ed.; Simon & Schuster Company: London, 1995.

4. Hendsch, Z. S.; Tidor, B. Do salt bridges stabilize proteins? A continuum electrostatic analysis. *Protein Sci.* **1994,** *3*, 211-226.

5. Dill, K. A. Dominant Forces in Protein Folding. *Biochemistry* **1990,** *29*, 7133-7155.

6. Berendsen, H. J. C.; Grigera, J. R.; Straatsma, T. P. The missing term in effective pair potentials. *J. Phys. Chem.* **1987,** *91*, 6269-6271.

7. Chen, J.; Stites, W. E. Packing Is a Key Selection Factor in the Evolution of Protein Hydrophobic Cores. *Biochem.* **2001,** *40*, 15280-15289.

8. Sharp, K. A.; Madan, B. Hydrophobic Effect, Water Structure, and Heat Capacity Changes. *J. Phys. Chem. B* **1997,** *101*, 4343-4348.

9. Pace, C. N.; Fu, H.; Fryar, K. L.; Landua, J.; Trevino, S. R.; Shirley, B. A.; Hendricks, M. M.; Iimura, S.; Gajiwala, K.; Scholtz, J. M.; Grimsley, G. R. Contribution of Hydrophobic Interactions to Protein Stability. *J. Mol. Biol.* **2011,** *408*, 514-528.

10.   Haran, G. How, when and why proteins collapse: the relation to folding. *Curr. Opin. Struct. Biol.* **2012,** *22*, 14-20.

11.   Teufel, D. P.; Johnson, C. M.; Lum, J. K.; Neuweiler, H. Backbone-Driven Collapse in Unfolded Protein Chains. *J. Mol. Biol.* **2011,** *409*, 250-262.

12.   Chaplin, M. F.; Bucke, C. *Enzyme Technology*1 ed.; Cambridge University Press: Cambridge, 1990.

13.   Dobson, C. M. Protein folding and misfolding. *Nature* **2003,** *426*, 884-890.

14.   Selkoe, D. J. Folding proteins in fatal ways. *Nature* **2003,** *426*, 900-904.

15.   Smith, A. Protein Misfolding. *Nature* **2003,** *426*, 883.

16.   Chiti, F.; Dobson, C. M. Protein Misfolding, Functional Amyloid, and Human Disease. *Annu. Rev. Biochem.* **2006,** *75*, 333-366.

17.   Uversky, V. N.; Fink, A. L. Protein Misfolding, Aggregation, and Conformational Disease. In *Protein Reviews;* Atassi, M. Z. Ed.; Springer: Singapore, 2006; Vol. 1,2.

18.   Luheshi, L. M.; Crowther, D. C.; Dobson, C. M. Protein Misfolding and Disease: From the Test Tube to the Organism. *Curr. Op. Chem. Biol.* **2008,** *12*, 25-31.

19.   MacCallum, J. L.; Perez, A.; Schnieders, M. J.; Hua, L.; Jacobson, M. P.; Dill, K. A. Assessment of protein structure refinement in CASP9. *Proteins* **2011,** *79 Suppl 10*, 74-90.

20. Perutz, M. F. Structure and Function of Haemoglobin I. A Tentative Atomic Model of Horse Oxyhaemoglobin. *J. Mol. Biol.* **1965,** *13*, 646-668.

21. Anfinsen, C. B. Principles that Govern the Folding of Protein Chains. *Science* **1973,** *181*, 223-230.

22. Levinthal, C. Mossbauer Spectroscopy in Biological Systems. In *Proceedings of a Meeting Held at Allerton House, Monticello, Illinois;* DeBrunner, J. T. P.; Munck, E. Eds.; University of Illinois Press: Chicago, 1969; pp. 22-24.

23. Dill, K. A.; Chan, H. S. From Levinthal to pathways to funnels. *Nat. Struct. Biol.* **1997,** *4*, 10-19.

24. Daggett, V.; Fersht, A. R. Is there a unifying mechanism for protein folding? *Trends Biochem. Sci.* **2003,** *28*, 18-25.

25. Jackson, S. E.; Fersht, A. Folding of Chymotrypsin Inhibitor 2. 1. Evidence for a Two-State Transition. *Biochem.* **1991,** *30*, 10428-10435.

26. Burton, R. E.; Myers, J. K.; Oas, T. G. Protein Folding Dynamics: Quantitative Comparison between Theory and Experiment. *Biochemistry* **1998,** *37*, 5337-5343.

27. Schonbrun, J.; Dill, K. A. Fast protein folding kinetics. *Proc. Natl. Acad. Sci. U.S.A.* **2003,** *100*, 12678-12682.

28. Sinha, K. K.; Udgaonkar, J. B. Barrierless evolution of structure during the submillisecond refolding reaction of a small protein. *Proc. Natl. Acad. Sci. U.S.A.* **2008,** *105*, 7998-8003.

29.   Zwanzig, R. Two-state models of protein folding kinetics. *Proc. Natl. Acad. Sci. U.S.A.* **1997,** *94*, 148-150.

30.   Aghera, N.; Earanna, N.; Udgaonkar, J. B. Equilibrium Unfolding Studies of Monellin: The Double-Chain Variant Appears To Be More Stable Than the Single-Chain Variant. *Biochemistry* **2011,** *50*, 2434-2444.

31.   Habazettl, J.; Reiner, A.; Kiefaber, T. NMR Structure of a Monomeric Intermediate on the Evolutionarily Optimized Assembly Pathway of a Small Tremerization Domain. *J. Mol. Biol.* **2009,** *389*, 103-114.

32.   Nabuchi, Y.; Murao, N.; Asoh, Y.; Takayama, M. Probing the Unfolding and Refolding Processes of Carbonic Anhydrase 2 Using Electrospray Ionization Mass Spectrometry Combined with pH Jump. *Anal. Chem.* **2007,** *79*, 8342-8349.

33.   Lin, M. M.; Mohammed, O. F.; S., J. G.; Zewail, A. H. Speed limit of protein folding evidenced in secondary structure dynamics. *Proc. Natl. Acad. Sci. U.S.A.* **2011,** *108*, 16622-16627.

34.   Karplus, M.; McCammon, J. A. Dynamics of Proteins: Elements and Function. *Ann. Rev. Biochem.* **1983,** *53*, 263-300.

35.   Frauenfelder, H.; Sligar, S. G.; Wolynes, P. G. The Energy Landscape and Motions of Proteins. *Science* **1991,** *254*, 1598-1603.

36.   McCammon, J. A. Protein dynamics. *Rep. Prog. Phys.* **1984,** *47*, 1-46.

37.   Falke, J. J. A Moving Story. *Science* **2002,** *295*, 1480-1481.

38.   Wuthrich, K.; Wagner, G. Internal motion in globular proteins. *Trends Biochem. Sci.* **1978,** *3*, 227-230.

39. Palmer III, A. G. NMR Probes of Molecular Dynamics: Overview and Comparison with Other Techniques. *Annu. Rev. Biophys. Biomol. Struct.* **2001,** *30*, 129 - 155.

40. Wand, A. J. Dynamic activation of protein function: A view emerging from NMR spectroscopy. *Nat. Struct. Biol.* **2001,** *8*, 926-931.

41. Weiss, S. Measuring conformational dynamics of biomolecules by single molecule fluorescence spectroscopy. *Nature Struct. Biol.* **2000,** *7*, 724-729.

42. Moffat, K. Time-resolved biochemical crystallography: a mechanistic perspective. *Chem.Rev.* **2001,** *101*, 1569-1581.

43. Daggett, V. Long timescale simulations. *Curr Opin Struct Biol* **2000,** *10*, 160-4.

44. Osborne, M. J.; Schnell, J.; Benkovic, S. J.; Dyson, H. J.; Wright, P. E. Backbone dynamics in dihydrofolate reductase complexes: role of loop flexibility in the catalytic mechanism. *Biochemistry* **2001,** *40*, 9846-59.

45. Faber, H. R.; Matthews, B. W. A mutant T4 lysozyme displays five different crystal conformations. *Nature* **1990,** *348*, 263-6.

46. Joseph, D.; Petsko, G. A.; Karplus, M. Anatomy of a conformational change: hinged "lid" motion of the triosephosphate isomerase loop. *Science* **1990,** *249*, 1425-8.

47. Forman-Kay, J. D. The 'dynamics' in the thermodynamics of binding. *Nature Structural Biology* **1999,** *6*, 1086-7.

48.   Wang, C.; Pawley, N. H.; Nicholson, L. K. The role of backbone motions in ligand binding to the c-Src SH3 domain. *J Mol Biol* **2001,** *313*, 873-87.

49.   Pu, J.; Karplus, M. How subunit coupling produces the γ-subunit rotary motion in F$_1$-ATPase. *Proc. Natl. Acad. Sci. U.S.A.* **2008,** *105*, 1192-1197.

50.   Belcheva, A.; Golemi-Kotra, D. A Close-up View of the VraSR Two-component System: A MEDIATOR OF STAPHYLOCOCCUS AUREUS RESPONSE TO CELL WALL DAMAGE. *J. Biol. Chem.* **2008,** *283*, 12354-12364.

51.   Sytina, O. A.; Heyes, D. J.; Hunter, C. N.; Alexandre, M. T.; van Stokkum, I. H.; van Grondelle, R.; Groot, M. L. Conformational changes in an ultrafast light-driven enzyme determine catalytic activity. *Nature* **2008,** *456*, 1001-1004.

52.   Skoog, D. A. *Principles of Instrumental Analysis*; Brooks/Cole Thomson Learning: Toronto, 1998.

53.   Antonini, E.; Brunori, M. *Hemoglobin and Myoglobin in Their Reactions With Ligands*; North-Holland Publishing Company: Amsterdam, London, 1971; Vol. 21.

54.   Brahms, S.; Brahms, J. Determination of Protein Secondary Structure in Solution by Vacuum Ultraviolet Circular Dichroism. *J. Mol. Biol.* **1980,** *138*, 149-178.

55.   Zubay, G. *Biochemistry* 4th ed.; Wm. C. Brown: Dubuque, IA, 1998.

56.   Kelly, S. W.; Jess, T. J.; Price, N. C. How to Study Protein by Circular Dichroism. *Biochim. Biophys. Acta* **2005,** *1751*, 119-139.

57.   Agashe, V. R.; Shastry, M. C. R.; Udgaonkar, J. B. Initial hydrophobic collapse in the folding of barstar. *Nature* **1995,** *377*, 754-757.

58.   Sadqi, M.; Lapidus, L. J.; Munoz, V. How fast is protein hydrophobic collapse? *Proc. Natl. Acad. Sci. U.S.A.* **2003,** *100*, 12117-12122.

59.   Deniz, A. A.; Laurence, T. A.; Beligere, G. S.; Dahan, M.; Martin, A. B.; Chemla, D. S.; Dawson, P. E.; Schultz, P. G.; Weiss, S. Single-molecule protein folding: Diffusion fluorescence resonance energy transfer studies of the denaturation of chymotrypsin inhibitor 2. *Proc. Natl. Acad. Sci. U.S.A.* **2000,** *97*, 5179-5184.

60.   Ishii, Y.; Yoshida, T.; Funatsu, T.; Wazawa, T.; Yanagida, T. Fluorescence resonance energy transfer between single fluorophores attached to a coiled-coil protein in aqueous solution. *Chem. Phys.* **1999,** *247*, 163-173.

61.   Elöve, G. A.; Bhuyan, A. K.; Roder, H. Kinetic Mechanism of Cytochrome c Folding: Involvement of the Heme and Its Ligands. *Biochemistry* **1994,** *33*, 6925-6935.

62.   Lee, S. P.; Engman, K. C.; Tezcan, F. A.; Gray, H. B.; Winkler, J. R. Structural features of cytochrome c' folding intermediates revealed by fluorescence energy-transfer kinetics. *Proc. Natl. Acad. Sci. U.S.A.* **2002,** *99*, 14778-14782.

63.   Kawamura-Konishi, Y.; Kihara, H.; Suzuki, H. Reconstitution of myoglobin from apoprotein and heme, monitored by stopped-flow absorption, fluorescence and circular dichroism. *Eur. J. Biochem.* **1988,** *170*, 589-595.

64.   Shen, L. L.; Hermans, J. Kinetics of Conformation Change of Sperm-Whale Myoglobin. I. Folding and Unfolding of Metmyoglobin following pH jump. *Biochemistry* **1972,** *11*, 1836-1841.

65.   Rhodes, G. *Crystallography Made Crystal Clear* 2nd ed.; Academic Press: San Diego, 2000.

66.   Kendrew, J. C.; Bodo, G.; Dintzis, H. M.; Parrish, R. G.; Wyckoff, H. W.; Phillips, D. C. A Three-Dimensional Model of the Myoglobin Molecule Obtained by X-Ray Analysis. *Nature* **1958,** *181*, 662-666.

67.   Petsko, G. A.; Ringe, D. Observation of unstable species in enzyme-catalyzed transformations using protein crystallography. *Curr Opin Chem Biol* **2000,** *4*, 89-94.

68.   Case, D. A. Molecular dynamics and NMR spin relaxation in proteins. *Acc Chem Res* **2002,** *35*, 325-31.

69.   Woodward, C. Is the slow-exchange core the protein folding core? *Trends Biochem. Sci.* **1993,** *18*, 359-360.

70.   Li, R.; Woodward, C. The hydrogen exchange core and protein folding. *Protein Science* **1999,** *8*, 1571-1590.

71.   Parker, M. J.; Marqusee, S. A Kinetic Folding Intermediate Probed by Native State Hydrogen Exchange. *J. Mol. Biol.* **2001,** *305*, 593-602.

72.   Chamberlain, A. K.; Handel, T. M.; Marqusee, S. Detection of rare partially folded molecules in equilibrium with the native conformation of RNaseH. *Nat. Struct. Biol.* **1996,** *3*, 782-787.

73.   Roder, H.; Elöve, G. A.; Englander, S. W. Structural characterization of folding intermediates in cytochrome c by H-exchange labelling and proton NMR. *Nature* **1988,** *335*, 700-704.

74.   Miranker, A.; Radford, S. E.; Karplus, M.; Dobson, C. M. Demonstration by NMR of folding domains in lysozyme. *Nature* **1991,** *349*, 633-636.

75. Nodet, G.; Abergel, D. An overview of recent developments in the interpretation and prediction of fast internal protein dynamics. *Eur. Biophys. J.* **2007,** *36*, 985-993.

76. Hvidt, A.; Linderstrom-Lang, K. Exchange of hydrogen atoms in insulin with deuterium atoms in aqueous solutions. *Biochem. Biophys. Acta* **1954,** *14*, 574-575.

77. Katta, V.; Chait, B. T. Conformational Changes in Proteins Probed by Hydrogen-exchange Electrospray-ionisation Mass Spectrometry. *Rapid Commun. Mass Spectrom.* **1991,** *5*, 214-217.

78. Smith, D. L.; Deng, Y.; Zhang, Z. Probing the Noncovalent Structure of Proteins by Amide Hydrogen Exchange Mass Spectrometry. *J. Mass Spectrom.* **1997,** *32*, 135-146.

79. Krishna, M. M. G.; Hoang, L.; Lin, Y.; Englander, S. W. Hydrogen exchange methods to study protein folding. *Methods* **2004,** *34*, 51-64.

80. Konermann, L.; Tong, X.; Pan, Y. Protein Structure and Dynamics Studied by Mass Spectrometry: H/D exchange, hydroxyl radical labeling, and related approaches. *J. Mass Spectrom.* **2008,** *43*, 1021-1036.

81. Xiao, H.; Hoerner, J. K.; Eyles, S. J.; Dobo, A.; Voigtman, E.; Melcuk, A. I.; Kaltashov, I. A. Mapping protein energy landscapes with amide hydrogen exchange and mass spectrometry: I. A generalized model for a two-state protein and comparison with experiment. *Protein Sci.* **2005,** *14*, 543-557.

82. Tanaka, K. The Origin of Macromolecule Ionization by Laser Irradiation (Nobel Lecture). *Angew. Chem. Int. Ed.* **2003,** *42*, 3861-3870.

83. Fenn, J. B. Electrospray Wings for Molecular Elephants (Nobel Lecture). *Angew. Chem. Int. Ed.* **2003,** *42*, 3871-3894.

84.   Karas, M.; Bachmann, D.; Hillenkamp, F. Influence of the wavelength in high-irradiance ultraviolet laser desorption mass spectrometry of organic molecules. *Anal. Chem.* **1985,** *57*, 2935-2939.

85.   Keller, B. O.; Li, L. Detection of 25,000 Molecules of Substance P by MALDI-TOF Mass Spectrometry and Investigations into the Fundamental Limits of Detection in MALDI. *J. Am. Soc. Mass Spectrom.* **2001,** *12*, 1055-1063.

86.   Iavarone, A. T.; Williams, E. R. Mechanism of Charging and Supercharging Molecules in Electrospray Ionization. *J. Am. Chem. Soc.* **2003,** *125*, 2319-2327.

87.   Kebarle, P.; Verkerk, U. H. Electrospray: From Ions in Solutions to Ions in the Gas Phase, What We Know Now. *Mass Spectrom. Rev.* **2009,** *28*, 898-917.

88.   Hogan, C. J.; Carroll, J. A.; Rohrs, H. W.; Biswas, P.; Gross, M. L. Combined Charged Residue-Field Emission Model of Macromolecular Electrospray Ionization. *Anal. Chem.* **2009,** *81*, 369-377.

89.   Iribarne, J. V.; Thomson, B. A. On the evaporation of small ions from charged droplets. *J. Chem. Phys.* **1976,** *64*, 2287-2294.

90.   Konermann, L.; Rodriguez, A. D.; Liu, J. On the formation of highly charged gaseous ions from unfolded proteins by electrospray ionization. *Anal Chem* **2012,** *84*, 6798-804.

91.   Kaltashov, I. A.; Abzalimov, R. R. Do Ionic Charges in ESI MS Provide Useful Information on Macromolecular Structure? *J. Am. Soc. Mass Spectrom.* **2008,** *19*, 1239-1246.

92.   Chowdhury, S. K.; Katta, V.; Chait, B. T. Probing Conformational Changes in Proteins by Mass Spectrometry. *J. Am. Chem. Soc.* **1990,** *112*, 9012-9013.

93.   Loo, J. A.; Loo, R. R. O.; Udseth, H. R.; Edmonds, C. G.; Smith, R. D. Solvent-induced Conformational Changes of Polypeptides Probed by Electrospray-ionization Mass Spectrometry. *Rapid. Comm. Mass. Spectrom.* **1991,** *5*, 101-105.

94.   Konermann, L.; Douglas, D. J. Unfolding of Proteins Monitored by Electrospray Ionization Mass Spectrometry: A Comparison of Positive and Negative Ion Modes. *J. Am. Soc. Mass Spectrom.* **1998,** *9*, 1248-1254.

95.   Mirza, U. A.; Cohen, S. L.; Chait, B. T. Heat-Induced Conformational Changes in Proteins Studied by Electrospray Ionisation Mass Spectrometry. *Anal. Chem.* **1993,** *65*, 1-6.

96.   Watson, J. T. *Introduction to Mass Spectrometry* third ed.; Lippincott - Raven: Philadelphia, New York, 1997.

97.   Roboz, J. *Mass Spectrometry: Instrumentation and Techniques*; Wiley: New York, 1968.

98.   March, R.; Todd, J. F. J. *Quadrupole Ion Trap Mass Spectrometry* Second edition ed.; Wiley: New York ; Toronto, 2005.

99.   Cotter, R. J. *Time-of-Flight Mass Spectrometry*; American Chemical Society: THE UNITED STATES OF AMERICA, 1997.

100.   Marshall, A. G.; Hendrickson, C. L. Fourier transform ion cyclotron resonance detection: principles and experimental configurations. *Int. J. Mass Spectrom* **2002,** *215*, 59-75.

101.   Marshall, A. G. Milestones in Fourier transform ion cyclotron resonance mass spectrometry technique development. *Int. J. Mass Spectrom* **2000,** *200*, 331-36.

102.   Comisaro.Mb; Marshall, A. G. Fourier-Transform Ion-Cyclotron Resonance Spectroscopy. *Chemical Physics Letters* **1974,** *25*, 282-283.

103.   Shi, S.-H.; Drader, J. J.; Freitas, M. A.; Hendrickson, C. L.; Marshall, A. G. Comparison and interconversion of the two most common frequecy-to-mass calibration functions for Fourier transform ion cyclotron resonance mass spectrometry. *Int. J. Mass Spectrom* **2000,** *195/196*, 591-98.

104.   Makarov, A. Electrostatic Axially Harmonic Orbital Trapping: A High-Performance Technique of Mass Analysis. *Anal. Chem.* **2000,** *72*, 1156-1162.

105.   Scigelova, M.; Makarov, A. Orbitrap Mass Analyzer - Overview and Applications in Proteomics. *Proteomics* **2006,** *6 Suppl. 2*, 16-21.

106.   Pringle, S. D.; Giles, K.; Wildgoose, J. L.; Williams, J. P.; Slade, S. E.; Thalassinos, K.; Bateman, R. H.; Bowers, M. T.; Scrivens, J. H. An investigation of the mobility separation of some peptide and protein ions using a new hybrid quadrupole/travelling wave IMS/oa-ToF instrument. *Int. J. Mass Spectrom.* **2007,** *261*, 1-12.

107.   Ruotolo, B. T.; Benesch, J. L.; Sandercock, A. M.; Hyung, S. J.; Robinson, C. V. Ion mobility-mass spectrometry analysis of large protein complexes. *Nat Protoc* **2008,** *3*, 1139-52.

108.   Mesleh, M. F.; Hunter, J. M.; Shvartsburg, A. A.; Schartz, G. C.; Jarrold, M. F. Structural information from ion mobility measurements: effects of the long-range potential. *J. Phys. Chem.* **1996,** *100*, 16082-86.

109.   Ruotolo, B. T.; Giles, K.; Campuzano, I.; Sandercock, A. M.; Bateman, R. H.; Robinson, C. V. Evidence for Macromolecular Protein Rings in the Absence of Bulk Water. *Science* **2005,** *310*, 1658-1661.

110. Uetrecht, C.; Barbu, I. M.; Shoemaker, G. K.; van Duijn, E.; Heck, A. J. R. Interrogating viral capsid assembly with ion mobility–mass spectrometry. *Nat. Chem.* **2011,** *3*, 126-132.

111. van Duijn, E.; Barendregt, A.; Synowsky, S.; Versluis, C.; Heck, A. J. R. Chaperonin Complexes Monitored by Ion Mobility Mass Spectrometry. *J. Am. Chem. Soc.* **2009,** *131*, 1452-1459.

112. Ahadi, E.; Konermann, L. Modeling the behavior of coarse-grained polymer chains in charged water droplets: Implications for the mechanism of electrospray ionization. *J. Phys. Chem. B* **2012,** *116*, 104-112.

113. Evans, S. V.; Brayer, G. D. High-resolution Study of the Three-dimensional Structure of Horse Heart Metmyoglobin. *J. Mol. Biol.* **1990,** *213*, 885-897.

114. de la Mora, F. J. Electrospray Ionization of large multiply charged species proceeds via Dole's charged residue mechanism. *Anal. Chim. Acta* **2000,** *406*, 93-104.

115. Ahadi, E.; Konermann, L. Ejection of solvated ions from electrosprayed methanol/water nanodroplets studied by molecular dynamics simulations. *J. Am. Chem. Soc.* **2011,** *133*, 9354-9363.

116. Thomson, B. A.; Iribarne, J. V. Field induced ion evaporation from liquid surfaces at atmospheric pressure. *J. Chem. Phys.* **1979,** *71*, 4451.

117. Gamero-Castaño, M.; de la Mora, F. Kinetics of small ion evaporation from the charge and mass distribution of multiply charged clusters in electrosprays. *J. Mass Spectrom.* **2000,** *35*, 790-803.

118. Labowsky, M. A model for solvated ion emission from electrospray droplets. *Rapid Commun. Mass Spectrom.* **2010,** *24*, 3079-3091.

119. Sali, A.; Glaeser, R.; Earnest, T.; Baumeister, W. From words to literature in structural proteomics. *Nature* **2003,** *422*, 216-25.

120. Huang, E. C.; Pramanik, B. N.; Tsarbopoulos, A.; Reichert, P.; Ganguly, A. K.; Trotta, P. P.; Nagabhushan, T. L.; Covey, T. R. Application of Electrospray Mass Spectrometry in Probing Protein-Protein and Protein-Ligand Noncovalent Interactions. *J. Am. Soc. Mass Spectrom.* **1993,** *4*, 624-630.

121. Light-Wahl, K. J.; Winger, B. E.; Smith, R. D. Observation of the multimeric forms of concanavalin A by electrospray ionization mass spectrometry. *J. Am. Chem. Soc.* **1993,** *115*, 5869-5870.

122. Light-Wahl, K. J.; Schwartz, B. L.; Smith, R. D. Observation of the Noncovalent Quaternary Association of Proteins by Electrospray Ionization Mass Spectrometry. *J. Am. Chem. Soc.* **1994,** *116*, 5271-5278.

123. Aquilina, J. A.; Benesch, J. L.; Bateman, O. A.; Slingsby, C.; Robinson, C. V. Polydispersity of a mammalian chaperone: mass spectrometry reveals the population of oligomers in alphaB-crystallin. *Proc Natl Acad Sci U S A* **2003,** *100*, 10611-6.

124. Ilag, L. L.; Videler, H.; McKay, A. R.; Sobott, F.; Fucini, P.; Nierhaus, K. H.; Robinson, C. V. Heptameric (L12)6/L10 rather than canonical pentameric complexes are found by tandem MS of intact ribosomes from thermophilic bacteria. *Proc Natl Acad Sci U S A* **2005,** *102*, 8192-7.

125. van Duijn, E.; Simmons, D. A.; van den Heuvel, R. H. H.; Bakkes, P. J.; van Heerikhuizen, H.; Heeren, R. M. A.; Robinson, C. V.; van der Vies, S. M.; Heck, A. J. R. Tandem Mass Spectrometry of Intact GroEL-Substrate Complexes Reveals Substrate-Specific Conformational Changes in the *trans* Ring. *J. Am. Chem. Soc.* **2006,** *128*, 4694-4702.

Chapter 2 — Irreversible Thermal Denaturation of Cytochrome *c* Studied by Electrospray Mass Spectrometry

2.1 Introduction

Studies on the structure and dynamics of proteins continue to be a focal area of biochemical research. A number of well established tools are available for experiments of this kind, including X-ray crystallography, NMR, calorimetry, and various spectroscopic techniques. Electrospray ionization (ESI) mass spectrometry (MS) has become another widely used approach for exploring the properties of proteins in solution, providing information complementary to that obtained by traditional methods [1]. The ESI process generates intact gas phase ions from proteins in solution. In the commonly used positive ion mode these $[M + n\text{H}]^{n+}$ species are multiply charged due to proton attachment.

ESI of natively folded proteins results in protonation states n similar to those predicted for water droplets of the same size that are charged to the Rayleigh limit. This finding supports the idea that ionization follows the charged residue model [2-6], although alternative scenarios have been proposed as well [7-9]. Much higher protonation states and wider charge state distributions are generally seen for proteins that are unfolded in solution. Based on this empirical relationship ESI-MS is now routinely being used for monitoring structural transitions in response to changes in pH, temperature, organic co-solvents, or covalent modifications [1,10-16]. The physical basis for the striking dependence of ESI charge states on the solution-phase protein conformation continues to be a matter of debate. Various explanations have been put forward, including differences in the steric accessibility of protonation sites, and changes of the corresponding pK_a

values [10,17]. It has also been argued that more extended conformations reduce the extent of Coulombic repulsion in multiply protonated ions [18]. In addition, the enhanced structural flexibility of unfolded proteins can favor intramolecular solvation of charged sites [19,20]. Other proposals invoke differences in gas phase basicity between protein and solvent [21]. Mechanisms involving conformation-dependent charge neutralization [22] or combinations of electrostatic and steric shielding [23] have been put forward, as well as proposals that ESI charge states reflect the protein surface area [24], and that they specifically monitor changes in tertiary (not secondary) structure [11].

Using ESI charge state distributions for protein structural studies offers a number of unique advantages. Differentiating co-existing conformers can be challenging when using traditional spectroscopic techniques, whereas multimodal ESI charge state distributions permit the direct visualization of individual species [25,26]. The gentle nature of the ESI process allows the transfer of intact protein-ligand and protein-protein complexes into the gas phase [6,27-29]. Thus, insights into conformations and interactions are obtained in a single experiment [17,30-36]. A further dimension can be added to these studies by incorporating ion mobility spectrometry [37,38].

A very interesting approach is to monitor the charge state distribution of a protein, while simultaneously measuring its hydrogen/deuterium exchange (HDX) behavior [39-42]. The two probes complement each other, since ESI charge states report on the "compactness" of a protein in solution [20], whereas HDX is governed largely by the hydrogen bonding behavior along the amide backbone. HDX at sites that are involved in stable hydrogen bonds or that are sterically shielded is mediated by conformational

fluctuations. Thus, proteins that are disordered and highly mobile undergo much faster isotope exchange than tightly folded conformers [43].

Because the individual components of bi- or multimodal ESI charge state distributions represent distinct solution-phase conformers, it is not surprising that different charge states in a single mass spectrum can be associated with different HDX properties [41,44-48]. However, not all cases show this behavior. Several studies have found that charge states representing very different coexisting protein structures can exhibit isotope exchange kinetics that are indistinguishable [49-51]. This conundrum is resolved when it is considered that coexisting conformers may interconvert in solution [52]. All species will exhibit the same HDX kinetics if interconversion is rapid on the HDX time scale. This relationship was first proposed in a seminal study by Wagner and Anderegg [53]. In that work it was reported that cytochrome *c* (cyt *c*) under mildly acidic conditions exhibits a bimodal charge state distribution, representing the presence of unfolded proteins in addition to the native conformers. The two forms showed very similar isotope exchange kinetics. The experiment was then repeated on samples that had been partially denatured in an irreversible manner by heat exposure. When the heated samples were transferred back to a native solvent environment at room temperature a bimodal charge state distribution was found to persist, corresponding to a mix of permanently unfolded protein and natively folded polypeptide chains. With interconversion being blocked, it was reported that high charge states showed more extensive HDX than low charge states. Those widely cited results [53] were instrumental for establishing ESI charge states as a well accepted probe for protein conformational studies.

Most unfolded proteins will spontaneously refold to the native state once placed in a non-denaturing solvent environment, i.e., ambient temperature, neutral pH, and in the absence of chemical denaturants [54]. A key question that was not explicitly addressed in Wagner and Anderegg's study [53] and in related previous work [55] is *why* heat exposure of cyt *c* results in the formation of conformers that are irreversibly unfolded. The reasons underlying the apparently different HDX characteristics for high and low charge states, therefore, remain unclear. Irreversible thermal denaturation has also been observed using other techniques for a number of different proteins. It was proposed that this phenomenon may be caused by a combination of factors, including partial aggregation and various covalent modifications [56-61]. The current study revisits the experiments of Wagner and Anderegg [53], with the aim of providing additional insights into the ESI-MS and HDX characteristics of cyt *c* after heat exposure. It is found that the formation of irreversibly denatured protein is linked to oxidative damage. Partial aggregation may play a role as well. Covalent oxygen adduction interferes with the analysis of HDX experiments, necessitating a re-examination of the question whether or not high and low charge states of heat-exposed cyt *c* exhibit distinct isotope exchange properties.

2.2 Experimental

2.2.1 Materials

Bovine heart cyt *c* (12230 Da [62]) was purchased from Sigma. Ammonium acetate and formic acid were from Fluka. Ammonia was obtained from Caledon Laboratory, and D_2O was from Cambridge Isotope Laboratories. Thermally denatured protein was generated using procedures very similar to those of ref. [53]. 25 mL aliquots containing 1 μM cyt *c* were heated in double distilled water (pH 6.5) for 1 or 2 hours at 90 °C in a water bath. Higher protein concentrations resulted in unacceptable levels of aggregation. After heat exposure the samples were flash frozen in liquid nitrogen, lyophilized, and subsequently re-dissolved to 500 μL in 5 mM aqueous ammonium acetate. The pH was adjusted to 7 by addition of ammonia. UV-Vis measurements ($\varepsilon_{Soret} = 1.06 \times 10^5$ M^{-1} cm^{-1} [63]) indicate the loss of *ca*. 30% protein during the procedure, yielding a final stock solution of about 35 μM. Native cyt *c* samples were prepared in 5 mM ammonium acetate at pH 7, and acid-denatured protein was generated by addition of formic acid to pH 2 (both without heating). Protein digestion was performed by trypsin spin columns (Sigma). The sequence of bovine cyt *c* (pdb code 2b4z [62]) along with its tryptic cleavage sites (↓) is indicated below.

¹GDVEK↓GK↓K↓IF VQK↓CAQCHTV EK↓GGK↓HK↓TGP NLHGLFGR↓K↓T

⁴¹GQAPGFSYTD ANK↓NK↓GITWG EETLMEYLEN PK↓K↓YIPGTK↓M

⁸¹IFAGIK↓K↓K↓GE R↓EDLIAYLK↓K↓ ATNE

2.2.2 Mass Spectrometry, LC/MS, and Hydrogen/Deuterium Exchange

All mass spectra were acquired on a Q-TOF Ultima API mass spectrometer (Waters) equipped with a Z-spray ESI source that was operated in positive ion mode. The capillary and cone voltages were 3 kV and 60 V, and RF lens 1 was set to 20 V unless indicated otherwise. Cone and desolvation gas flow rates were 50 L h^{-1} and 500 L h^{-1}, respectively. The desolvation temperature was set to 120 °C and that of the source to 80 °C. For characterizing protein charge state distributions cyt *c* was infused directly into the ion source at a flow rate of 5 μL min^{-1} using a syringe pump (Harvard Apparatus, Boston, MA). The protein concentrations used were 5 μM for native and acid-denatured cyt *c*, whereas the low signal intensities after heat exposure necessitated a higher protein concentration of 35 μM. LC/MS experiments were conducted using a Waters 1525μ HPLC pump with a C18 (Symmetry 300) 2.1 mm × 100 mm reversed-phase column at a flow rate of 100 μL min^{-1} and a water/acetonitrile gradient in the presence of 0.1% formic acid. The injection loop volume was 25 μL at a protein concentration of 25 to 35 μM. Identities of tryptic peptides were confirmed by MS/MS. These measurements were carried out in data-dependent acquisition mode, where the instrument automatically switches to tandem MS once a peptide of interest elutes from the column. HDX experiments were performed by mixing protein solution with D$_2$O in a 1:2 ratio. The mixture was transferred into a syringe and directly infused into the ion source of the mass spectrometer. The *x*-axis was converted from *m/z* to mass *M* for individual ionic signals according to $M = (m/z \times n) - (0.667 \times 2.014 \times n) - (0.333 \times 1.008 \times n)$ where *n* is the charge state of the corresponding ion. Bovine cyt *c* contains a total of 192 exchangeable

hydrogens [53]. Hydrogen back exchange in the gas phase is negligible under the conditions used here [64].

2.2.3 Optical Spectroscopy

UV-Vis absorption spectra were recorded on a Varian Cary 100 spectrophotometer (Palo Alto, CA). To facilitate the comparison of spectra obtained under different conditions the data were normalized to unity at the Soret maximum. Fluorescence emission spectra were acquired on a Fluorolog-3 instrument (Horiba Jobin Yvon, Edison, NJ), using an excitation wavelength of 280 nm and protein concentrations that were normalized to 5 μM. Protein-free solutions were used as blanks in all absorption and fluorescence experiments. CD spectra were recorded on a Jasco J-810 spectropolarimeter (Easton, MD) with a 1 mm path length cuvette. The protein concentration used for CD experiments was 35 μM, and the measured spectra were converted to mean residue ellipticity [53,65]. HCl was used instead of formic acid for CD measurements on acid-denatured cyt *c* in order to avoid complications related to excessive light absorption in the far UV.

2.3 Results and Discussion

ESI-MS, optical spectroscopy, and HDX measurements were used to examine the effects of heat exposure on the structure of cyt *c*. Samples that had undergone thermal denaturation and subsequent lyophilization were compared to native cyt *c,* and to samples

at pH 2 (1.2% formic acid) where the protein is known to be extensively unfolded [11]. Protein that had undergone heat exposure was studied in the same solvent environment as native cyt c, i.e., pH 7 in 5 mM ammonium acetate at room temperature (22 ± 1 °C).

2.3.1 ESI Charge State Distributions

The ESI mass spectrum of native cyt c shows a narrow charge state distribution that encompasses only the 7+ and 8+ peaks, representing a tightly folded solution-phase conformation (**Figure 2**-1A). A much wider distribution centered around 15+ and extending all the way to 20+ is observed for the acid-denatured protein at pH 2 (**Figure 2**-1D). These observations are in line with previous reports [11,25,53]. Protein that had been heat exposed for 1 h retains its most intense charge state at 8+, but the relative intensity of the 7+ peak is diminished. In addition, higher charge states extending up to at least 14+ are observed (**Figure 2**-1B). The relative intensity of highly charged ions is further elevated for a heating period of 2 h (**Figure 2**-1C). The appearance of these mass spectra was found to be stable for days. Extending the heating period to more than 2 hours resulted in data with increasingly poor signal-to-noise ratio (not shown). The results depicted in **Figure 2**-1B, C are consistent with earlier observations [53,55] that heat exposure of cyt c generates a sub-population of proteins that are irreversibly unfolded. In the mass spectra of **Figure 2**-1C, D, these non-native proteins give rise to charge states centered around 11+.

Compared to the data in **Figure 2-1**B, C, somewhat higher charge states with considerably higher relative intensities were seen in ref. [53] for heat-denatured
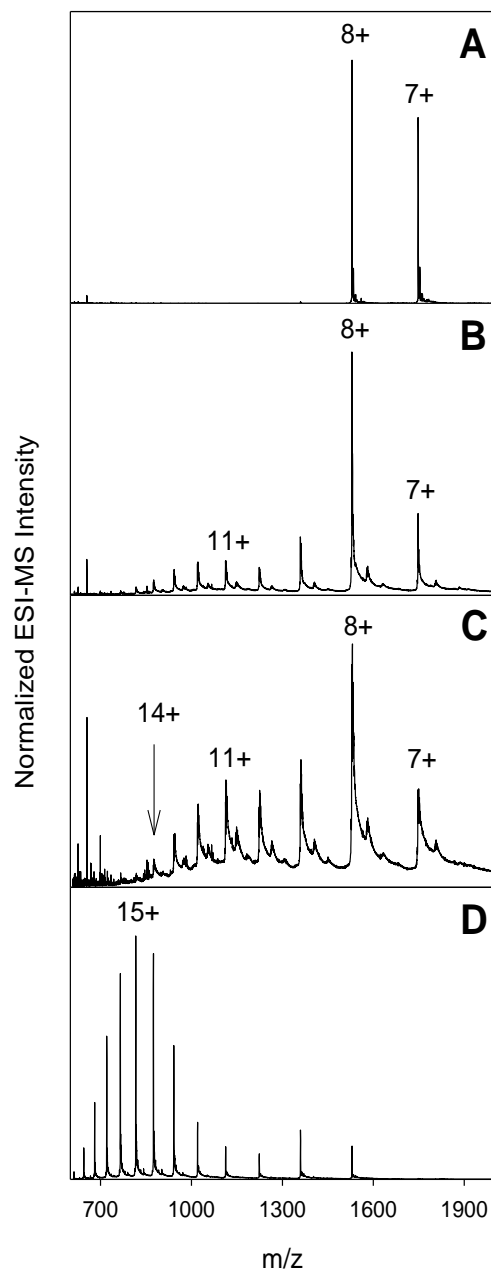
Figure 2-1. ESI mass spectra of bovine cyt *c* recorded at room temperature under different conditions. (A) Native protein at pH 7; (B) after heat exposure for 1 h (pH 7); (C) after heat exposure for 2 h (pH 7); (D) Acid denatured cyt *c* at pH 2 without prior heat exposure.

conformers, an effect that is tentatively attributed to differences in instrumentation. Quadrupole instruments of the type used in ref. [53] may discriminate against ions with high *m/z* [66], resulting in skewed spectra when compared to the TOF-MS data reported here. Other instrument characteristics such as the ion source design could play a role as well.

2.3.2 Optical Spectroscopy

Cyt *c* represents a convenient model system because it offers several optical probes for monitoring the occurrence of structural changes. The UV-Vis absorption spectrum reports on the heme environment [11,63]. Coordination of the heme iron with its native His18 and Met80 ligands leads to a Soret absorption maximum at 409 nm. Displacement of these ligands upon acid unfolding induces a blue shift to 394 nm. A much smaller shift to 407 nm is seen after two hours of heat exposure (**Figure 2**-2A). A prominent feature in the spectrum of the heated protein is a sloped baseline that strongly increases for shorter wavelengths. This effect can be attributed to Rayleigh scattering caused by small particles that are suspended in solution, representing a hallmark of partial protein aggregation [61]. Unfortunately, quantifying the extent of aggregation is not straightforward because scattering is affected both by the particle size and number density.

The CD spectrum of native cyt *c* shows minima at 208 and 222 nm, features that attest to a largely helical secondary structure (**Figure 2**-2B). In contrast, the acid-denatured protein has its main minimum at 202 nm which is consistent with the prevalence of random coil-like elements [67]. Also heat exposure induces some

secondary structure perturbations, as evidenced by the differences between the solid and the dashed spectra in Figure 2-2B. The change in ellipticity at 222 nm between these two data sets suggests a 20% loss in helicity after heating, a finding that is consistent with the results of Wagner and Anderegg [53].

The single Trp residue (Trp59) in native cyt c is virtually non-fluorescent due to efficient Förster resonance energy transfer to the heme, from where the excitation energy is dissipated as heat [11,68]. Unfolding disrupts this quenching mechanism by increasing the heme-Trp distance. As a result, exposure of the protein to pH 2 leads to a dramatic increase in fluorescence intensity. A fluorescence increase is also seen for cyt c after heating, but the signal intensity in this case is only *ca*. 20% of that seen for the acid-unfolded protein (**Figure 2**-2C).

The data presented so far confirm that heat exposure of cyt c causes irreversible unfolding for a sub-population of proteins in the sample. A shift to higher ESI charge states indicates a more expanded conformation. Changes in the UV-Vis and fluorescence spectra point to tertiary structure alterations, and CD spectroscopy shows a reduced α helicity. However, the overall magnitude of these heat-induced structural changes is moderate when compared to the more dramatic effects seen upon acid-induced unfolding. Heat exposed cyt c aggregates to a certain extent, which is consistent with the behavior seen for other proteins [61]. Although non-native aggregates can sometimes be observed directly by ESI-MS [20,34] this is not the case under the conditions of this work, even when extending the mass range for the measurements in **Figure 2**-1B, C (data not shown).
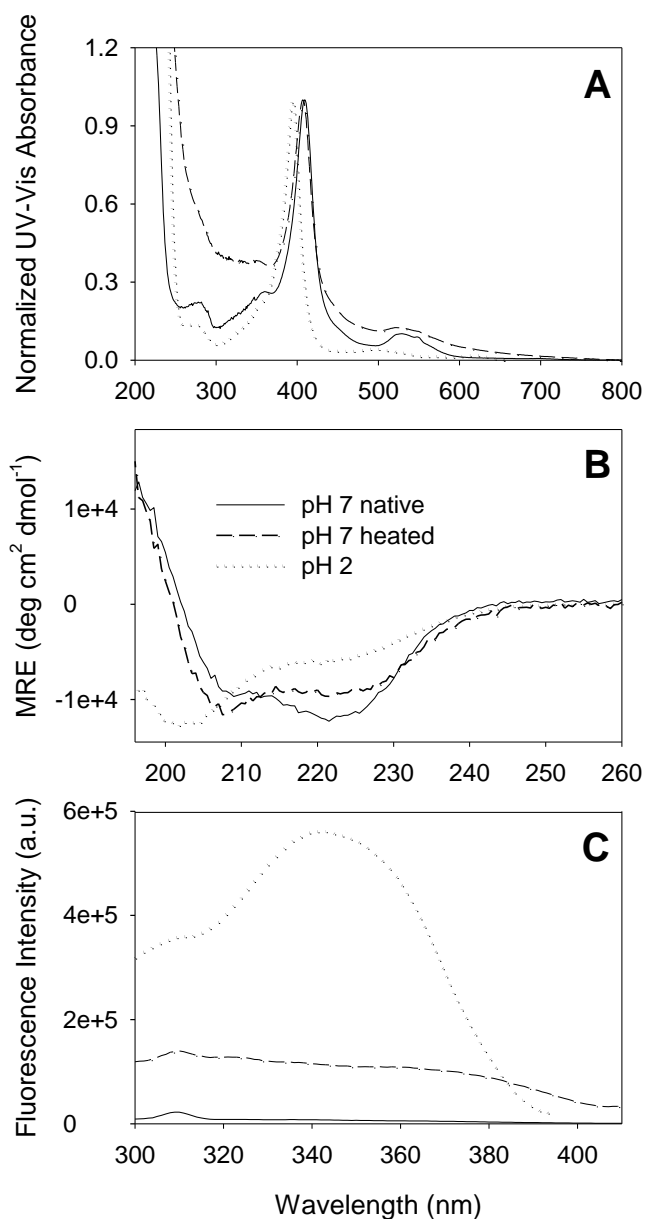
Figure 2-2. Optical spectra of native cyt *c* at pH 7 (solid lines), after 2 hours of heating at pH 7 (dashed lines), and acid-denatured cyt *c* at pH 2 (dotted lines). (A) UV-Vis spectra, normalized to unity at the Soret maximum; (B) CD spectra, expressed as mean residue ellipticity (MRE); (C) fluorescence emission spectra.

2.3.3 Oxidative Modifications

A striking feature in the ESI mass spectra of thermally treated cyt *c* (**Figure 2**-1B, C) is the occurrence of extensive peak broadening and tailing, resulting in data with relatively poor signal-to-noise ratio. Close inspection of individual peaks reveals that the heated protein has undergone oxidative modifications. All charge states show a signal corresponding to the mass of unmodified cyt *c*, but there are additional satellite peaks shifted by +16 Da and multiples thereof (**Figure 2**-3A, B). Covalent modifications of this type may be induced by exposure to H_2O_2 or $\cdot OH$ [69,70], but it has been demonstrated that oxidation can also occur during heat exposure in the absence of such reactive compounds [61]. The mechanisms of protein oxidation can be quite complex, but many reaction pathways result in the incorporation of oxygen atoms into amino acid side chains, thereby accounting for the observed +16 Da adducts [69]. Previous ESI-MS studies on thermally denatured cyt *c* [53,55] did not address the possible occurrence of protein oxidation, and close-ups of individual peaks were not shown. However, the spectra for heated samples in refs. [53,55] had a "noisy" appearance reminiscent of the data in **Figure 2-1**B, C, making it likely that oxidation also took place under the conditions of those previous investigations.

Thermally-induced oxidation is less pronounced for low charge states than for highly charged protein ions. After one hour of heating, for example, the base peak for cyt *c* 7+ and 8+ corresponds to the mass of the unmodified protein. This is followed by smaller +16 Da and +32 Da adducts (**Figure 2-3**A). Residual unmodified cyt *c* is also seen for higher charge states, but the most intense peak in these cases is for singly oxidized protein, followed by a progression up to at least five-fold oxidation (**Figure 2-**

3B). It is common to report protein oxidation levels as "fraction unmodified", F_u, defined as A_u/A_{tot} [69]. In this expression A_u is the peak area corresponding to the unmodified protein, and A_{tot} is the area of the entire mass distribution including unmodified and oxidized species. Peak integration for determining A_{tot} in the current work was performed over the mass range from zero to five oxidations. Analysis of ESI-MS data after one hour of heating (Figure 1B) results in F_u values around 0.35 for charge states 7+ and 8+. F_u gradually decreases for higher charge states, down to a value of 0.16 for 14+ (**Figure 2-3**C). Depending on their location within the protein, oxidative modifications can severely disrupt the native fold [71-73]. This is consistent with the observation that cyt *c* with elevated oxidation levels is preferentially seen in high charge states (**Figure 2-3**B). These data imply that oxidative modifications are a major contributing factor to the formation of irreversibly denatured cyt *c* after heat exposure.

Tryptic peptide mapping was used for locating major modification sites within the heated protein. Some oxidation was found to occur within the region covered by peptide T12 (residues 56-72). Marker fragments b_4+16 (*m/z* 474.2) and $y_8"+16$ (*m/z* 1039.5) reveal oxygen incorporation at both Met65 and Trp59. Also T15 (residues 80-86) carries a +16 Da modification. Observation of b_2+16 (*m/z* 261.1, **Figure 2-4**), along with unmodified $y_6"$ (*m/z* 648.4) pinpoints Met80 as the site of oxidation in this segment. These results for T12 and T15 are consistent with previous work that found Met and Trp to be among the amino acids with the highest intrinsic reactivities [69]. Oxidation was also observed for T4-5 (residues 9-22). Unfortunately, the interpretation of MS/MS spectra (not shown) for this peptide is complicated by the presence of heme which is covalently attached to Cys14 and Cys17 via thioiether bonds. Luckily, some insights can be obtained by collisional activation of the intact protein during ESI, leading to the
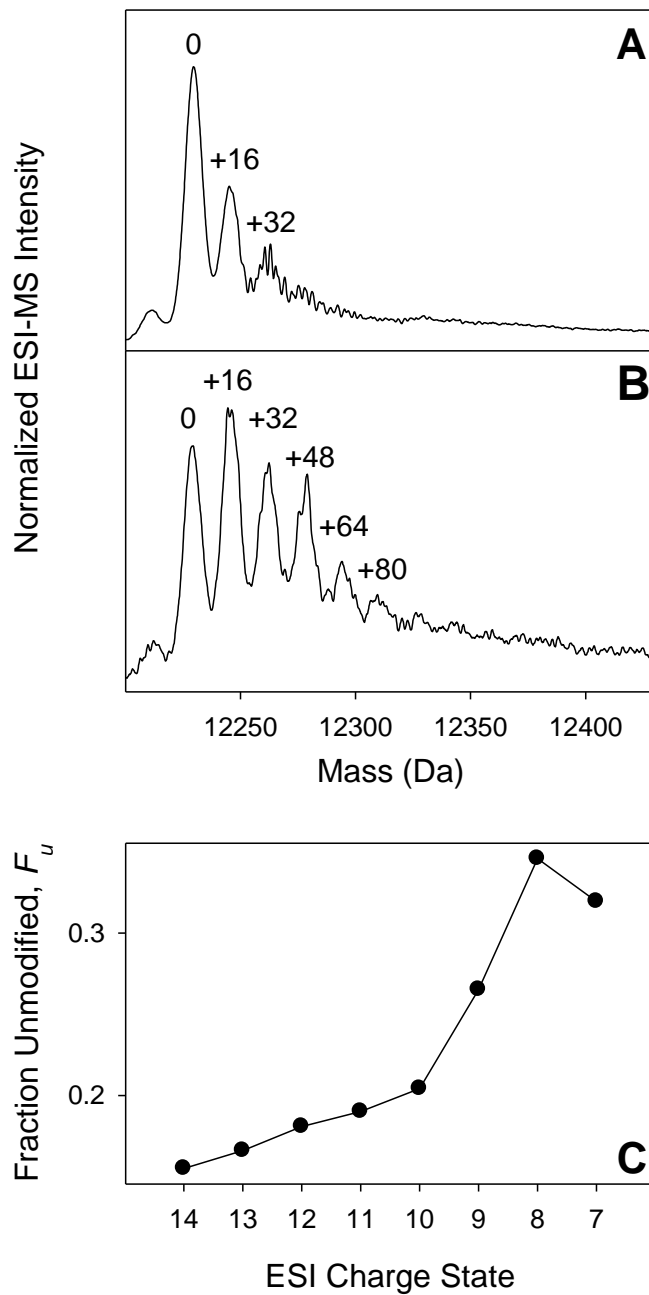
Figure 2-3. ESI-MS data for cyt *c* after 1 hour of heating. (A) 8+ charge state plotted on a mass scale. (B) 13+ charge state plotted on a mass scale. Notation: "0" represents the mass of the unmodified protein; "+16", "+32" *etc.* represents adduction of one, two *etc.* oxygens. (C) Oxidation level of individual charge states, expressed as fraction of unmodified protein, F_u.
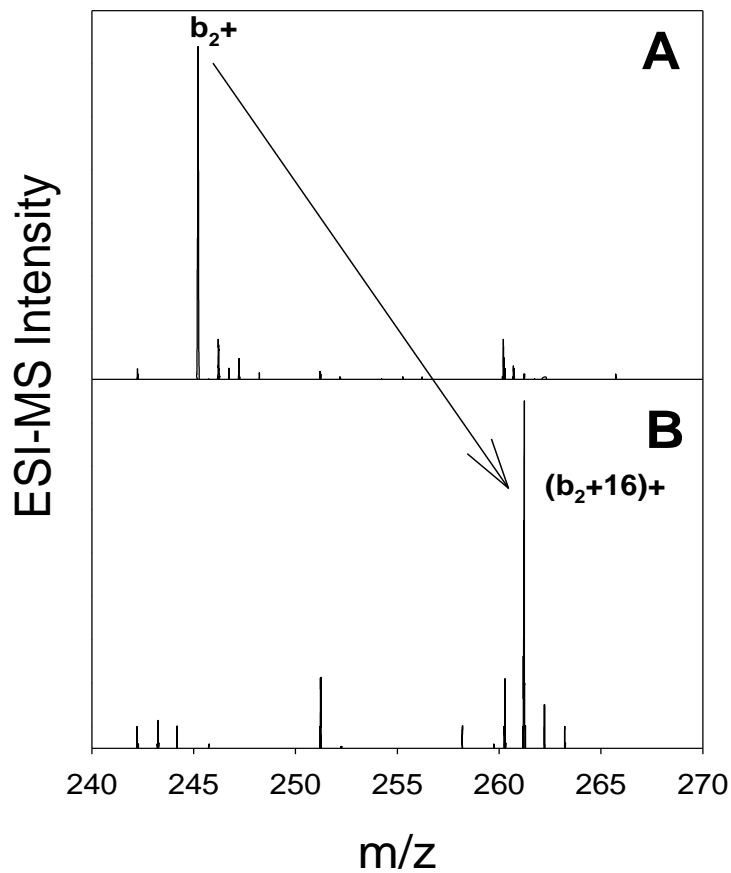
Figure 2-4. Partial tandem mass spectra of tryptic peptide T15 (MIFAGIK, residues 80-86). (A) unmodified peptide obtained from the native protein; (B) oxidized peptide after heat exposure of cyt c for 1 h.
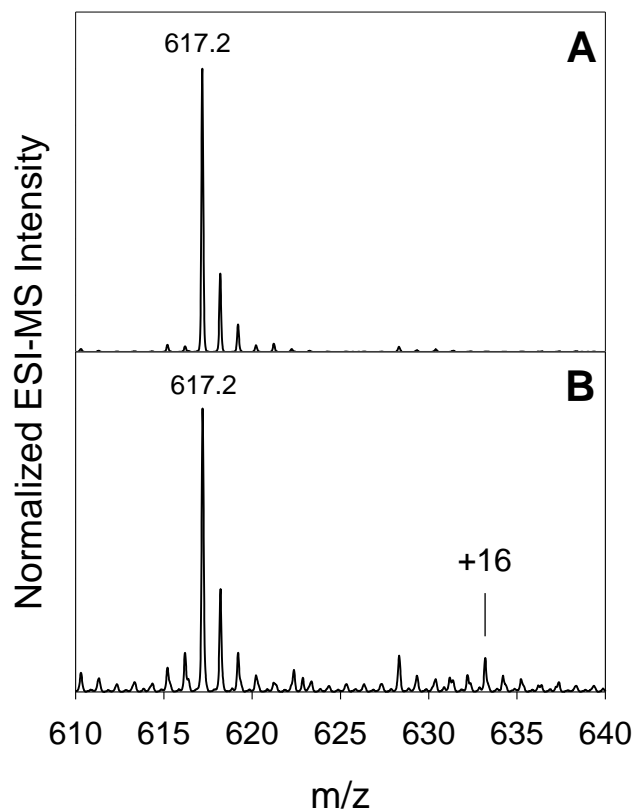
Figure 2-5. Partial ESI mass spectra recorded under "harsh" declustering conditions (cone voltage 150 V, RF lens 1 voltage 170 V) where [heme + H]$^+$ is released as collision induced dissociation product [74]. (A) Native protein; (B) after heat exposure for 1 h.

formation of protonated heme as a major fragmentation product [74]. Collision-induced dissociation of non-heated cyt *c* produces a clean heme signal at *m/z* 617.2 that is accompanied only by its isotope peaks (**Figure 2-5**A). Analysis of heat exposed protein results in additional ions including (heme + 16 Da), and a host of other unidentified species (**Figure 2-5**B). This result strongly suggests that heme itself undergoes covalent modifications during heat exposure, an interpretation that is supported by studies on myoglobin under oxidizing conditions [75]. In addition to the modifications uncovered here, other sites of oxidation likely exist. Based on the known reactivity of sulfur-containing residues [69], the thioether groups of Cys14 and Cys17 in T4-5 represent possible candidates.

2.3.4 Hydrogen/Deuterium Exchange

Unheated cyt *c* in 0.33% formic acid shows a bimodal charge state distribution (not shown), representing the presence of co-populated unfolded and native proteins. As reported previously [53], exposing the protein under these conditions to D_2O results in HDX kinetics that are very similar for all charge states. As an example, **Figure 2-6**A shows mass distributions for the 7+ and 13+ peaks after 7 minutes of exchange. The peak maxima are shifted by 97 and 98 Da, respectively, relative to unlabeled cyt *c*. This corresponds to a relative HDX level around 97 / (0.66 × 192) = 77%. As discussed in the *Introduction*, the observation of virtually the same exchange kinetics for all charge states can be attributed to the rapid interconversion of native and non-native conformers under the conditions of partial acid-unfolding [49-51,53].
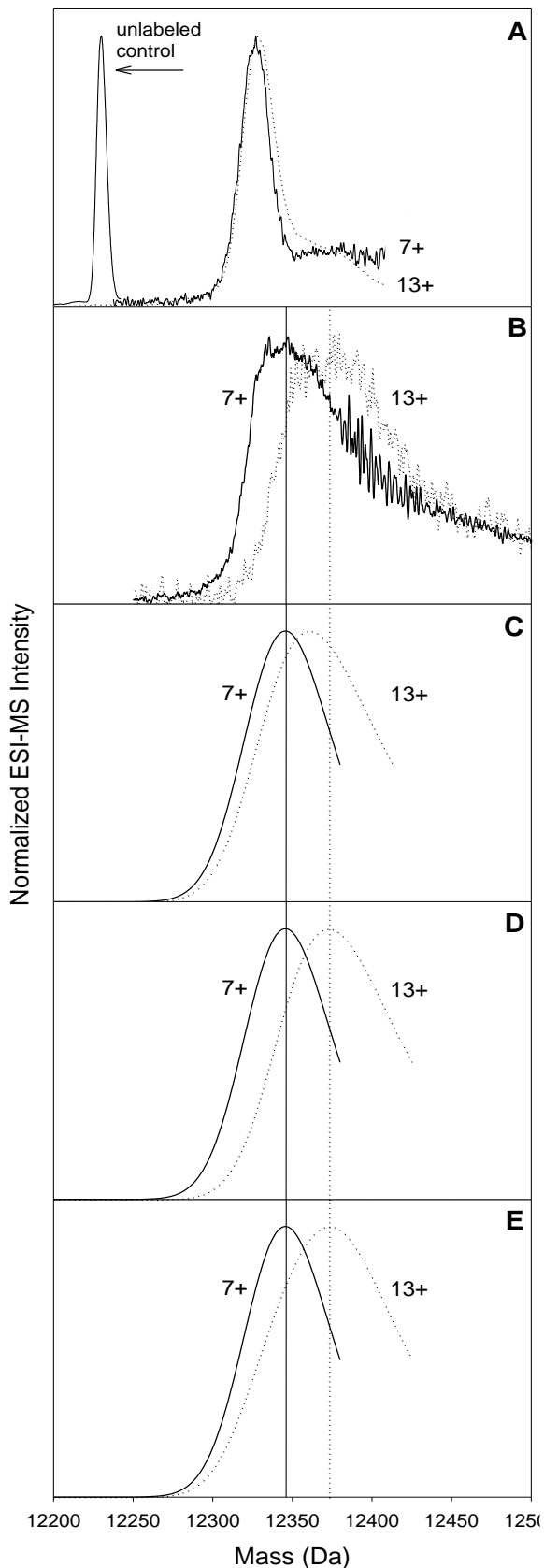
Figure 2-6. ESI mass distributions for two representative cyt *c* charge states obtained after incubation in 66% D_2O. Solid lines: 7+, dotted lines: 13+. (A) Partially denatured (unheated) cyt *c* with 0.33% formic acid. Integration was performed for HDX times of 7 ± 1 minutes. (B) Cyt *c* after 1 hour of heating in neutral solution. Integration was performed for HDX times of 17.5 ± 2.5 minutes. Also shown in panel A is the mass distribution of the unlabeled protein. Panels (C), (D), and (E) represent different peak shape simulations, aimed at reproducing the experimental 7+ and 13+ data in (B). Details are provided in the text. Vertical lines indicate approximate centroids for the distributions in (B).

A key finding of Wagner and Anderegg's work [53] was the observation of different HDX mass shifts for high and low charge states of heated cyt *c*. Also in the current work the heat exposed protein shows mass distributions for all 10+ to 15+ peaks that are very different from those of the 7+ and 8+ charge states (exemplified for 7+ and 13+ in **Figure 2-6**B for $t \approx 17.5$ min). The accurate determination of HDX levels is complicated by peak broadening and by the limited signal-to-noise ratio of the data. From the approximate centroids (vertical lines in **Figure 2-6**B) it is estimated that high charge states show a mass shift that is 25 - 30 Da larger than for low charge states. At this juncture it is tempting to directly follow the arguments of ref. [53] and conclude that this difference is due to vastly different HDX characteristics, caused by non-interconverting folded and unfolded polypeptide chains in heat-exposed samples. However, this interpretation may be overly simplistic because the observed mass shifts result from a combination of HDX *and* protein oxidation. In other words, it is not immediately clear if highly charged ions really show elevated HDX levels. Alternatively, the differences in **Figure 2-6**B might be caused solely by the more extensive oxidation of highly charged ions (**Figure 2-3**A, B), which will shift the mass envelope to the right even if all peaks showed the same HDX behavior. To examine if such a "trivial" explanation can account for the effects seen in Figure 5B we resort to peak shape simulations.

HDX induces centroid mass shifts in addition to peak broadening [76]. The mass distribution of a broadened peak *p* after HDX may be approximated as a convolution of the protein's shifted mass profile *f* with a Gaussian distribution function *D* [64]. This can be expressed as

$$p(M) = [f * D](M) \qquad (1)$$

where

$$[f * D](M) = \int_{-\infty}^{\infty} f(\tau)D(M - \tau)d\tau \qquad (2)$$

A FORTRAN program was written for the numerical evaluation of eq 2. The procedure is illustrated in Figure 2-7, where the mass profile f is modeled as the sum of five Gaussians that are spaced by 16 Da. Width and intensity progression were chosen to mimic the 7+ and 8+ charge states of heated cyt c (**Figure 2-3**A). The entire profile f was then shifted by 106 Da to account for a mass increase due to HDX. A Gaussian band with an FWHM of 50 Da serves as distribution function D. Convolution of f and D according to eq 2 results in an unstructured peak p. The presence of +16, +32, etc. oxygen adducts in f causes p to be slightly asymmetric, with a maximum that is shifted by an additional 10 Da relative to the non-oxidized protein (indicated by the arrows in **Figure 2-7**). We will now examine a few hypothetical HDX scenarios based on the known oxidation patterns of high and low charge states in heated cyt c. The simulation procedure outlined in **Figure 2-7** does not account for nonspecific solvent adducts that are frequently observed on the high mass side of ESI-MS peaks. Comparisons with experimental data will therefore focus on the low mass portion of the simulated curves, not far past the peak maxima. To emphasize this point the simulated profiles will be displayed as truncated on the high mass side.
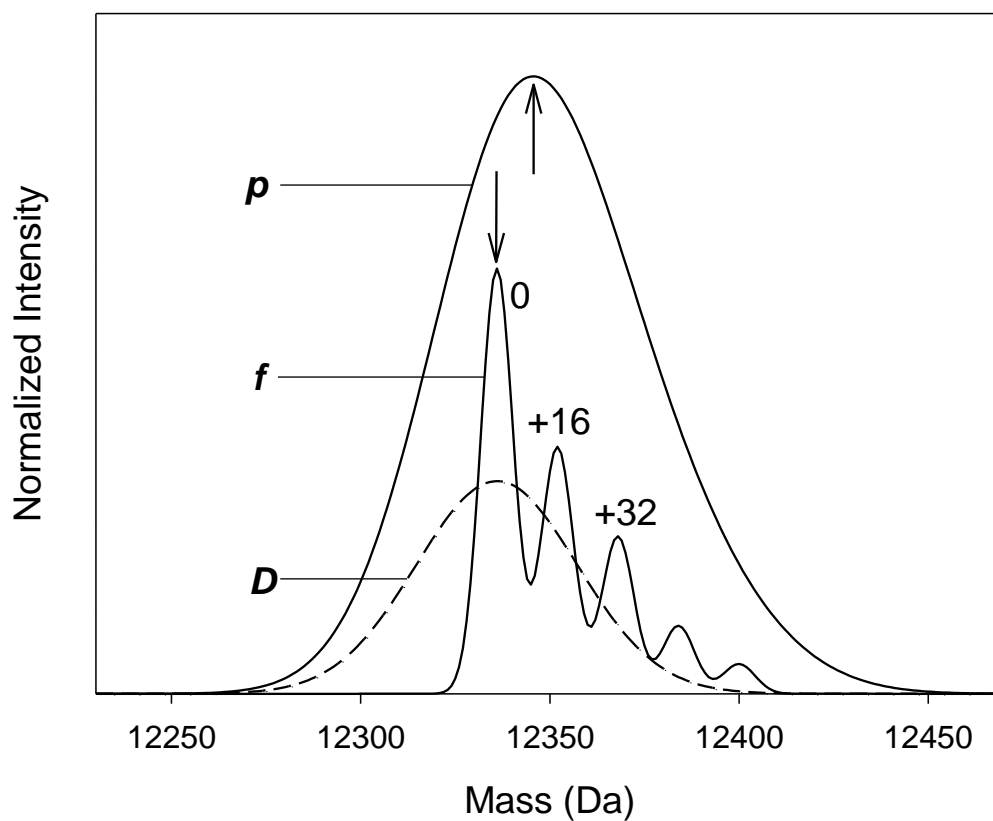
Figure 2-7. Illustration of how the peak shape *p* is generated as convolution product of a mass profile *f* and a Gaussian distribution function *D*. Labels 0, +16 and +32 represent the degree of oxygen adduction as in Figure 3A. Arrows highlight the positions of peak maxima. Intensity scaling of the three curves relative to each other is arbitrary. Additional information is provided in the text.

(*a*) We first consider a hypothetical scenario where all oxidation levels in high and low charge states show the same HDX behavior, corresponding to the "trivial" case outlined above. The parameters used for Figure 6 (HDX mass shift = 106 Da, fwhm of *D* = 50 Da) provide a low mass portion and peak maximum that are in reasonable agreement with the experimental 7+ data for the heated protein (solid lines in **Figure 2-6**B, C). For reasons of simplicity, this parameter set will be retained for modeling the low charge state behavior in all cases considered here. Using a profile *f* that mimics the elevated oxidation level of the high charge states (**Figure 2-3**B) under otherwise identical simulation conditions results in a peak maximum that is shifted further to the right (dotted profile in **Figure 2-6**C). However, comparison with the experimental 13+ data in Figure 2-6B reveals that this simulated mass shift falls short of that seen for the measured 13+ signal. It is concluded that the "trivial" case considered here cannot account for the experimentally observed difference in mass shift after HDX.

(*b*) The previous scenario is now modified by assuming that the entire peak envelope of the 13+ charge state undergoes an additional shift due to more extensive HDX. Acceptable agreement with the experimental data is obtained if this additional shift is chosen to be 12 Da (dotted lines in **Figure 2-6**B, D). Under these conditions the measured centroids are well reproduced for both 7+ and 13+, as well as the fact that the low mass portions (between 12300 and 12350 Da) of both experimental peaks rise almost in parallel (**Figure 2-6**D).

(*c*) As a third possibility we consider a scenario where protein ions exhibit different HDX properties depending on whether they are oxidized or not, irrespective of their charge state. For example, unoxidized 13+ might show the same isotope exchange

properties as unoxidized 7+, whereas all oxidatively modified 13+ species undergo more extensive HDX. Such a scenario is tested in **Figure 2-6**E, where only the oxygen-bearing components of 13+ experience an additional HDX mass shift of 9 Da. The peak maxima obtained in this way are consistent with the measured data. However, the parallel rise of the experimental peaks between 12300 and 12350 Da is not well reproduced by the simulation.

The simulations of **Figure 2-6** confirm that there is a genuine difference in the experimentally observed HDX levels of high and low charge states after heat exposure (as in scenario *b*). "Trivial" mass shifts resulting from oxygen adduction (scenario *a*) are not large enough to account for the measured effects. We conclude that a significant sub-population of protein in the heat-exposed sample is oxidatively damaged in such a way that its members can no longer interconvert with conformers that are tightly folded. Partial unfolding of the modified proteins makes them appear in higher charge states, while at the same time giving rise to more extensive HDX. This interpretation provides a straightforward explanation for the ESI-MS and HDX behavior of cyt *c* after heat exposure that was previously reported by Wagner and Anderegg [53].

A more subtle point is that ESI-MS also shows the presence of high charge states for *un*oxidized cyt *c* after heating, represented by the "0" component in **Figure 2-3**B. Charge states in this range are not observed without prior heating (**Figure 2-1**A). Thus, heat exposure seems to result in conditions that can lock protein chains in a non-native structure, even in the absence of oxidative modifications. The inadequacy of simulation scenario (*c*) suggests that rapid interconversion of these species with more compact conformers does not take place. It is instructive to examine possible reasons that could

cause the irreversible denaturation of unoxidized protein after heat exposure. Cyt *c* does not possess any -S-S- bridges, thus eliminating the possibility of disulfide shuffling [59]. A small degree of Asn or Gln deamidation (-NH$_2$ → -OH, mass shift = +1 Da per affected residue) [77] cannot be excluded, but our data show that the bulk of the protein is unaffected by this process. Formation of *cis* isomers at the protein's four X-Pro peptide bonds may slow down the normal sub-second time scale of cyt *c* folding [78] by several orders of magnitude [79]. However, X-Pro *cis/trans* isomerization is reversible on a time scale of seconds to minutes, and would thus not be expected to generate proteins that are permanently locked in a non-native structure. An important point to remember is that the UV-Vis data of **Figure 2-2**A demonstrate the occurrence of partial aggregation after heating. Previous work has shown that dissociation of protein aggregates during ESI can generate highly protonated monomeric ions via asymmetric charge partitioning [20]. It is also known that interconversion between aggregated proteins and those that are free in solution is minimal [80]. In addition, conformational distortion of polypeptide chains within amorphous aggregates may promote rapid HDX. Thus, partial aggregation of the heated protein could generate a sub-population of cyt *c* molecules that (*i*) remain unoxidized, (*ii*) appear in high charge states, (*iii*) do not interconvert with the native state, and (*iv*) show a higher level of HDX than coexisting tightly folded conformers. While this aggregation mechanism is a plausible scenario, other possibilities cannot be ruled out.

2.4 Conclusions

Heat exposure of cyt *c* results in a sub-population of irreversibly denatured protein chains, i.e., species that cannot attain their native state even when placed under "physiological" solvent conditions. The non-native molecules co-exist with tightly folded species, giving rise to bimodal ESI charge state distributions and perturbed optical spectra. This work demonstrates that the denatured conformers are heavily affected by oxidative modifications. Oxidation sites include Met65, Met80, Trp59, and the heme group. Modifications of Trp59 and Met80, in particular, are expected to be highly disruptive because in the native structure these residues are located within the tightly packed protein core [62]. Protein oxidation appears to be the main reason that prevents refolding to the native state for a considerable fraction of cyt *c* molecules after heating. This interpretation is supported by previous reports of oxidative damage induced by different means for other proteins [71-73,81]. With interconversion being blocked, oxidation-denatured protein chains undergo more extensive HDX than native conformers in the same solution. Unfortunately, oxygen adducts interfere with the analysis of isotope exchange data. Uncovering the presence of HDX differences requires a careful analysis of the measured peak shapes through comparisons with simulated mass spectra. Convolution integrals of the type used in this work (eq 2) are a useful tool for interpreting HDX data in the presence of interfering contributions. In addition to oxidation, partial aggregation appears to contribute to the formation of irreversibly denatured protein after heating. These findings represent an extension of previous work by Wagner and Anderegg [53] and Mirza et al. [55] who first reported on the interesting properties of cyt *c* after heat exposure, without examining the physical reasons for the observed behavior.

2.5 References

1.   Kaltashov, I. A.; Eyles, S. J. Studies of Biomolecular Conformations and Conformational Dynamics by Mass Spectrometry. *Mass Spectrom. Rev.* **2002,** *21*, 37-71.

2.   de la Mora, F. J. Electrospray Ionization of large multiply charged species proceeds via Dole's charged residue mechanism. *Anal. Chim. Acta* **2000,** *406*, 93-104.

3.   Felitsyn, N.; Peschke, M.; Kebarle, P. Origin and number of charges observed on multiply-protonated native proteins produced by ESI. *Int. J. Mass Spectrom. Ion Proc.* **2002,** *219*, 39-62.

4.   Nesatyy, V. J.; Suter, M. J.-F. On the conformation-dependent neutralization theory and charging of individual proteins and their non-covalent complexes in the gas phase. *J. Mass Spectrom.* **2004,** *39*, 93-97.

5.   Iavarone, A. T.; Williams, E. R. Mechanism of Charging and Supercharging Molecules in Electrospray Ionization. *J. Am. Chem. Soc.* **2003,** *125*, 2319-2327.

6.   Heck, A. J. R.; Van den Heuvel, R. H. H. Investigation of intact protein complexes by mass spectrometry. *Mass Spectrom. Rev.* **2004,** *23*, 368-389.

7.   Hogan, C. J.; Carroll, J. A.; Rohrs, H. W.; Biswas, P.; Gross, M. L. Charge Carrier Field Emission Determines the Number of Charges on Native State Proteins in Electrospray Ionization. *J. Am. Chem. Soc.* **2008,** *130*, 6929-6927.

8.   Samalikova, M.; Grandori, R. Protein Charge-State Distributions in Electrospray-Ionization Mass Spectrometry Do Not Appear To Be Limited by the Surface Tension of the Solvent. *J. Am. Chem. Soc.* **2003,** *125*, 13352-13353.

9.   Nguyen, S.; Fenn, J. B. Gas-phase ions of solute species from charged droplets of solutions. *Proc. Natl. Acad. Sci. U.S.A.* **2007,** *104*, 1111-1117.

10.   Chowdhury, S. K.; Katta, V.; Chait, B. T. Probing Conformational Changes in Proteins by Mass Spectrometry. *J. Am. Chem. Soc.* **1990,** *112*, 9012-9013.

11.   Konermann, L.; Douglas, D. J. Acid-Induced Unfolding of Cytochrome *c* at Different Methanol Concentrations: Electrospray Ionization Mass Spectrometry Specifically Monitors Changes in the Tertiary Structure. *Biochemistry* **1997,** *36*, 12296-12302.

12.   Grandori, R.; Matecko, I.; Muller, N. Uncoupled analysis of secondary and tertiary protein structure by circular dichroism and electrospray ionization mass spectrometry. *J. Mass Spectrom.* **2002,** *37*, 191-196.

13.   Loo, J. A.; Edmonds, C. G.; Udseh, H. R.; Smith, R. D. Effect of Reducing Disulfide-Containing Proteins on Electrospray Ionisation Mass Spectra. *Anal. Chem.* **1990,** *62*, 693-698.

14.   Lin, H.; Dass, C. Conformational changes in β-endorphin as studied by electrospray ionization mass spectrometry. *Rapid Commun. Mass Spectrom.* **2001,** *15*, 2341-2346.

15.   Kaltashov, I. A.; Abzalimov, R. R. Do Ionic Charges in ESI MS Provide Useful Information on Macromolecular Structure? *J. Am. Soc. Mass Spectrom.* **2008,** *19*, 1239-1246.

16.   Cai, X.; Dass, C. Conformational analysis of proteins and peptides. *Curr. Org. Chem.* **2003,** *7*, 1841-8154.

17.   Katta, V.; Chait, B. T. Observation of the Heme-Globin Complex in Native Myoglobin by Electrospray-Ionisation Mass Spectrometry. *J. Am. Chem. Soc.* **1991,** *113*, 8534-8535.

18.   Grandori, R. Origin of the conformation dependence of protein charge-state distributions in electrospray ionization mass spectrometry. *J. Mass. Spectrom.* **2003,** *38*, 11-15.

19.   Wu, J.; Lebrilla, C. B. Intrinsic Basicity of Oligomeric Peptides that Contain Glycine, Alanine, and Valine - The Effects of the Alkyl Side Chain on Proton Transfer Reactions. *J. Am. Soc. Mass. Spectrom.* **1995,** *6*, 91-101.

20.   Abzalimov, R. R.; Frimpong, A. K.; Kaltashov, I. A. Gas-phase processes and measurements of macromolecular properties in solution: On the possibility of false positive and false negative signals of protein unfolding. *Int. J. Mass Spectrom.* **2006,** *253*, 207-216.

21.   Schnier, P. D.; Gross, D. S.; Williams, E. R. On the Maximum Charge State and Proton Transfer Reactivity of Peptide and Protein Ions Formed By Electrospray Ionization. *J. Am. Soc. Mass Spectrom.* **1995,** *6*, 1086-1097.

22.   Samalikova, M.; Grandori, R. Role of opposite charge in protein electrospray ionization mass spectrometry. *J. Mass Spectrom.* **2003,** *38*, 941-947.

23.   Konermann, L. A Minimalist Model for Exploring Conformational Effects on the Electrospray Charge State Distribution of Proteins. *J. Phys. Chem. B* **2007,** *111*, 6534-6543.

24.   Kaltashov, I. A.; Mohimen, A. Estimates of Protein Surface Area in Solution by Electrospray Ionization Mass Spectrometry. *Anal. Chem.* **2005,** *77*, 5370-5379.

25.   Grandori, R. Detecting equilibrium cytochrome *c* folding intermediates by electrospray ionization mass spectrometry: Two partially folded forms populate the molten globule state. *Protein Sci.* **2002,** *11*, 453-458.

26.   Mohimen, A.; Dobo, A.; Hoerner, J. K.; Kaltashov, I. A. A Chemometric Approach to Detection and Characterization of Multiple Protein Conformers in Solution Using Electrospray Ionization Mass Spectrometry. *Anal. Chem.* **2003,** *75*, 4139-4147.

27.   Yin, S.; Xie, Y.; Loo, J. A. Mass Spectrometry of Protein-Ligand Complexes: Enhanced Gas-Phase Stability of Ribonuclease-Nucleotide Complexes. *J. Am. Soc. Mass Spectrom.* **2008,** *19*, 1199-1208.

28.   Benesch, J. L. P.; Ruotolo, B. T.; Simmons, D. A.; Robinson, C. V. Protein Complexes in the Gas Phase: Technology for Structural Genomics and Proteomics. *Chem. Rev.* **2007,** *107*, 3544-3567.

29.   Wang, W.; Kitova, E. N.; Klassen, J. S. Influence of solution and gas phase processes on protein-carbohydrate binding affinities determined by nanoelectrospray Fourier transform ion cyclotron resonance mass spectrometry. *Anal. Chem.* **2003,** *75*, 4945-4955.

30.   Feng, R.; Konishi, Y. Stepwise Refolding of Acid-Denatured Myoglobin: Evidence from Electrospray Mass Spectrometry. *J. Am. Soc. Mass Spectrom.* **1993,** *4*, 638-645.

31.   Vis, H.; Heinemann, U.; Dobson, C. M.; Robinson, C. V. Detection of a Monomeric Intermediate Associated with Dimerization of Protein Hu by Mass Spectrometry. *J. Am. Chem. Soc.* **1998,** *120*, 6427-6428.

32.   Wilson, D. J.; Rafferty, S. P.; Konermann, L. Kinetic Unfolding Mechanism of the Inducible Nitric Oxide Synthase Oxygenase Domain Determined by Time-Resolved Electrospray Mass Spectrometry. *Biochemistry* **2005,** *44*, 2276-2283.

33.   Nabuchi, Y.; Murao, N.; Asoh, Y.; Takayama, M. Probing the Unfolding and Refolding Processes of Carbonic Anhydrase 2 Using Electrospray Ionization Mass Spectrometry Combined with pH Jump. *Anal. Chem.* **2007,** *79*, 8342-8349.

34. Smith, A. M.; Jahn, T. R.; Ashcroft, A. E.; Radford, S. E. Direct Observation of Oligomeric Species formed in the Early Stages of Amyloid Formation using Electrospray Ionization Mass Spectrometry. *J. Mol. Biol.* **2006,** *364*, 9-19.

35. Nemirovskiy, O. V.; Ramanathan, R.; Gross, M. L. Investigation of Calcium-Induced, Noncovalent Association of Calmodulin with Melittin by Electrospray Ionization Mass Spectrometry. *J. Am. Soc. Mass Spectrom.* **1997,** *8*, 809-812.

36. Invernizzi, G.; Samalikova, M.; Brocca, S.; Lotti, M.; Molinari, H.; Grandori, R. Comparison of bovine and porcine β-lactoglobulin: a mass spectrometric analysis. *J. Mass Spectrom.* **2006,** *41*, 717-727.

37. Borysik, A. J. H.; Read, P.; Little, D. R.; Bateman, R. H.; Radford, S. E.; Ashcroft, A. E. Separation of β2-microglobulin conformers by high-field asymmetric waveform ion mobility spectrometry (FAIMS) coupled to electrospray ionisation mass spectrometry. *Rapid Commun. Mass Spectrom.* **2004,** *18*, 2229-2234.

38. Smith, D. P.; Giles, K.; Bateman, R. H.; Radford, S. E.; Ashcroft, A. E. Monitoring Copopulated Conformational States During Protein Folding Events Using Electrospray Ionization-Ion Mobility Spectrometry-Mass Spectrometry. *J. Am. Soc. Mass Spectrom.* **2007,** *18*, 2180-2190.

39. Katta, V.; Chait, B. T. Hydrogen/Deuterium Exchange Electrospray Ionisation Mass Spectrometry: A Method for Probing Protein Conformational Changes in Solution. *J. Am. Chem. Soc.* **1993,** *115*, 6317-6321.

40. Anderegg, R. J.; Wagner, D. S. Mass Spectrometric Characterization of a Protein-Ligand Interaction. *J. Am. Chem. Soc.* **1995,** *117*, 1374-1377.

41. Jaquinod, M.; Guy, P.; Halgand, F.; Caffrey, M.; Fitch, J.; Cusanovich, M.; Forest, E. Stability study of Rhodobacter capsulatus ferrocytochrome c2 wild-type and site-directed mutants using hydrogen/deuterium exchange monitored by electrospray ionization mass spectrometry. *FEBS Letters* **1996,** *380*, 44-48.

42. Nemirovskiy, O.; E., G. D.; Gross, M. L. Electrospray Ionization Mass Spectrometry and Hydrogen/Deuterium Exchange for Probing the Interaction of Calmodulin with Calcium. *J. Am. Soc. Mass Spectrom.* **1999,** *10*, 711-718.

43. Krishna, M. M. G.; Hoang, L.; Lin, Y.; Englander, S. W. Hydrogen exchange methods to study protein folding. *Methods* **2004,** *34*, 51-64.

44. Maier, C. S.; Schimerlik, M. I.; Deinzer, M. L. Thermal Denaturation of *Escherichia coli* Thioredoxin Studied by Hydrogen/Deuterium Exchange and Electrospray Ionization Mass Spectrometry: Monitoring a Two-State Protein Unfolding Transition. *Biochemistry* **1999,** *38*, 1136-1143.

45. Kim, M.-Y.; Maier, C. S.; Reed, D. J.; Deinzer, M. L. Conformational changes in chemically modified *Escherichia coli* thioredoxin monitored by H/D exchange and electrospray mass spectrometry. *Protein Sci.* **2002,** *11*, 1320-1329.

46. Eyles, S. J.; Dresch, T.; Gierasch, L. M.; Kaltashov, I. A. Unfolding Dynamics of a β-Sheet Protein Studied by Mass Spectrometry. *J. Mass Spectrom.* **1999,** *34*, 1289-1295.

47. Simmons, D. A.; Dunn, S. D.; Konermann, L. Conformational Dynamics of Partially Denatured Myoglobin Studied by Time-Resolved Electrospray Mass Spectrometry With Online Hydrogen-Deuterium Exchange. *Biochemistry* **2003,** *42*, 5896-5905.

48. Pan, J. X.; Wilson, D. J.; Konermann, L. Pulsed Hydrogen Exchange and Electrospray Charge-State Distribution as Complementary Probes of Protein Structure in Kinetic Experiments: Implications for Ubiquitin Folding. *Biochemistry* **2005,** *44*, 8627-8633.

49. Babu, K. R.; Douglas, D. J. Methanol-Induced Conformations of Myoglobin at pH 4.0. *Biochemistry* **2000,** *39*, 14702-14710.

50.	Babu, K. R.; Moradian, A.; Douglas, D. J. The Methanol-Induced Conformational Transitions of β-Lactoglobulin, Cytochrome c, and Ubiquitin at Low pH: A Study by Electrospray Ionization Mass Spectrometry. *J. Am. Soc. Mass Spectrom.* **2001,** *12*, 317-328.

51.	Wang, F.; Tang, X. Conformational Heterogeneity and Stability of Apomyoglobin Studied by Hydrogen/Deuterium Exchange and Electrospray Ionization Mass Spectrometry. *Biochemistry* **1996,** *35*, 4069-4078.

52.	Bai, Y.; Sosnick, T. R.; Mayne, L.; Englander, S. W. Protein Folding Intermediates: Native State Hydrogen Exchange. *Science* **1995,** *269*, 192-197.

53.	Wagner, D. S.; Anderegg, R. J. Conformation of Cytochrome c Studied by Deuterium Exchange-Electrospray Ionization Mass Spectrometry. *Anal. Chem.* **1994,** *66*, 706-711.

54.	Anfinsen, C. B. Principles that Govern the Folding of Protein Chains. *Science* **1973,** *181*, 223-230.

55.	Mirza, U. A.; Cohen, S. L.; Chait, B. T. Heat-Induced Conformational Changes in Proteins Studied by Electrospray Ionisation Mass Spectrometry. *Anal. Chem.* **1993,** *65*, 1-6.

56.	Potekhin, S. A.; Kovrigin, E. L. Folding under inequilibrium conditions as possible reason for partial irreversibility of heat-denatured proteins: computer simulation study. *Biophys. Chem.* **1998,** *73*, 241-248.

57.	Kreimer, D. I.; Shnyrov, V. L.; Villar, E.; Silman, I.; Weiner, L. Irreversible thermal denaturation of Torpedo californica acetylcholinesterase. *Protein Sci.* **1995,** *4*, 2349-2357.

58.   Miller, S.; Schuler, B.; Seckler, R. Phage P22 tailspike protein: Removal of head-binding domain unmasks effects of folding mutations on native-state thermal stability. *Protein Sci.* **1998,** *7*, 2223-2232.

59.   Tani, F.; Shirai, N.; Onishi, T.; Venelle, F.; Kyoden, Y.; Doi, E. Temperature control for kinetic refolding of heat-denatured ovalbumin. *Protein Sci.* **1997,** *6*, 1491-1502.

60.   Boys, B. L.; Konermann, L. A Temperature-Jump Stopped-Flow System fo Monitoring Chemical Kinetics Triggered by Rapid Cooling. *Talanta* **2007,** *71*, 1276-1281.

61.   Benjwal, S.; Verma, S.; Röhm, K.-H.; Gursky, O. Monitoring protein aggregation during thermal unfolding in circular dichroism experiments. *Protein Sci.* **2006,** *15*, 635-639.

62.   Mirkin, N.; Jaconcic, J.; Stojanoff, V.; Moreno, A. High resolution X-ray ctystallographic structure of bovine heart cytochrome c and its application to the design of an electron transfer biosensor. *Proteins: Struct. Funct. Gen.* **2008,** *70*, 83-92.

63.   Babul, J.; Stellwagen, W. Participation of the Protein Ligands in the Folding of Cytochrome c. *Biochemistry* **1972,** *7*, 1195-1200.

64.   Ferguson, P. L.; Pan, J.; Wilson, D. J.; Dempsey, B.; Lajoie, G.; Shilton, B.; Konermann, L. Hydrogen/Deuterium Scrambling During Quadrupole-Time-of-Flight MS/MS Analysis of a Zinc-Binding Protein Domain. *Anal. Chem.* **2007,** *79*, 153-160.

65.   Bychkova, V. E.; Dujsekina, A. E.; Klenin, S. I.; Tiktopulo, E. I.; Uversky, V. N.; Ptitsyn, O. B. Molten Globule-Like State of Cytochrome c under Conditions Simulating Those Near the Membrane Surface. *Biochemistry* **1996,** *35*, 6058-6063.

66. March, R.; Todd, J. F. J. *Quadrupole Ion Trap Mass Spectrometry*Second edition ed.; Wiley: New York ; Toronto, 2005.

67. Brahms, S.; Brahms, J. Determination of Protein Secondary Structure in Solution by Vacuum Ultraviolet Circular Dichroism. *J. Mol. Biol.* **1980,** *138*, 149-178.

68. Sosnick, T. R.; Mayne, L.; Englander, S. W. Molecular Collapse: The Rate-Limiting Step in Two-State Cytochrome c Folding. *Proteins: Struct. Biol. Genet.* **1996,** *24*, 413-426.

69. Xu, G.; Chance, M. R. Hydroxyl Radical-Mediated Modification of Proteins as Probes for Structural Proteomics. *Chem. Rev.* **2007,** *107*, 3514-3543.

70. Tong, X.; Wren, J. C.; Konermann, L. γ-Ray-Mediated Oxidative Labeling for Detecting Protein Conformational Changes by Electrospray Mass Spectrometry. *Anal. Chem.* **2008,** *80*, 2222-2231.

71. Sharp, J. S.; Tomer, K. B. Analysis of the Oxidative Damage-Induced Conformational Changes of Apo- and Holocalmodulin by Dose-Dependent Protein Oxidative Surface Mapping. *Biophys. J.* **2007,** *92*, 1682-1692.

72. Shum, W.-K.; Maleknia, S. D.; Downard, K. M. Onset of oxidative damage in α-crystallin by radical probe mass spectrometry. *Anal. Biochem.* **2005,** *344*, 247-256.

73. Chao, C.-C.; Ma, Y.-S.; Stadtman, E. R. Modification of protein surface hydrophobicity and methionine oxidation by oxidative systems. *Proc. Natl. Acad. Sci. U.S.A.* **1997,** *94*, 2969-2974.

74. Li, Y.-T.; Hsieh, Y.-L.; Henion, J. D.; Ganem, B. Studies on Heme Binding in Myoglobin, Hemoglobin, and Cytochrome c by Ion Spray Mass Spectrometry. *J. Am. Soc. Mass Spectrom.* **1993,** *4*, 631-637.

75. Sugiyama, K.; Highet, R. J.; Woods, A.; Cotter, R. J.; Osawa, Y. Hydrogen peroxide-mediated alteration of the heme prosthetic group of metmyoglobin to an iron chlorin product: Evidence for a novel oxidative pathway. *Proc. Natl. Acad. Sci. U.S.A.* **1997,** *94*, 796-801.

76. Xiao, H.; Hoerner, J. K.; Eyles, S. J.; Dobo, A.; Voigtman, E.; Melcuk, A. I.; Kaltashov, I. A. Mapping protein energy landscapes with amide hydrogen exchange and mass spectrometry: I. A generalized model for a two-state protein and comparison with experiment. *Protein Sci.* **2005,** *14*, 543-557.

77. Zabrouskov, V.; Han, X.; Welker, E.; Zhai, H.; Lin, C.; van Wijk, K. J.; Scheraga, H. A.; McLafferty, F. W. Stepwise Deamidation of Ribonuclease A at Five Sites Determined by Top Down Mass Spectrometry. *Biochemistry* **2006,** *45*, 987-992.

78. Englander, S. W.; Sosnick, T. R.; Mayne, L. C.; Shtilterman, M.; Qi, P. X.; Bai, Y. Fast and Slow Folding in Cytochrome c. *Acc. Chem. Res.* **1998,** *31*, 737-744.

79. Houry, W. A.; Scheraga, H. A. Nature of the Unfolded State of Ribonuclease A: Effect of Cis-Trans X-Pro Peptide Bond Isomerisation. *Biochemistry* **1996,** *35*, 11719-11733.

80. Dobson, C. M. Protein folding and misfolding. *Nature* **2003,** *426*, 884-890.

81. Tong, X.; Wren, J. C.; Konermann, L. Effects of Protein Concentration on the Extent of γ-Ray-Mediated Oxidative Labeling Studied by Electrospray Mass Spectrometry. *Anal. Chem.* **2007,** *79*, 6376-6382.

Chapter 3 – Protein-Protein Binding Affinities In Solution Determined by Electrospray Mass Spectrometry

3.1 Introduction

Many proteins form noncovalent complexes with ligands such as metal ions, prosthetic groups, or other proteins. Multi-protein complexes are of particular interest, because they play a central role in numerous biological processes. The architecture of these supramolecular assemblies ranges from dimers all the way to MDa systems that encompass dozens of subunits [2]. Various experimental methods have been applied for studying protein-protein interactions. These include optical and calorimetric assays [4], nuclear magnetic resonance spectroscopy [5], surface plasmon resonance[6], micro-array chip [7], yeast two-hybrid screen [8], and analytical ultracentrifugation (AUC) [9]. Mass spectrometry (MS) offers a number of complementary avenues for characterizing protein-protein interactions [10]. Hydrogen/deuterium exchange MS monitors changes in structure and dynamics upon binding [11-13]. Similarly, alterations in solvent accessibility can be probed by covalent labeling in solution, followed by a MS-based readout [14,15]. Affinity purification/MS has proven to be highly effective as well [16,17].

Conceptually the most straightforward technique for monitoring noncovalent complexes by MS is the "direct" approach. This method involves the transfer of intact solution phase assemblies into the gas phase by electrospray (ESI) or related ionization processes, followed by detection in a suitable mass analyzer [18-22]. Attractive features of this strategy include its speed, sensitivity, and selectivity. Numerous laboratories have

used the direct ESI-MS approach for characterizing protein-protein complexes [18-22], as well as other noncovalent assemblies [23-27].

One question that remains somewhat unclear is to what extent the direct ESI-MS approach is suitable for determining solution phase binding *affinities*. This issue has been explored in considerable detail for protein-small molecule complexes [28-31]. In comparison, affinity measurements for protein-protein interactions have received less attention. We will consider the simple example of a homodimer D that is in equilibrium with its monomeric form M in solution according to

$$D \; \rightleftarrows \; 2\,M \tag{1}$$

The binding affinity of the complex is reflected in the dissociation constant

$$K_d = \frac{[M]^2}{[D]} \tag{2}$$

where $[M]$ and $[D]$ denote the equilibrium concentrations of monomer and dimer, respectively. Assuming that the concentration ratio

$$R_{sol} = \frac{[D]}{[M]} \tag{3}$$

in solution is known, the dissociation constant can be calculated as

$$K_d = [P]_0 \frac{1}{R_{sol}(2R_{sol}+1)} \tag{4}$$

where $[P]_0 = [M] + 2[D]$ is the total protein concentration, expressed on a monomer basis. It is important to recognize that ESI-MS does *not* directly report the value of R_{sol}. Instead, these experiments provide the ion abundance ratio $R_{ESI\text{-}MS}$ which is given by

$$R_{ESI-MS} = \frac{I_D}{I_M} \tag{5}$$

where I_D and I_M are the integrated signal intensities of dimeric and monomeric ions. The relationship between signal intensity and solution-phase concentration is given by

$$I_D = \gamma_D [D] \tag{6a}$$

$$I_M = \gamma_M [M] \tag{6b}$$

The response factors γ reflect the extent to which M and D species in bulk solution are converted to measurable ESI-MS signals [32]. The magnitude of γ depends on several factors, including how efficiently the species are (i) transformed into gaseous ions, (ii) transmitted from the ESI source into the vacuum and through the mass spectrometer, and (iii) converted into electronic signals at the detector. Knowledge of γ_M/γ_D is vital for the use of ESI-MS as a tool for binding affinity measurements on the basis of equation (4), since

$$R_{sol} = \frac{\gamma_M}{\gamma_D} R_{ESI-MS} \tag{7}$$

Methods for determining ESI-MS response factors have been proposed [32,33], but those approaches are not straightforward and their general applicability remains unclear. Hence, it is common to postulate that $\gamma_M/\gamma_D \approx 1$ [34].

In addition to discussing K_d values, a useful quantity that expresses the extent of protein interactions in solution is the fraction bound, f_{sol}, defined as

$$f_{sol} = 2\frac{[D]}{[P]_0} \tag{8}$$

ESI-MS provides a related value, $f_{ESI\text{-}MS}$, that is based on ion intensities according to

$$f_{ESI-MS} = 2\frac{I_D}{I_M + 2I_D} \tag{9}$$

Analogous to the discussion above, it is seen that $f_{sol} = f_{ESI\text{-}MS}$ only if $\gamma_M = \gamma_D$.

The assumption that free and bound solution-phase species have the same γ value is relatively unproblematic in the case of small molecule binding to a large receptor, where the free and bound forms generate ions that cover a very similar m/z range [25,29,30]. For protein complexes, however, the situation is not as simple. The formation of protein-protein interactions may be associated with changes in physicochemical properties that can affect the response factors [35,36]. The most obvious of these parameters are size and molecular weight. Smaller species tend to produce higher signal intensities [37]. Mass (or m/z) discrimination effects of this type can be caused by various factors, including insufficient collisional focusing during ion transfer [19,20,38,39].

Discrimination phenomena can also be related to the ESI mechanism. Formation of a protein complex can change the percentage of solvent-exposed hydrophobic residues, for example when monomers undergo a folding transition upon binding. Differences between γ_M and γ_D would be expected in such a case, because hydrophobicity is closely linked to the ESI ionization efficiency [3,40]. Also, solution phase equilibria may shift due to acidification caused by redox reactions in the ESI capillary [29,41,42], or as the result of concentration changes in the shrinking ESI droplets [43]. Luckily, these equilibrium shifts tend to be small under typical operating conditions [37,44]. Of greater concern is the possibility that nonspecific complexes can be formed from ESI droplets that contain two or more protein molecules. ESI-induced artifacts of this type give rise to false-positive results, i.e., the observation of gas-phase complexes that did not exist in solution [19,34,37,45]. Conversely, protein complexes may get disrupted during or after ESI, for example by collision-induced dissociation (CID) [21,37,46-49].

Whereas regular ESI employs flow rates in the µL min^{-1} range, nanoESI sources are operated in the nL min^{-1} regime [50,51]. It is often implied that nanoESI methods provide a better reflection of solution-phase binding equilibria due to the purported greater "softness" of the ionization process [19]. Nano-ESI-MS certainly offers some advantages due to its low sample consumption. The notion that it better reflects solution-phase binding equilibria, however, is not undisputed [28,46].

The preceding considerations show that ESI-MS may provide a distorted view of solution phase binding equilibria in certain cases. To examine the applicability of the direct ESI-MS approach for protein-protein affinity measurements, the current work focuses on two systems, β-lactoglobulin (BLG) [34,52,53]. and hemoglobin (Hb) [54-56].

We test the effects of different ion sources. The extent to which differential protein ionization efficiencies, inadvertent fragmentation, and artifactual clustering affect the measured data are explored. Dramatically skewed results are obtained when employing improper ion transfer settings. Nonetheless, we find that under carefully controlled conditions the mass spectra reflect the protein binding behavior in solution remarkably well.

3.2 Experimental

3.2.1 Materials

Bovine BLG (monomer mass 18281 Da, pdb code 1BEB) was purchased from Sigma (St. Louis, MO, USA). Protein purity was confirmed by SDS gel electrophoresis. Hb (pdb code 2QSS) was isolated from fresh cow blood in its oxygenated (ferro) form following established procedures [56]. The masses of the Hb α and β subunits (including heme, excluding oxygen) are 15669 and 16570 Da, respectively. Prior to ESI-MS, the proteins were extensively dialyzed against 10 mM aqueous ammonium acetate. The resulting stock solutions were diluted to the desired protein concentrations in 150 mM ammonium acetate (pH 6.8). Protein concentrations were verified by UV-Vis absorption spectroscopy. BLG concentrations throughout this work are expressed on a monomer basis, Hb concentrations are reported on the basis of heterodimeric $\alpha\beta$ complexes.

3.2.2 Mass Spectrometry

All mass spectra were recorded under gentle ESI condition using a quadrupole-time-of-flight instrument (Q-TOF Ultima, Waters, Milford, MA). The cone voltage and RF1 lens DC offset were adjusted to provide the highest relative signals for protein non-covalent complexes. Cone voltage values were in the range of 40 V to 70 V, and the RF1 voltage was between 50 V and 70 V. The desolvation temperature was set to 40 °C, down from its factory-recommended standard value of around 250 °C. The source block temperature was adjusted to 80 °C. Cone and desolvation gas flow rates were 100 and 500 L h^{-1}, respectively. Mass calibration was performed over the range from *m/z* 600 to 7000 using 2 μg μL^{-1} CsI in 1:1 (v/v) water/2-propanol. The ion transmission of the quadrupole is strongly dependent on the "MS profile" parameters, as discussed in the Results and Discussion section. Changing the hexapole RF settings was found to have only minor effects, and all spectra were recorded with a gain of 10 and an offset of 0.8. The maximum signal intensity in the spectra discussed below was on the order of 100 counts per second, roughly one order of magnitude below the saturation level. Increasing the pressure in the source region did not significantly affect the measured R_{ESI} values, revealing that extensive collisional focusing occurs even under standard experimental conditions for the Q-TOF employed here. This is in contrast to other instruments previously used in our laboratory, where the source pressure has dramatic effects [57]. Three different ESI sources were tested, a pulled capillary Waters nanoESI source, an automated chip-based nanoESI system (Advion Triversa, Ithaca, NY), and a regular Waters Z-spray source. The ESI voltages used for the three sources were 1.5 - 1.8 kV, 1.5 - 1.7 kV, and 3 kV, respectively. Pulled capillary nanoESI measurements employed

borosilicate emitters with a Au/Pd coating (Proxeon, Cambridge MA). Solution flow through these capillaries was assisted by gentle nitrogen back pressure of less than 1 psi. The nanoESI flow rate under these conditions was estimated gravimetrically to be around 25 nL min^{-1}, consistent with the manufacturer's specifications. The nozzles of the Advion nanoESI chips had a diameter of 5 μm, and flow rates were in the range of 50 to 100 nL min^{-1}. Flow rates of the Z-spray source were controlled by a syringe pump (Harvard 22, Boston, MA). All spectra were acquired in positive ion mode. Peak area measurements for determination of I_M and I_D was conducted by using integration windows of $\Delta m/z =$ 100 around each peak.

3.3 Results and Discussion

3.3.1 Quadrupole Transmission Profile

Q-TOF analyzers are one of the most commonly used type of mass spectrometer for studies on noncovalent protein complexes [18-22]. Intact mass measurements on Q-TOF instruments are conducted by operating the quadrupole ("Q") in RF-only mode where it serves as an ion guide [58-60]. It is important to note that an RF-only quadrupole does not transmit all ions with the same efficiency. Instead, it acts as a broad-band filter that does not allow passage of species with m/z values less than ~ $0.8 \times M^*$, where M^* depends on the RF amplitude. On the high mass side the transmission drops gradually, and only ions up to ca. $5 \times M^*$ can pass through the device. Commercial Q-TOF instruments allow the RF amplitude (and hence M^*) to be ramped during data acquisition, thereby permitting analysis of a wider m/z window [61].

The choice of RF-only quadrupole settings has dramatic consequences for the relative peak intensities in different m/z regions of a mass spectrum. Figure 1 illustrates this effect for Hb. The experiments were conducted under semi-denaturing conditions (pH 3.6), to ensure that the protein exists in various solution phase binding states that cover a wide m/z range (unbound α and β subunits, as well as $\alpha\beta$ and $(\alpha\beta)_2$ complexes) [56]. For the instrument used here the quadrupole transmission is controlled by seven parameters. *Dwell$_1$* and *dwell$_2$* reflect the fraction of time that the quadrupole is operated at $M_1{}^*$ and $M_2{}^*$, respectively. *Ramp$_{12}$* is the time fraction during which the device is ramped from $M_1{}^*$ to $M_2{}^*$. Similarly, *ramp$_{23}$* refers to the ramp time spent between $M_2{}^*$ and a third value $M_3{}^*$. **Figure 3-1** (left hand side panels) depicts transmission profiles that were simulated for different quadrupole parameters, while the panels on the right show the corresponding mass spectra. Except for modifications of these quadrupole parameters, all data in **Figure 3-1** were recorded under identical conditions.

When trying to ensure uniform transmission over a wide m/z range it is tempting to use settings where the RF amplitude is continuously ramped between a minimum value $M_1{}^*$ and a maximum value $M_2{}^*$. Unfortunately, this strategy leads to an overall transmission profile that strongly favors the m/z range around $M_2{}^*$, while discriminating against lower values (**Figure 3-1A**). This behavior is a consequence of the asymmetric profile shape at any given M^* (see above) [61]. The Hb spectrum recorded under such conditions, with $M_1{}^* = 400$ and $M_2{}^* = 4000$, is dominated by $\alpha\beta$ ions, while peak intensities for $(\alpha\beta)_2$ and unbound subunits are much lower (**Figure 3-1B**). **Figures 3-1C, D** represent quadrupole settings that were chosen to strongly favor low m/z values.
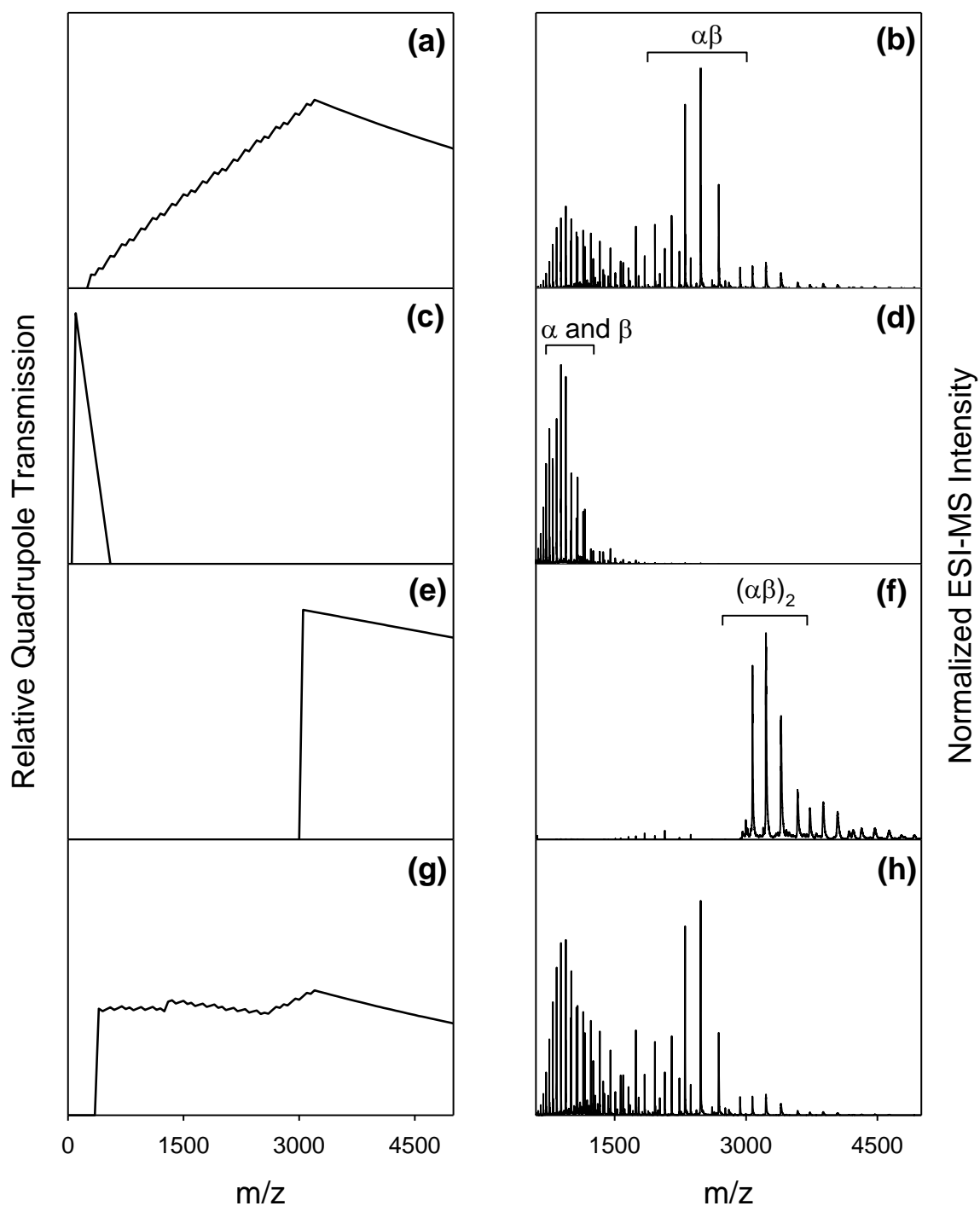
Figure 3-1. Simulated quadrupole transmission profiles (left) and corresponding measured ESI mass spectra of Hb (right) at pH 3.6. The data were recorded using a Z-spray ESI source with a flow rate of 3 μL min^{-1} and a (αβ) concentration of 100 μM. Parameters for operation of the RF-only quadrupole (M_1^*, $dwell_1$, $ramp_{12}$, M_2^*, $dwell_2$, $ramp_{23}$, and M_3^*) were as follows: (a, b) 400, 5%, 95%, 4000, 0%, 0%, 4000; (c, d) 100, 100%, 0%, 100, 0%, 0%, 100; (e, f) 3800, 100%, 0%, 3800, 0%, 0%, 3800; (g, h) 1600, 3%, 0%, 400, 37%, 60%, 4000. Binding states of Hb subunits are indicated as α and β, αβ, and (αβ)$_2$.

The resulting mass spectrum exclusively shows free α and β species. In contrast, **Figure 3-1E** demonstrates the effects of "high mass settings", yielding data that are dominated by $(\alpha\beta)_2$ (**Figure 3-1F**). By carefully adjusting the quadrupole RF parameters it is possible to achieve a transmission profile that is relatively uniform between *m/z* 300 and 4500 (**Figure 3-1G**). Under these conditions unbound subunits and $\alpha\beta$ appear with comparable peak intensities, while $(\alpha\beta)_2$ signals are much lower (**Figure 3-1H**).

Overall, **Figure 3-1** illustrates that ESI mass spectra for samples containing co-existing protein binding states are strongly dependent on the transmission characteristics of the mass analyzer. In fact, the ion intensity ratio of a complex and its unbound constituents can have any value between zero and infinity, depending on the choice of quadrupole settings (**Figure 1D, F**). It is surprising that the quadrupole transmission properties hardly receive any mention in the pertinent ESI-MS literature, where ion intensity ratios ($R_{ESI\text{-}MS}$, Equation 5) are used to estimate binding affinities in solution. The instrument settings of **Figure 3-1G** appear to be most suitable for binding affinity measurements because they result in fairly uniform transmission characteristics. Hence, this profile was used for all subsequent measurements of this work.

3.3.2 Effects of Different ESI Sources

The binding behavior of two model proteins, BLG and Hb was studied by ESI-MS under native solvent conditions (150 mM ammonium acetate, pH 6.8). BLG forms homodimers in solution. X-ray analyses of the binding interface show a number of hydrogen bonds between the AB loops of both subunits. Inter-subunit H-bonds also occur

between two β strands, in addition to a pair of salt bridges [34,52,53]. Hb is usually referred to as a "dimer of dimers", because its solution phase behavior is dominated by $(\alpha\beta)_2 = 2 \alpha\beta$ equilibration under native conditions [54-56,62]. Subunit interactions in Hb are mediated by nonpolar and van der Waals contacts, as well as hydrogen bonds and salt bridges [63]. Hb dissociation into unbound α and β only plays a role under non-native conditions, as in **Figure 3-1** [54-56]. On the basis of these considerations, the dissociation behavior of both BLG and Hb can be interpreted within the framework provided by Equations 1 - 9. For Hb, this requires $\alpha\beta$ and $(\alpha\beta)_2$ to be interpreted as "*M*" and "*D*", respectively.

Mass spectra of both protein systems were acquired under four different ionization conditions: (1) nanoESI employing a pulled capillary emitter, (2) an automated chip-based nanoESI source, and a regular Z-spray ESI source operated at (3) 1 μL min^{-1} and (4) 50 μL min^{-1}. Data acquired for BLG show monomers and homodimers, consistent with earlier observations (**Figure 3-2**) [34,52]. Analysis of these spectra reveals that the apparent extent of BLG dimerization under all four ionization conditions is quite similar, with f_{ESI-MS} values of 0.69, 0.66, 0.79, and 0.72 for **Figure 3-2**A, C, E, and G, respectively. Similar measurements were conducted with Hb, for assessing the abundance of $\alpha\beta$ and $(\alpha\beta)_2$ ions. Native Hb mass spectra obtained under the four ionization conditions resulted in f_{ESI-MS} values of 0.70, 0.67, 0.83, and 0.80 (Figure 3-2B, D, F, H, respectively). As expected [54-56], unbound α and β are virtually undetectable for the solvent conditions of **Figure 3-2**.
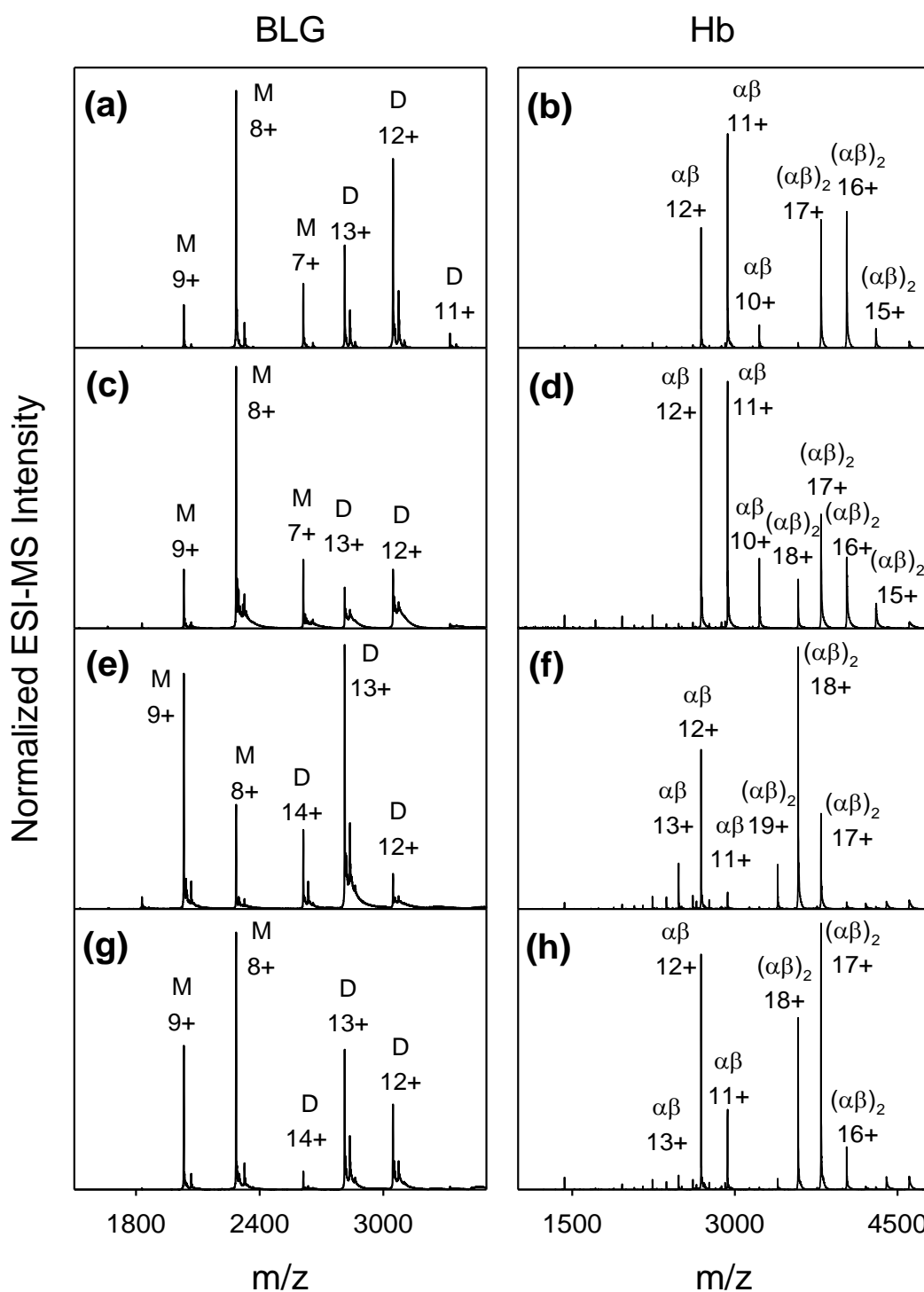
Figure 3-2. ESI mass spectra of 10 μM BLG (panels on left), and 34 μM Hb (panels on right). The data were acquired with (a, b) pulled capillary nanoESI source, (c, d) chip-based nanoESI source, (e, f) Z-spray ESI source at 1 μL min^{-1}, and (g, h) Z-spray ESI source at 50 μL min^{-1}. *M* and *D* in the BLG spectra denote monomers and dimers, respectively. Binding states of Hb subunits are denoted as αβ and (αβ)$_2$, with protonation states indicated. Except for differences in ESI voltage (see text), all spectra were acquired under identical instrument settings.

The data of **Figure 3-2** demonstrate that the choice of ion source can affect the outcome of binding affinity measurements to a certain extent. However, the differences are surprisingly small, as f_{ESI-MS} values measured under the four conditions agree within 25%. Our observations do *not* support the commonly held notion that nanoESI is "softer" and thus better suited for studying noncovalent systems, at least not for the proteins studied here. This finding is in line with the results of other protein binding experiments [28,46]. Consistent with earlier reports [19,47]. we also found nanoESI-MS measurements to be less reproducible than those conducted with a regular ESI source. If f_{ESI-MS} values are to be used for judging the quality of the spectra in **Figure 3-2**, one has to conclude that a regular ESI source operated at 1 μL min^{-1} provides the most favorable conditions for the observation of protein complexes (**Figure 3-2**E, F).

3.3.3 Testing the Fidelity of ESI-MS Data for Affinity Measurements

Several potential pitfalls have to be considered when assessing the solution-phase binding affinity of protein complexes by ESI-MS (see Introduction). Luckily, the most pertinent points are addressable by direct analysis of the measured spectra.

Protein binding in solution can be associated with conformational changes. In these cases the subunits will be more tightly folded within the complex than in the free state [64]. Such a scenario should increase the response factor γ_M relative to γ_D (Equation 6) because partial unfolding enhances the effective hydrophobicity and thereby increases the ionization efficiency [3,40]. Whether or not this case applies to the systems studied here can be determined by applying a simple test. The average ESI charge state is linked

to the protein surface area in solution. For natively folded proteins a linear relationship between ln(*surface area*) and ln(*average ESI charge state*) has been demonstrated, with a slope of 0.69 ± 0.02 [1]. **Figure 3-3** shows a ln-ln plot of this type for BLG monomers and dimers, as well as for Hb $\alpha\beta$ and $(\alpha\beta)_2$. All data points fall on a straight line with a slope of 0.66 ± 0.03, consistent with the results of ref [1]. Solution-phase unfolding greatly enhances the degree of protonation during ESI [65-68], and therefore would lead to major deviations from linear behavior in **Figure 3-3**. Thus, we conclude that complex formation is not associated with major conformational changes for the proteins studied here. In other words, a selective enhancement of free protein signals (γ_M) caused by conformational effects can be excluded.

Another point that has to be addressed is the possible disruption of noncovalent complexes by CID during ion sampling or transport [29,49]. In other words, we have to scrutinize whether BLG monomer peaks and Hb $\alpha\beta$ signals in Figure 2 encompass significant contributions from inadvertently formed gas phase fragments. Charge partitioning during CID can occur in a symmetric or asymmetric fashion, subject to conservation of overall charge [69]. On the basis of the very narrow charge state distributions for both BLG monomers and Hb $\alpha\beta$ ions (**Figure 3-2**), CID with asymmetric charge partitioning can immediately be excluded. On the other hand, symmetric fragmentation of BLG dimers would result in monomeric species with charge states centered around $13/2 \approx 6$ - 7, whereas $(\alpha\beta)_2$ would produce $\alpha\beta$ fragments with charges in the range of $17/2 \approx 8$ - 9. The observed charge states for both BLG monomers and Hb $\alpha\beta$ ions fall outside these expected ranges (**Figure 3-2**). This behavior implies that the extent of inadvertent gas phase fragmentation is negligible for the conditions used
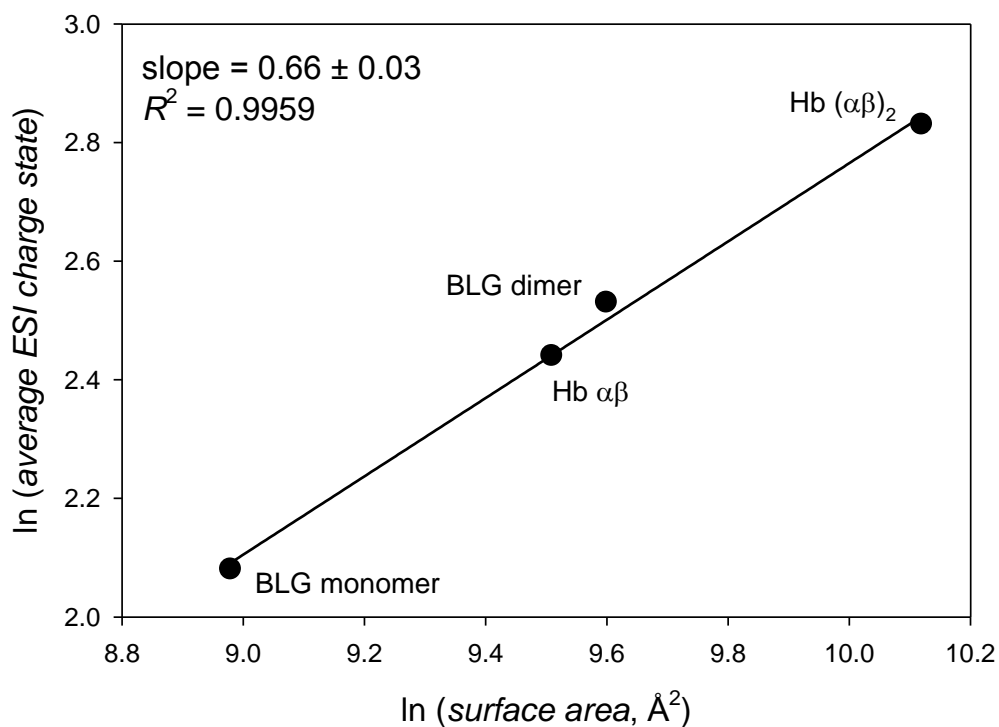
Figure 3-3. Plot of ln(average ESI charge state) vs. ln(surface area, $\mathring{A}^2$), following the approach of ref [1]. Average charge states for each protein were calculated as described previously [3] on the basis of integrated peak areas, averaged over all spectra shown in Figure 2. Solvent accessible surface areas were calculated for BLG monomers and dimers from pdb file 1BEB using the program GetArea (http://curie.utmb.edu/getarea.html). PDB file 2QSS for used for Hb.

here. In the case of Hb, this conclusion is further supported by earlier experiments where CID of $(\alpha\beta)_2$ was deliberately induced, resulting in spectra that are completely different from those depicted in **Figure 3-2** [58].

A third potential concern is the formation of nonspecific protein-protein complexes during ESI [34,37,45]. Such an effect would lead to an overrepresentation of bound protein states in the spectra. Any ESI-mediated clustering artifacts is strongly dependent on the size of the initially formed ESI droplets. The volume of these droplets is proportional to the solution flow rate [3,70-72]. Larger droplets undergo a greater number of evaporation/fission cycles, thereby increasing the protein concentration in the final droplets that produce gas phase analyte ions [19,37]. Thus, the formation of nonspecific aggregates should be enhanced at higher flow rates. Comparison of mass spectra recorded at 1 μL min^{-1} (**Figure 3-2E, F**) and 50 μL min^{-1} (**Figure 3-2**G, H) shows that increasing the flow rate does *not* lead to higher signals for bound species. Therefore, the f_{ESI-MS} values measured for BLG and Hb are not significantly affected by nonspecific clustering. It is interesting to note that abundance of dimeric BLG and Hb $(\alpha\beta)_2$ actually *de*creases slightly when the flow rate is raised. This may be due to more favorable desolvation at 1 μL min^{-1} (**Figure 3-2E, F**).

In summary, the mass spectra of **Figure 3-2** appear to be free of major ESI-induced complexation and fragmentation artifacts. Moreover, the linear relationship of **Figure 3-3** suggests that conformationally-induced differences in the ionization efficiency of free and bound proteins are small. The quadrupole transmission has been adjusted to ensure that *m/z*-dependent discrimination effects are at a minimum (**Figure 3-**

1G). Only after considering all of these points it is justified to assume that $\gamma_M \approx \gamma_D$ (Equation 6). Hence, the value of R_{ESI-MS} should closely match the concentration ratio R_{sol} (Equation 7), such that dissociation constants can be determined directly from ESI-MS intensity ratios (Equation 4). The validity of these considerations is confirmed by the results discussed in the subsequent section.

3.3.4 Concentration-Dependent Measurements

For any dissociation equilibrium in solution (Equation 1) the fraction of bound protein depends on the total concentration $[P]_0$. Elevated protein concentrations will increase the value of f_{sol}. **Figure 3-4** depicts the results of comparative ESI measurements on BLG and Hb, where $[P]_0$ was altered by two orders of magnitude. The data were acquired using a standard Z-spray ESI source at 1 μL min^{-1}. As expected, the resulting spectra show an increased abundance of bound protein at elevated $[P]_0$. Dissociation constants were determined from the measured R_{ESI} values at different $[P]_0$, assuming that $\gamma_M/\gamma_D = 1$ (Equations 4, 7). The resulting K_d values are summarized in **Table 1**. BLG dissociation constants determined in this way at different protein concentrations agree within a factor of two. When averaging these data a value of $K_d = (2.2 \pm 0.7)$ μM is obtained. This result is in reasonable agreement with the literature value of 4.9 μM, which was measured by AUC for BLG [53]. The spread in the ESI-MS-derived K_d values for Hb is somewhat larger, between 1.3 and 3.6 μM. However, this level of variability is quite common when measuring dissociation constants under different conditions [73].
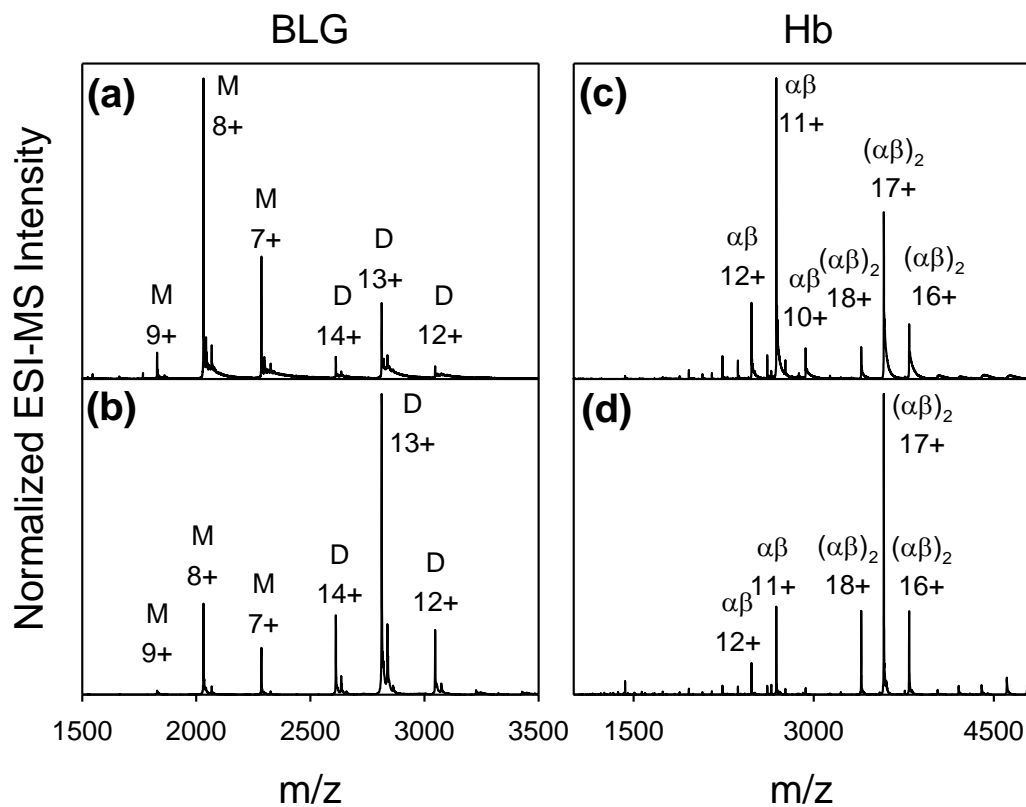
Figure 3-4. ESI mass spectra of BLG acquired at a protein concentration of (a) 1 μM [f_{ESI-MS} = 0.36] and (b) 90 μM [f_{ESI-MS} = 0.89]. Panels (c), (d) show data measured for 3.4 μM and 170 μM Hb, with f_{ESI-MS} values of 0.65 and 0.90, respectively. The data were recorded using a Z-spray ESI source at 1 μL min^{-1}.

Table 1. Dissociation constants K_d measured by ESI-MS at different protein concentrations $[P]_0$. The data used for these calculations were acquired using a regular Z-spray ESI source operated at 1 μL min^{-1} (Figures 2, 4). All values are in units of μM.

BLG	$[P]_0$	1	10	90
	K_d	2.2	1.2	2.5
Hb	$[P]_0$	3.4	34	170
	K_d	1.3	2.4	3.6

Most importantly, the average K_d value of (2.4 ± 1) μM for Hb is consistent with a the results of various solution-phase assays that provided a dissociation constant of 2 μM [62,74].

The fact that similar K_d values are obtained at different protein concentrations confirms that the spectral changes seen in **Figure 3-4** indeed reflect equilibrium shifts in solution. More importantly, the consistency of ESI-MS-derived K_d values with previous solution-phase data provides an *a posteriori* justification for the supposition that $\gamma_M \approx \gamma_D$ under the carefully adjusted conditions of this work.

3.4 Conclusions

This work demonstrates the feasibility of using the direct ESI-MS approach for quantitative measurements of protein-protein binding affinities (K_d values) in solution. In contrast to traditional methods for studying biomolecular interactions, ESI-MS relies on the detection of biomolecular assemblies in the gas phase. Special care must be taken, therefore, to ensure that the data obtained are not affected by artifacts related to the ionization or detection processes. In contrast to typical protein-small molecule complexes, free and bound forms of protein-protein assemblies cover a much wider *m/z* range in the spectra. This aspect leads to unique challenges. A key aspect that has received little attention in previous studies are the parameter settings of RF-only quadrupoles in the ion path. These elements are present in Q-TOF instruments, as well as in other types of mass analyzers. Only carefully adjusted conditions provide a relatively uniform transmission

profile. When studying protein-protein assemblies, practitioners may by tempted to employ quadrupole parameters that maximize the relative abundance of bound species. It can be very misleading to employ data acquired under such skewed conditions for binding affinity measurements (**Figure 3-1**). In addition, we caution that other ion optics such as hexapoles and stacked lenses may also be associated with *m/z*-dependent discrimination effects [58]. Some of these factors are not easily controllable by the user, and they are not as well characterized as the quadrupole behavior. A proper test for the uniformity of the overall transmission profile are comparisons between ESI-MS-derived K_d values and solution-phase measurements for a number of well studied model systems.

Except for its lower sample consumption, the use of nanoESI does not offer any advantages for the two protein systems studied in this work. In fact, the highest abundance of BLG dimers and Hb $(\alpha\beta)_2$ complexes (and the best agreement with previously measured K_d values) was obtained with a regular ESI source operated at 1 μL min^{-1} (**Figure 3-2**).

Mass spectra of protein-protein complexes and their free constituents can be subjected to a number of simple controls. In cases where formation of a protein complex is associated with major conformational changes one would expect the ionization efficiencies of free and bound forms to be significantly different. For complexes with known X-ray structures, a ln-ln plot of the type depicted in **Figure 3-3** is a useful tool for determining whether or not such conformational factors are prevalent. Comparison of the ESI charge states for free and bound species gives an indication whether the measured spectra are affected by CID artifacts. Flow-rate-dependent measurements can reveal the extent to which nonspecific aggregates are formed. Another important test for the fidelity

of the direct ESI-MS approach are binding affinity measurements conducted at various protein concentrations, all of which should provide very similar values of K_d. In future work it will be interesting to extend the measurements of this study to a range of additional protein complexes. We are hopeful that the direct ESI-MS approach will become well established for determining protein-protein binding affinities, similar to the case of protein-small molecule interactions where this strategy is already fairly commonplace.

3.5 Reference

1.   Kaltashov, I. A.; Mohimen, A. Estimates of Protein Surface Area in Solution by Electrospray Ionization Mass Spectrometry. *Anal. Chem.* **2005,** *77*, 5370-5379.

2.   Robinson, C. V.; Sali, A.; Baumeister, W. The molecular sociology of the cell. *Nature* **2007,** *450*, 973-982.

3.   Kuprowski, M. C.; Konermann, L. Signal Response of Co-Existing Protein Conformers in Electrospray Mass Spectrometry. *Anal. Chem.* **2007,** *79*, 2499-2506.

4.   van Holde, K.; Johnson, W.; Shing Ho, P. *Principles of Physical Biochemistry*second ed.; Pearson Prentice Hall: Upper Saddle River, NJ, 2006.

5.   Hajduk, P.; Meadows, R. P.; Fesik, S. W. NMR-based screening in drug discovery. *Q. Rev. Biophys.* **1999,** *32*, 211-240.

6.   McDonnell, J. M. Surface plasmon resonance: towards an understanding of the mechanisms of biological molecular recognition. *Curr. Opin. Chem. Biol.* **2001,** *5*, 572-577.

7.   Zhu, H.; Bilgin, M.; Bangham, R.; Hall, D.; Casamayor, A.; Bertone, P.; Lan, N.; Jansen, R.; Bidlingmaier, S.; Houfek, T.; Mitchell, T.; Miller, P.; Dean, R. A.; Gerstein, M.; Snyder, M. Global Analysis of Protein Activities Using Proteome Chips. *Science* **2001,** *293*, 2101.

8.   Titz, B.; Schlesner, M.; Uetz, P. What do we learn from high-throughput protein interaction data? *Exp. Rev. Proteomics* **2004,** *1*, 111-121.

9.   Cole, J. L.; Hansen, J. C. Analytical ultracentrifugation as a contemporary biomolecular research tool. *J. Biomol. Tech.* **1999,** *10*, 163-176.

10.   Clark, S. M.; Konermann, L. Determination of Ligand-Protein Dissociation Constants by Electrospray Mass Spectrometry-Based Diffusion Measurements. *Anal. Chem.* **2004,** *76*, 7077-7083.

11.   Xu, Y.; Schmitt, S.; Tang, L.; Jakob, U.; Fitzgerald, M. C. Thermodynamic Analysis of a Molecular Chaperone Binding to Unfolded Protein Substrates. *Biochemistry* **2010,** *49*, 1346-1353.

12.   Zhu, M. M.; Rempel, D. L.; Du, Z.; Gross, M. L. Quantification of Protein-Ligand Interactions by Mass Spectrometry, Titration, and H/D Exchange: PLIMSTEX. *J. Am. Chem. Soc.* **2003,** *125*, 5252-5253.

13.   Marcsisin, S. R.; Engen, J. R. Hydrogen exchange mass spectrometry: what is it and what can it tell us? *Anal. Bioanal. Chem.* **2010,** *397*, 967-972.

14.   Xu, G.; Chance, M. R. Hydroxyl Radical-Mediated Modification of Proteins as Probes for Structural Proteomics. *Chem. Rev.* **2007,** *107*, 3514-3543.

15.   Mendoza, V. L.; Vachet, R. W. Probing Protein Structure by Amino Acid-specific Covalent Labeling and Mass Spectrometry. *Mass Spectrom. Rev.* **2009,** *28*, 785-815.

16.   Rigaut, G.; Shevchenko, A.; Rutz, B.; Wilm, M.; Mann, M.; Seraphin, B. A generic protein purification method for protein complex characterization and proteome exploration. *Nat. Biotech.* **1999,** *17*, 1030-1032.

17.   Schriemer, D. C. Biosensor Alternative: Frontal Affinity Chromatography. *Anal. Chem.* **2004,** *76*, 441A-448A.

18.   Loo, J. A. Studying noncovalent protein complexes by electrospray ionization mass spectrometry. *Mass Spectrom. Rev.* **1997,** *16*, 1-23.

19.   Benesch, J. L. P.; Ruotolo, B. T.; Simmons, D. A.; Robinson, C. V. Protein Complexes in the Gas Phase: Technology for Structural Genomics and Proteomics. *Chem. Rev.* **2007,** *107*, 3544-3567.

20.   Heck, A. J. R.; Van den Heuvel, R. H. H. Investigation of intact protein complexes by mass spectrometry. *Mass Spectrom. Rev.* **2004,** *23*, 368-389.

21.   Daniel, J. M.; Friess, S. D.; Rajagopalan, S.; Wendt, S.; Zenobi, R. Quantitative determination of noncovalent binding interactions using soft ionization mass spectrometry. *Int. J. Mass Spectrom.* **2002,** *216*, 1-27.

22.   Ashcroft, A. E. Mass Spectrometry and the Amyloid Problem - How Far Can We Go in the Gas Phase? *J. Am. Soc. Mass Spectrom.* **2010,** *21*, 1087-1096.

23.   Ganem, B.; Li, Y.-T.; Henion, J. D. Observation of Noncovalent Enzyme-Substrate and Enzyme-Product Complexes by Ion-Spray Mass Spectrometry. *J. Am. Chem. Soc.* **1991,** *113*, 7818-7819.

24.   Katta, V.; Chait, B. T. Observation of the Heme-Globin Complex in Native Myoglobin by Electrospray-Ionisation Mass Spectrometry. *J. Am. Chem. Soc.* **1991,** *113*, 8534-8535.

25.   Frycak, P.; Schug, K. A. On-Line Dynamic Titration: Determination of Dissociation Constants for Noncovalent Complexes Using Gaussian Concentration Profiles by Electrospray Ionization Mass Spectrometry. *Anal. Chem.* **2007,** *79*, 5407-5413.

26.   Rostom, A. A.; Fucini, P.; Benjamin, D. R.; Juenemann, R.; Nierhaus, K. H.; Hartl, F. U.; Dobson, C. M.; Robinson, C. V. Detection and selective dissociation

of intact ribosomes in a mass spectrometer. *Proc. Natl. Acad. Sci. U.S.A.* **2000,** *97*, 5185-5190.

27.   Bothner, B.; Siuzdak, G. Electrospray Ionization of a Whole Virus: Analyzing Mass, Structure, and Viability. *ChemBioChem* **2004,** *5*, 258-260.

28.   Jecklin, M. C.; Touboul, D.; Bovet, C.; Wortmann, A.; Zenobi, R. Which Electrospray-Based Ionization Method Best Reflects Protein-Ligand Interactions Found in Solution? A Comparison of ESI, nanoESI, and ESSI for the Determination of Dissociation Constants with Mass Spectrometry. *J. Am. Soc. Mass Spectrom.* **2008,** *19*, 332-343.

29.   Wang, W.; Kitova, E. N.; Klassen, J. S. Influence of solution and gas phase processes on protein-carbohydrate binding affinities determined by nanoelectrospray Fourier transform ion cyclotron resonance mass spectrometry. *Anal. Chem.* **2003,** *75*, 4945-4955.

30.   Jørgensen, T. J. D.; Roepstorff, P.; Heck, A. J. R. Direct Determination of Solution Binding Constants for Noncovalent Complexes between Bacterial Cell Wall Peptide Analogues and Vancomycin Group Antibiotics by Electrospray Ionization Mass Spectrometry. *Anal. Chem.* **1998,** *70*, 4427-4432.

31.   Pan, J.; Xu, K.; Yang, X.; Choy, W. Y.; Konermann, L. Solution-phase chelators for suppressing nonspecific protein-metal interactions in electrospray mass spectrometry. *Anal. Chem.* **2009,** *81*, 5008-5015.

32.   Gabelica, V.; Rosu, F.; De Pauw, E. A Simple Method to Determine Electrospray Response Factors of Noncovalent Complexes. *Anal. Chem.* **2009,** *81*, 6708-6715.

33.   Wilcox, J. M.; Rempel, D. L.; Gross, M. L. Method of Measuring Oligonucleotide-Metal Affinities: Interactions of the Thrombin Binding Aptamer with K+ and Sr2+. *Anal. Chem.* **2008,** *80*, 2365–2371.

34.   Sun, J.; Kitova, E. N.; Sun, N.; Klassen, J. S. Method for Identifying Nonspecific Protein-Protein Interactions in Nanoelectrospray Ionization Mass Spectrometry. *Anal. Chem.* **2007,** *79*, 8301-8311.

35.   Chalcraft, K. R.; Lee, R.; C., M.; Britz-McKibbin, P. Virtual Quantification of Metabolites by Capillary Electrophoresis-Electrospray Ionization-Mass Spectrometry: Predicting Ionization Efficiency Without Chemical Standards. *Anal. Chem.* **2009,** *81*, 2506-2515.

36.   Oss, M.; Kruve, A.; Herodes, K.; Leito, I. Electrospray Ionization Efficiency Scale of Organic Compounds. *Anal. Chem.* **2010,** *82*, 2865-2872.

37.   Peschke, M.; Verkerk, U. H.; Kebarle, P. Features of the ESI Mechanism that Affect the Observation of Multiply Charged Noncovalent Protein Complexes and the Determination of the Association Constant by the Titration Method. *J. Am. Soc. Mass Spectrom.* **2004,** *15*, 1424-1434.

38.   Chernushevich, I. V.; Thomson, B. A. Collisional cooling of large ions in electrospray mass spectrometry. *Anal. Chem.* **2004,** *76*, 1754-1760.

39.   Schmidt, A.; Bahr, U.; M., K. Influence of Pressure in the First Pumping Stage on Analyte Desolvation and Fragmentation in Nano-ESI MS. *Anal. Chem.* **2001,** *73*, 6040-6046.

40.   Cech, N. B.; Enke, C. G. Practical Implication of Some Recent Studies in Electrospray Ionization Fundamentals. *Mass Spectrom. Rev.* **2001,** *20*, 362-387.

41.   Van Berkel, G. J.; Zhou, F.; Aronson, J. T. Changes in Bulk solution pH Caused by the Inherent Controlled-Current Electrolytic Process of an Electrospray Ion Source. *Int. J. Mass Spectrom. Ion Proc.* **1997,** *162*, 55-67.

42. Konermann, L.; Silva, E. A.; Sogbein, O. F. Electrochemically Induced pH
     Changes Resulting in Protein Unfolding in the Ion Source of an Electrospray Mass
     Spectrometer. *Anal. Chem.* **2001,** *73*, 4836-4844.

43. Wang, H.; Agnes, G. R. Kinetically Labile Equilibrium Shifts Induced by the
     Electrospray Process. *Anal. Chem.* **1999,** *71*, 4166-4172.

44. Wortmann, A.; Kistler-Momotova, A.; Zenobi, R.; Heine, M. C.; Wilhelm, O.;
     Pratsinis, S. E. Shrinking Droplets in Electrospray Ionization and Their Influence
     on Chemical Equilibria. *J. Am. Soc. Mass Spectrom.* **2007,** *18*, 385-393.

45. Hossain, B. M.; Konermann, L. Pulsed Hydrogen/Deuterium Exchange MS/MS
     for Studying the Relationship between Noncovalent Protein Complexes in
     Solution and in the Gas Phase after Electrospray Ionization. *Anal. Chem.* **2006,**
     78, 1613-1619.

46. Loo, J. A. Electrospray Ionization Mass Spectrometry: a Technology for Studying
     Noncovalent Macromolecular Complexes. *Int. J. Mass Spectrom.* **2000,** *200*, 175-
     186.

47. Bovet, C.; Wortmann, A.; Eiler, S.; Granger, F.; Ruff, M.; Gerrits, B.; Moras, D.;
     Zenobi, R. Estrogen receptor-ligand complexes measured by chip-based
     nanoelectrospray mass spectrometry: An approach for the screening of endocrine
     disruptors. *Protein Sci.* **2007,** *16*, 938-946.

48. Bich, C.; Baer, S.; Jecklin, M. C.; Zenobi, R. Probing the Hydrophobic Effect of
     Noncovalent Complexes by Mass Spectrometry. *J. Am. Soc. Mass Spectrom.*
     2010, *21*, 286-289.

49. Tesic, M.; Wicki, J.; Poon, D., K. Y.; Withers, S. G.; Douglas, D. J. Gas Phase
     Noncovalent Protein Complexes that Retain Solution Binding Properties: Binding
     of Xylobiose Inhibitors to the β-1, 4 Exoglucanase from *Cellulomonas fimi*. *J. Am.
     Soc. Mass Spectrom.* **2007,** *18*, 64-73.

50.   Wilm, M.; Mann, M. Analytical Properties of the Nanoelectrospray Ion Source. *Anal. Chem.* **1996,** *68*, 1-8.

51.   Juraschek, R.; Dulcks, T.; Karas, M. Nanoelectrospray - More than just a Minimized-Flow Electrospray Ionization Source. *J. Am. Soc. Mass Spectrom.* **1999,** *10*, 300-308.

52.   Invernizzi, G.; Samalikova, M.; Brocca, S.; Lotti, M.; Molinari, H.; Grandori, R. Comparison of bovine and porcine β-lactoglobulin: a mass spectrometric analysis. *J. Mass Spectrom.* **2006,** *41*, 717-727.

53.   Sakurai, K.; Goto, Y. Manipulating Monomer-Dimer Equilibrium of Bovine β-Lactoglobulin by Amino Acid Substitution. *J. Biol. Chem.* **2002,** *277*, 25735-25740.

54.   Eaton, W. A.; Henry, E. R.; Hofrichter, J.; Mozzarelli, A. Is cooperative oxygen binding by hemoglobin really understood. *Nat. Struct. Biol.* **1999,** *6*, 351 - 358.

55.   Perutz, M. F. Stereochemistry of Cooperative Effects in Haemoglobin. *Nature* **1970,** *228*, 726-739.

56.   Boys, B. L.; Kuprowski, M. C.; Konermann, L. Symmetric Behavior of Hemoglobin α- and β- Subunits during Acid-Induced Denaturation Observed by Electrospray Mass Spectrometry. *Biochemistry* **2007,** *46*, 10675-10684.

57.   Boys, B. L.; Konermann, L. Folding and Assembly of Hemoglobin Monitored by Electrospray Mass Spectrometry Using an On-line Dialysis System. *J. Am. Soc. Mass Spectrom.* **2007,** *18*, 8-16.

58.   Chernushevich, I. V.; Loboda, A. V.; Thomson, B. A. An introduction to quadrupole time-of-flight mass spectrometry. *J. Mass Spectrom.* **2001,** *36*, 849 - 865.

59. Douglas, D. J. Linear Quadrupoles in Mass Spectrometry. *Mass Spec. Rev.* **2009,** *28*, 937-960.

60. March, R.; Todd, J. F. J. *Quadrupole Ion Trap Mass Spectrometry*Second edition ed.; Wiley: New York ; Toronto, 2005.

61. Sobott, F.; Hernandez, H.; McCammon, M. G.; Tito, M. A.; Robinson, C. V. A Tandem Mass Spectrometer for Improved Transmission and Analysis of Large Macromolecular Assemblies. *Anal. Chem.* **2002,** *74*, 1402-1407.

62. Thomas, J. O.; Edelstein, S. J. Observation of the Dissociation of Unliganded Hemoglobin. *J. Biol. Chem.* **1972,** *247*, 7870-7874.

63. Antonini, E.; Brunori, M. *Hemoglobin and Myoglobin in Their Reactions With Ligands*; North-Holland Publishing Company: Amsterdam, London, 1971; Vol. 21.

64. Gunasekaran, K.; Tsai, C.-J.; Kumar, S.; Zanuy, D.; Nussinov, R. Extended disordered proteins: targeting function with less scaffold. *Trends Biochem. Sci.* **2003,** *28*, 81-85.

65. Dobo, A.; Kaltashov, I. A. Detection of Multiple Protein Conformational Ensembles in Solution via Deconvolution of Charge-State Distributions in ESI MS. *Anal. Chem.* **2001,** *73*, 4763-4773.

66. Grandori, R. Detecting equilibrium cytochrome *c* folding intermediates by electrospray ionization mass spectrometry: Two partially folded forms populate the molten globule state. *Protein Sci.* **2002,** *11*, 453-458.

67. Konermann, L.; Douglas, D. J. Acid-Induced Unfolding of Cytochrome *c* at Different Methanol Concentrations: Electrospray Ionization Mass Spectrometry

Specifically Monitors Changes in the Tertiary Structure. *Biochemistry* **1997,** *36*, 12296-12302.

68.   Borysic, A. J. H.; Radford, S. E.; Ashcroft, A. E. Co-populated Conformational Ensembles of b2-Microglobulin Uncovered Quantitatively by Electrospray Ionization Mass Spectrometry. *J. Biol. Chem.* **2004,** *279*, 27069-27077.

69.   Jurchen, J. C.; Williams, E. R. Origin of Asymmetric Charge Partitioning in the Dissociation of Gas-Phase Protein Homodimers. *J. Am. Chem. Soc.* **2003,** *125*, 2817-2826.

70.   Pan, P.; McLuckey, S. A. Electrospray Ionization of Protein Mixtures at Low pH. *Anal. Chem.* **2003,** *75*, 1491-1499.

71.   Loscertales, I. G.; de la Mora, J. F. Experiments on the kinetics of field evaporation of small ions from droplets. *J. Chem. Phys.* **1995,** *103*, 5041-5060.

72.   Schmidt, A.; Karas, M.; Dülcks, T. Effect of Different Solution Flow Rates on Analyte Signals in Nano-ESI MS, or: When Does ESI Turn into Nano-ESI. *J. Am. Soc. Mass Spectrom.* **2003,** *14*, 492-500.

73.   Powell, K. D.; Ghaemmaghami, S.; Wang, M. Z.; Ma, L.; Oas, T. G.; Fitzgerald, M. C. A General Mass Spectrometry-Based Assay for the Quantitation of Protein-Ligand Binding Interactions in Solution. *J. Am. Chem. Soc.* **2002,** *124*, 10256-10257.

74.   Riggs, A. F. Self-association, cooperativity and supercooperativity of oxygen binding by hemoglobins. *J. Exper. Biol.* **1998,** *201*, 1073-1084.

Chapter 4 –Assembly of Hemoglobin from Denatured Monomeric Subunits: Effects of Heme Ligation and Off-Pathway Intermediates Studied by Electrospray Mass Spectrometry

4.1 Introduction

The mechanisms by which small monomeric proteins fold to their native conformations have been explored in great detail [1]. Funneled energy landscapes can account for the fact that folding occurs rapidly and with high-yield [2], although misfolding and aggregation can also take place [3,4]. While most folding studies have dealt with the behavior of isolated proteins *in vitro*, there are also efforts to decipher cotranslational events [5] and chaperone involvement [6] that can be important *in vivo*.

While monomeric proteins have been quite amenable to mechanistic folding investigations, the situation is more difficult for multi-subunit systems. Protein complexes play a major role in numerous cellular processes [7,8]. Folding of these noncovalent assemblies requires the formation of intramolecular contacts, as well as intermolecular binding. In addition, many protein complexes incorporate metal ions or other cofactors [9-13]. Only relatively few time-resolved studies on the folding/assembly mechanisms of protein complexes have appeared in the literature [8,11,14]. Experimental investigations in this area are complicated by the fact that commonly used spectroscopic probes cannot distinguish between intra- and intermolecular events [15]. Also, the yield of folding/binding reactions tends to be low due to off-pathway aggregation [3,16]. On the other hand, similar aggregation phenomena can also occur *in vivo*. Thus, the observation

of these off-pathway events *in vitro* can provide valuable insights into the kinetic competition between aberrant aggregation and proper assembly of protein complexes [3,12].

Hemoglobin (Hb) acts as oxygen transporter in red blood cells [17-19]. The native tetrameric Hb structure comprises two α and two β subunits. The eight helices in β-globin are termed A – H, whereas helix D is missing in the slightly shorter α subunit. The Hb quaternary structure represents a $(\alpha^h\beta^h)_2$ "dimer of dimers", where the superscript "h" indicates the presence of a heme in each subunit. The tetramer is stabilized by hydrophobic contacts, hydrogen bonds, van der Waals interactions, and salt bridges. The α1β1 (and α2β2) interfaces are linked by close contacts, whereas α1β2 (and α2β1) binding is less extensive [20]. The heme is sandwiched between helices E and F. Helix F provides the proximal (αHis87 and βHis91) ligand for the heme iron. Reversible oxygen binding to ferrous (Fe^{2+}) heme takes place on the distal side. Autooxidation can generate metHb (with ferric iron, Fe^{3+}) that is incapable of O_2 binding [21]. Under physiological conditions $(\alpha^h\beta^h)_2$ is in equilibrium with $\alpha^h\beta^h$. The tetramer-dimer dissociation constant is on the order of 10^{-6} M for oxyHb, whereas much tighter binding with $K_d \approx 10^{-11}$ M is observed in the deoxy state [22,23].

Numerous investigations have focused on the Hb oxygen binding properties [20,24,25], but much less is known about the mechanism of Hb folding and assembly. The protein can be refolded *in vitro* from isolated apo-globin subunits (α^a and β^a) and free heme [26]. Deciphering the mechanism of this process is complicated by the considerable heterogeneity of the reaction mixture which comprises various subunit combinations and

heme binding states [27,28]. Also, the refolding yield tends to be low due to precipitation of α^a and β^a [29]. Some earlier studies employed mixing of prefolded α^h and β^h [30-33]. Assembly under these conditions requires the dissociation of non-native $(\alpha^h)_2$ and $(\beta^h)_4$ complexes into monomeric species. This is followed by formation of $\alpha^h\beta^h$, which then generates $(\alpha^h\beta^h)_2$ [28,33]. Other species such as $\alpha^h\beta^a$ may be involved as on-pathway or off-pathway intermediates [27,31,34,35]. In red blood cell precursors a chaperone termed AHSP (α-hemoglobin stabilizing protein) can sequester α^h and/or α^a, thereby suppressing aggregation, and facilitating binding to β-globin [27,36].

Native electrospray ionization (ESI) mass spectrometry (MS) provides information on protein interactions and conformations. By transferring intact noncovalent assemblies into the gas phase it is possible to determine their subunit stoichiometry via simple mass measurements [37-40]. Binding affinity estimates may be obtained from ion intensity ratios [41-44]. ESI charge state distributions are sensitive to the solution-phase conformation, because folded and unfolded proteins follow different ionization mechanisms [45]. Compact conformers form low charge states, whereas unfolded proteins generate wide distributions of highly protonated ions [46-52]. ESI-MS can therefore simultaneously report on the assembly status and the conformation of proteins [51]. Also, co-existing species can be monitored individually, whereas traditional spectroscopic tools only provide population-averaged data [53]. By analyzing a reaction mixture at various time points it is possible to uncover the temporal sequence of events during the assembly of noncovalent protein complexes [54-58].

A number of studies have explored Hb subunit interactions by ESI-MS [35,42,57,59-63], but a comprehensive view of the Hb folding/assembly mechanism has not been obtained yet. The implications of recent *un*folding studies for the Hb *re*folding mechanism are not clear [35,63], because denaturation was triggered by acidification which induces irreversible heme precipitation [64]. Denaturants such as urea are problematic because they are incompatible with on-line ESI-MS. Our group monitored the refolding of metHb by ESI-MS, starting from monomeric apo-subunits after acetonitrile-induced denaturation at pH 10 [57]. In that work it was possible to return the protein to a folded tetrameric state via solvent exchange to an aqueous environment at pH 8. A convoluted assembly mechanism involving a number of intermediates was observed under those conditions [57]. Unfortunately, the refolding experiments of our earlier work were conducted using Hb samples that had been obtained commercially as lyophilized powder [64]. Subsequent investigations revealed that such commercial Hb samples exhibit high levels of oxidative modifications, a factor that significantly affects the protein behavior [60,61,63].

In the current work we investigate the Hb assembly mechanism, using freshly prepared Hb that is virtually free of oxidative modifications. Surprisingly, it is found that the refolding procedure developed earlier provides poor results for these higher quality samples [57], necessitating the development of an optimized experimental approach. By conducting comparative ESI-MS analyses of Hb assembly under "low-yield" "high-yield" conditions it is possible to uncover the mechanistic basis of the different outcomes.

4.2 Experimental

4.2.1 Materials

Bovine oxyHb was purified as described,[63] from fresh cow blood that had been collected over 0.3% (w/v) sodium citrate. Briefly, plasma and buffy coat were removed by 30 minutes of centrifugation at 5,500 g. The red blood cell pellet was washed with 0.9% (w/v) NaCl and re-centrifuged four times. Red blood cells were then ruptured osmotically by exposure to distilled water with 10% (v/v) toluene. Stromal impurities were extracted into the organic layer. The resulting hemolysate was centrifuged at 15,000 g for 30 minutes, and dialyzed against 10 mM ammonium acetate with multiple buffer exchanges on ice. Stock solutions obtained in this way were flash frozen in liquid nitrogen and stored at -80 °C. Mass analyses reveal that oxidative damage of the Hb samples obtained in this way is negligible, consistent with earlier results [63]. Cyano-metHb was prepared by first oxidizing oxyHb to metHb via addition of 1.2-fold molar excess (on a heme basis) potassium ferricyanide for 5 minutes at room temperature. CN^- binding was achieved by addition of 1.2 fold molar excess of KCN. The resulting cyano-metHb was filtered through a 3×25 cm G-25 Sephadex column with 10 mM ammonium acetate in water (pH 7) as mobile phase. The Hb subunit masses were found to agree with those expected based on the amino acid sequence (15,053 Da for α^a and 15,954 Da for β^a) to within $\pm$ 1 Da [21]. Heme accounts for an additional 616 Da. As reported previously [63], the extent of oxidative damage for protein samples obtained in this way is negligible.

4.2.2 Dialysis-Mediated Hb Refolding

Denaturation of oxyHb was achieved by addition of ammonia to pH 10, followed by addition of 40% acetonitrile (v/v), for a final Hb concentration of 60 μM (based on protein tetramers). Some experiments were conducted by adding 2 mM KCN to the Hb solution, prior to exposure to acetonitrile and basic pH. After seven minutes 1 mL samples of denatured protein was transferred into a slide-A-Lyzer dialysis cassette (Pierce, Rockford, IL) with a 7 kDa cutoff, followed by dialysis against 1 L aqueous ammonium acetate solution at pH 8. The solvent exchange goes to completion within ~40 minutes [57]. Dialysis experiments were conducted at 22 °C or at 4 °C. Aliquots were taken at various time points during dialysis for ESI-MS and for optical measurements. Control experiments on native Hb revealed a slight (27%) decrease in protein concentration after 18 h of dialysis. Part of this effect is caused by solution influx into the dialysis chamber which leads to a 10% volume increase. The remainder (17%) is attributed to protein loss through the membrane.

4.2.3 ESI Mass Spectrometry

Hb samples were analyzed using a Q-TOF Ultima API instrument (Waters, Manchester, UK) equipped with a Z-spray source. Gentle ESI conditions were used that had previously been shown to preserve $(\alpha^h\beta^h)_2$ complexes[42] (capillary voltage 3 kV, cone voltage 60 V, RF lens 1 voltage 35 V, source temperature 80 °C, and desolvation temperature 40 °C). Cone and desolvation gas flow rates were 150 L h^{-1} and 500 L h^{-1}, respectively. The quadrupole profile was adjusted to ensure uniform transmission across

the *m/z* range of interest [42]. The protein solution was infused into the ESI source at 5 µL min^{-1} using a syringe pump. Each spectrum shown below represents the sum of around 100 scans, with an acquisition time of 2 s per scan. All ESI-MS data were recorded at a nominal tetramer concentration of 60 µM, i.e., aliquots removed from the dialysis cassette were infused directly without further processing or dilution.

4.2.4 UV-Vis Spectroscopy

Absorption spectra were recorded on a Varian Cary 100 Spectrophotometer (Palo Alto, CA). Data were acquired in 1 cm cuvettes, and all samples were diluted to a nominal tetramer concentration of 2 µM. Protein concentrations were determined using $\varepsilon_{541} = 13.8$ mM^{-1} cm^{-1} for oxyHb, $\varepsilon_{500} = 10.0$ mM^{-1} cm^{-1} for metHb, and $\varepsilon_{540} = 11.5$ mM^{-1} cm^{-1} for cyano-metHb [17,65]. These numbers are per heme equivalent; for determining the absorption coefficient of $(\alpha^h\beta^h)_2$ each value has to be multiplied by four.

4.3 Results and Discussion

4.3.1 Hb Unfolding and Refolding Monitored by Optical Spectroscopy

Prior to conducting ESI-MS investigations it is instructive to characterize the protein behavior by UV-Vis absorption spectroscopy. The heme absorption spectrum is sensitive to the porphyrin environment, iron ligation, and iron oxidation state. UV-Vis

measurements have been the primary tool for probing Hb structural changes for many years [17].

Hb obtained using the isolation procedure outlined above displays a dominant Soret peak at 415 nm, along with maxima at 541 nm and 577 nm. The presence of these bands is consistent with oxyHb, where all ferrous heme groups are oxygenated (**Figure 4-1A**, black) [17,63]. Hb denaturation was conducted by exposure to 40% acetonitrile at pH 10 [57]. The resulting spectrum has a greatly reduced Soret absorption with a maximum at 400 nm, reflecting major changes in heme environment. At the same time, spectral alterations in the 500-600 nm range indicate the occurrence of heme $Fe^{2+} \rightarrow Fe^{3+}$ autooxidation (**Figure 4-1A**, red) [17,21].

Hb refolding was triggered by dialysis-mediated acetonitrile removal, in combination with a pH decrease from 10 to 8 [57]. Initial experiments were conducted at 22 °C. The UV-Vis spectrum of Hb recorded 18 h after initiation of refolding displays a Soret maximum at 406 nm (**Figure 4-1B**, green), consistent with metHb and distal ligation by H_2O or OH^- [17]. From the known metHb absorption coefficient (see Methods) the refolding yield under these conditions can be determined to be ~48%. Partial aggregation and/or precipitation is the most likely culprit responsible for this low yield. Interestingly, the same procedure results in a yield of almost 100% for commercially obtained metHb [57]. Standard commercial samples are characterized by high oxidation levels at methionine and other residues, particularly in β-globin [63]. These oxidation events
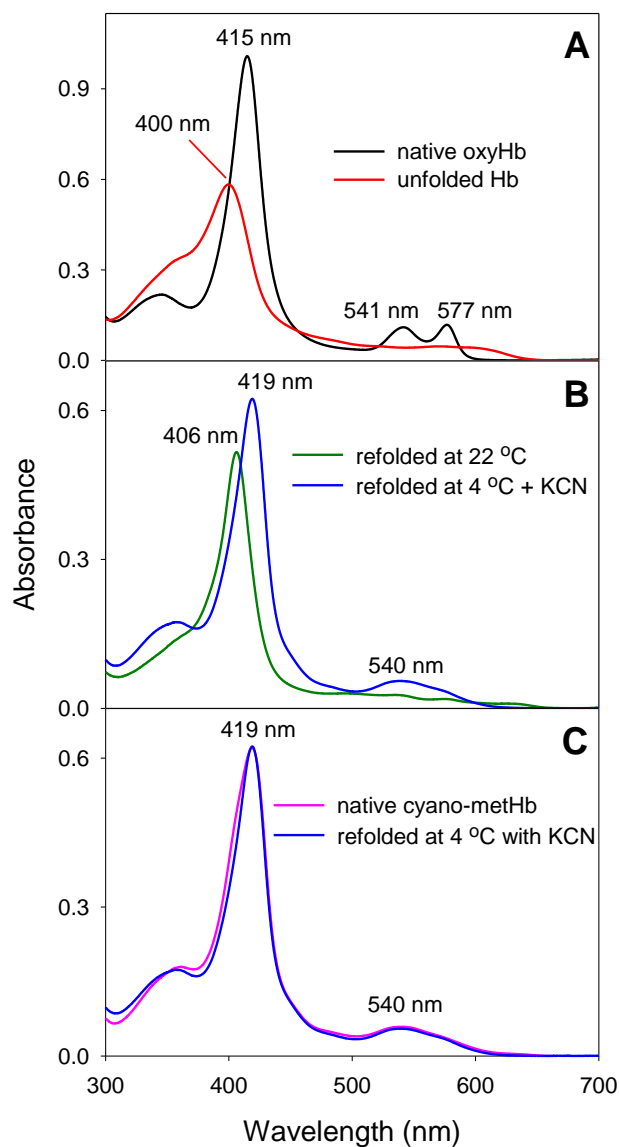
Figure 4-1. UV-Vis absorption spectra of bovine Hb under different conditions. (A) Freshly isolated oxyHb at pH 7 (black), and denatured protein in 40% acetonitrile at pH 10. (B) Hb after refolding at room temperature (green), and after refolding at 4 °C with 2 mM KCN (blue). (C) Comparison of native cyano-metHb (pink) with protein that had been refolded at 4 °C with 2 mM KCN (blue).

decrease the overall protein hydrophobicity [66], and reduce the aggregation propensity. **Figure 4-1**B reveals that the procedure of ref.[57] performs poorly for the freshly prepared Hb used here, which is virtually free of oxidative modifications.

To improve the refolding conditions the temperature was lowered to 4 °C, resulting in an increased yield of ~70% (data not shown). A further improvement to ~85% was achieved by supplementing the Hb solution with 2 mM KCN prior to denaturation. The UV-Vis spectrum after refolding at 4 °C with KCN has a Soret maximum at 419 nm (**Figure 4-1**B, blue), corresponding to cyano-metHb where the distal coordination site is occupied by CN$^-$ [17]. The absorption properties of KCN-refolded samples are virtually indistinguishable from those of freshly prepared cyano-metHb (**Figure 4-1**C). Control experiments conducted with KCl revealed that the enhanced refolding yield is not simply an ionic strength effect (data not shown).

Attempts to increase the refolding yield even further via addition of free heme were not successful for any of the conditions employed here (data not shown). This behavior indicates that the loss of free heme through the dialysis membrane is not a limiting factor, pointing to weak residual heme-protein interactions in the denatured state as suggested previously [67].

In summary, the optical data of **Figure 4-1** reveal that the Hb refolding behavior strongly depends on the conditions used. For investigating the mechanistic basis of the observed outcomes we will focus on (*i*) *low-yield conditions* (22 °C, no KCN); and (*ii*) *high-yield conditions* (4 °C, with KCN). Heme is moderately soluble in aqueous solution at pH 8, forming dimers and larger porphyrin aggregates [64]. In contrast, free heme in

the presence of KCN gets converted to hemin dicyanide ($h(CN)_2$) that has a much higher solubility and does not self-associate [68,69].

4.3.2 ESI-MS Characterization of Refolded Hb

The UV-Vis data of **Figure 4-1** only reflect the local heme environment. Quaternary structural information can be obtained by ESI-MS. For reference, **Figure 4-2**A shows a typical mass spectrum of native oxyHb. Monomeric subunits are virtually absent. The data are dominated by the canonical $(\alpha^h\beta^h)_2$ assembly, with some contributions from $\alpha^h\beta^h$. For the instrument settings used here the ion intensity ratio approximately matches the tetramer:dimer ratio in solution [42].

Quite a different spectrum is obtained after refolding under low-yield conditions (**Figure 4-2**A). The relative intensities of $(\alpha^h\beta^h)_2$ and $\alpha^h\beta^h$ are significantly reduced. Instead, the data are dominated by α^h in charge states 8+ and 9+, representing folded holo-α-globin monomers [53,57,63]. The mass spectrum also shows α^h ions in higher charge states that originate from solution-phase conformers that are more unfolded. In addition, each of the $\alpha^h\beta^h$ peaks exhibits a $(\alpha^h)_2$ satellite signal.

ESI-MS data obtained after high-yield refolding are dominated by cyanide-bound $(\alpha^h\beta^h)_2$ (**Figure 4-2**C). The tetramer:dimer ratio resembles that of the native protein in **Figure 4-2**A. The contributions of free α^h and $(\alpha^h)_2$ in Figure 4-2C are significantly reduced relative to **Figure 4-2**B.
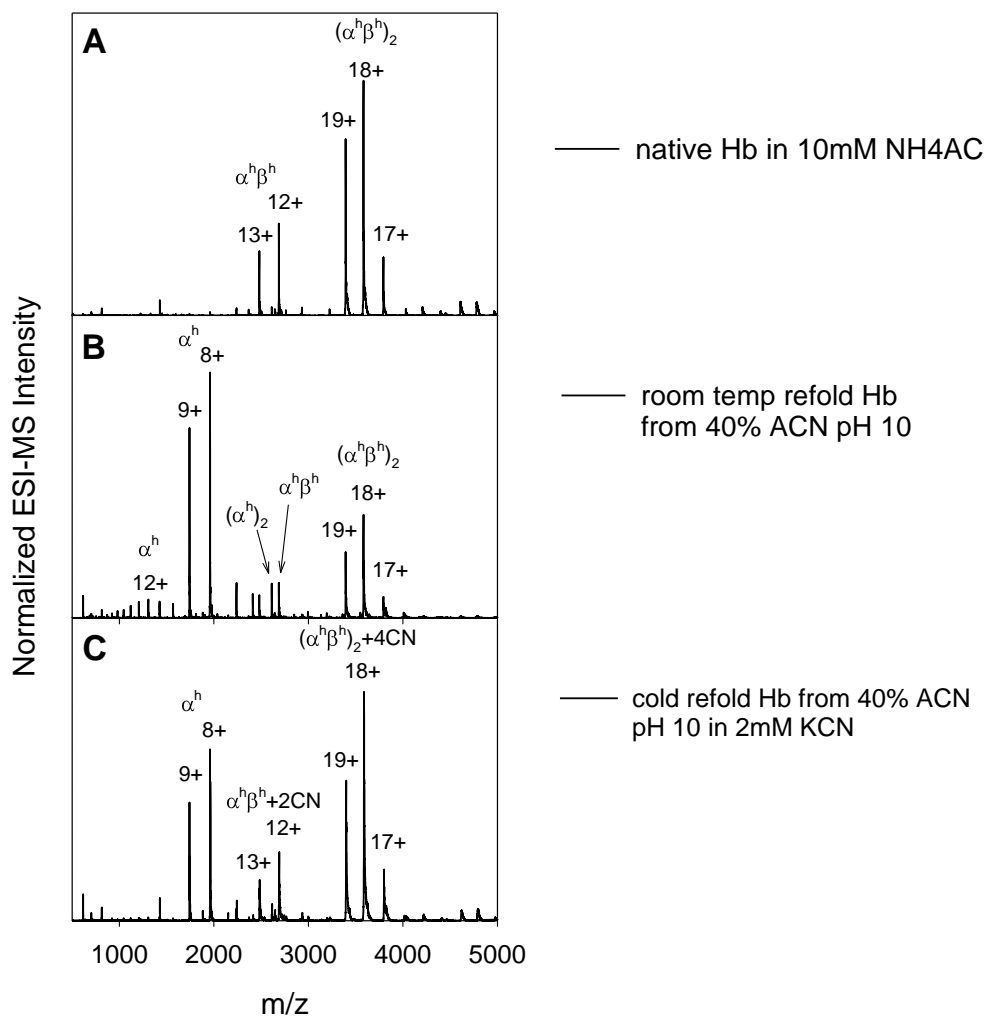
Figure 4-2. ESI mass spectra of (A) native oxyHb; (B) Hb after refolding under "low-yield conditions", (22 °C without KCN); (C) Hb after refolding under and "high-yield conditions" (4 °C with KCN).

Overall, the ESI-MS data of **Figure 4-2** confirm that Hb samples after low-yield refolding are strongly perturbed (**Figure 4-2**B). In contrast, high-yield conditions mainly produce native tetramers (**Figure 4-2**C). Interestingly, the mass spectra of both refolded samples reveal an α/β imbalance, where free α^h and $(\alpha^h)_2$ are not matched by any β-globin species. Considering that the initial samples had an $\alpha{:}\beta$ molar ratio of unity, this imbalance implies the loss of β-globin during refolding due to aggregation and/or precipitation. This β-globin-deficiency is substantially more pronounced under low-yield conditions (**Figure 4-2**B).

4.3.3 Time-Dependent ESI-MS Measurements

The Hb assembly status can be tracked during refolding by ESI-MS analysis of aliquots taken at various time points. Under low-yield conditions the $t = 0$ spectrum shows monomeric α^a, α^h, β^a, and β^h in a wide range of charge states (**Figure 4-3**A). These data confirm that the initial denaturing solvent environment converts native Hb into a structurally heterogeneous ensemble of monomers [57]. The presence of apo and holo ions for both globins reveals that heme-protein interactions are not completely disrupted. The spectrum also shows α-globin that is bound to a heme dimer (α^{2h}) consistent with partial heme dimerization under the conditions used here [64]. Starting at $t = 3$ min α^h ions in low charge states become the most abundant species (**Figure 4-3**B). In addition, there are notable contributions from $\alpha^h\beta^h$ and $(\alpha^h)_2$. After 12 minutes α^a has all but vanished, while $(\alpha^h\beta^h)_2$ starts to appear(**Figure 4-3**C). Figure 3D represents the $t = 18$ h
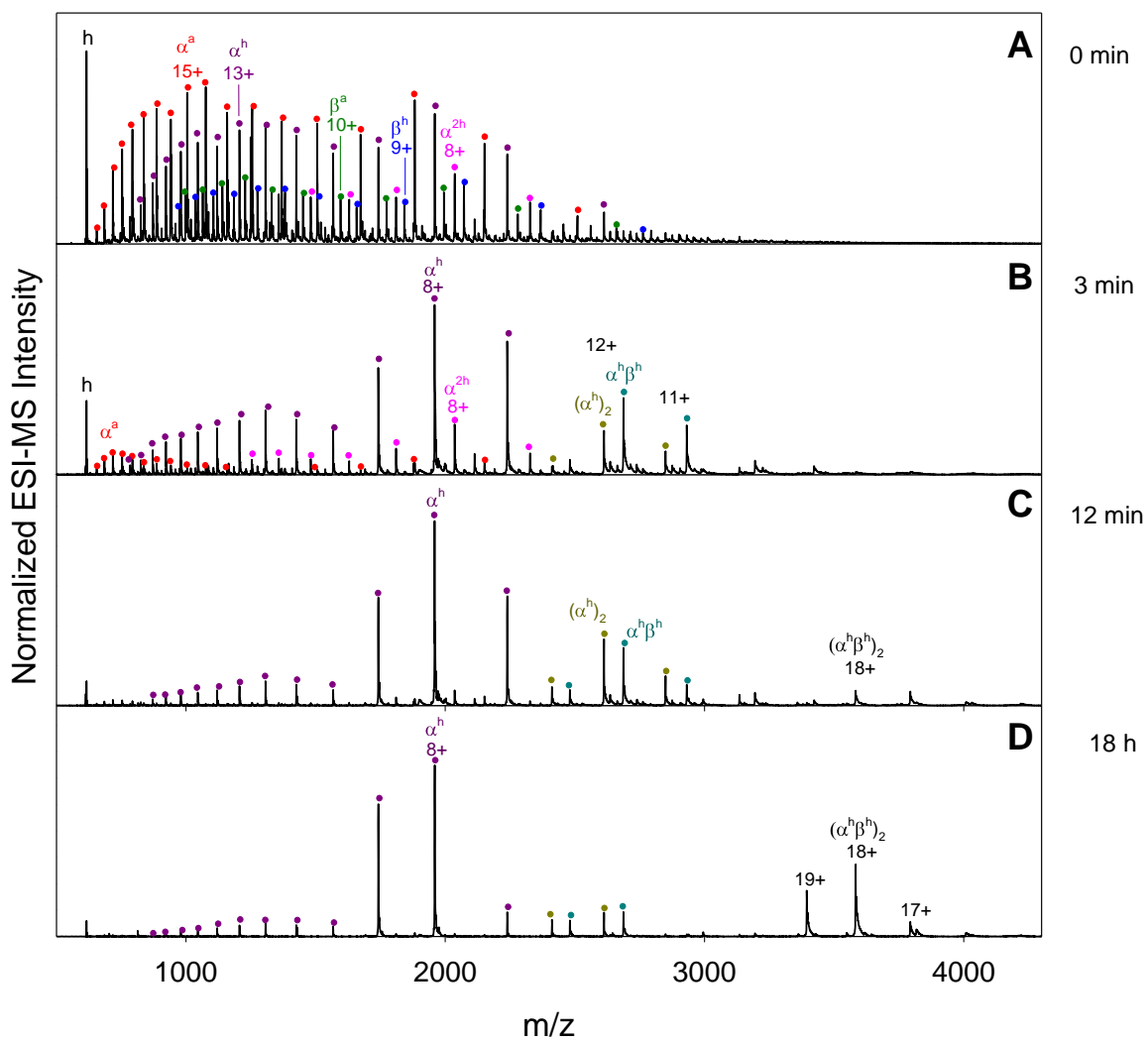
Figure 4-3. ESI-MS spectra taken at different time points during Hb refolding under low-yield conditions. (A) denatured state at $t = 0$ (40% acetonitrile at pH 10), (B) 3 minutes, (C) 12 minutes, (D) 18 hours. The protein ion notation is discussed in the text, free heme is denoted as "h". The intensity in the free heme region of panel A has been rescaled, as indicated.

end point of the reaction. Although the relative contribution of $(\alpha^h\beta^h)_2$ has increased further, the spectrum remains dominated by α^h in low charge states.

The data of **Figure 4-3** provide interesting clues as to why refolding experiments conducted at 22 °C without KCN result in a low $(\alpha^h\beta^h)_2$ yield. Inspection of the mass spectra reveals that all time points show a β-globin deficiency. This imbalance is already apparent at $t = 0$, where the combined total ion count of α^a and α^h is roughly three times higher than that of β^a and β^h (**Figure 4-3**A). These observations point to aggregation-mediated loss of β-globin in the denatured state and early during refolding as the main reason responsible for the limited yield.

ESI-MS data recorded under high-yield conditions provide quite a different picture (**Figure 4-4**). Peak tailing results from heterogeneous adduct formation caused by the presence of KCN in the reaction mixture. These salt effects are well known in ESI-MS [70]. For the spectra of Figure 4 the extent of adduct formation decreases as the salt concentration drops during dialysis. The denatured state in the presence of KCN displays non-native charge state distributions for both globins (**Figure 4-4**A), similar to those seen under low-yield conditions (**Figure 4-3**A). Strikingly, however, **Figure 4-4**A shows comparable ion intensities for α^a and β^a, as well as for α^h and β^h. In other words, the α/β imbalance at $t = 0$ is much less pronounced in **Figure 4-4**A. However, signs of β-globin deficiency start to appear after 3 minutes (**Figure 4-4**B). A close match in α and β intensities as seen at this time point only for highly charged ions. In contrast, the low charge state range displays dominant α^h signals as well as $(\alpha^h)_2$ without matching β-globin contributions. $\alpha^h\beta^h$ dominates the spectrum after 12 minutes (**Figure 4-4**C). After
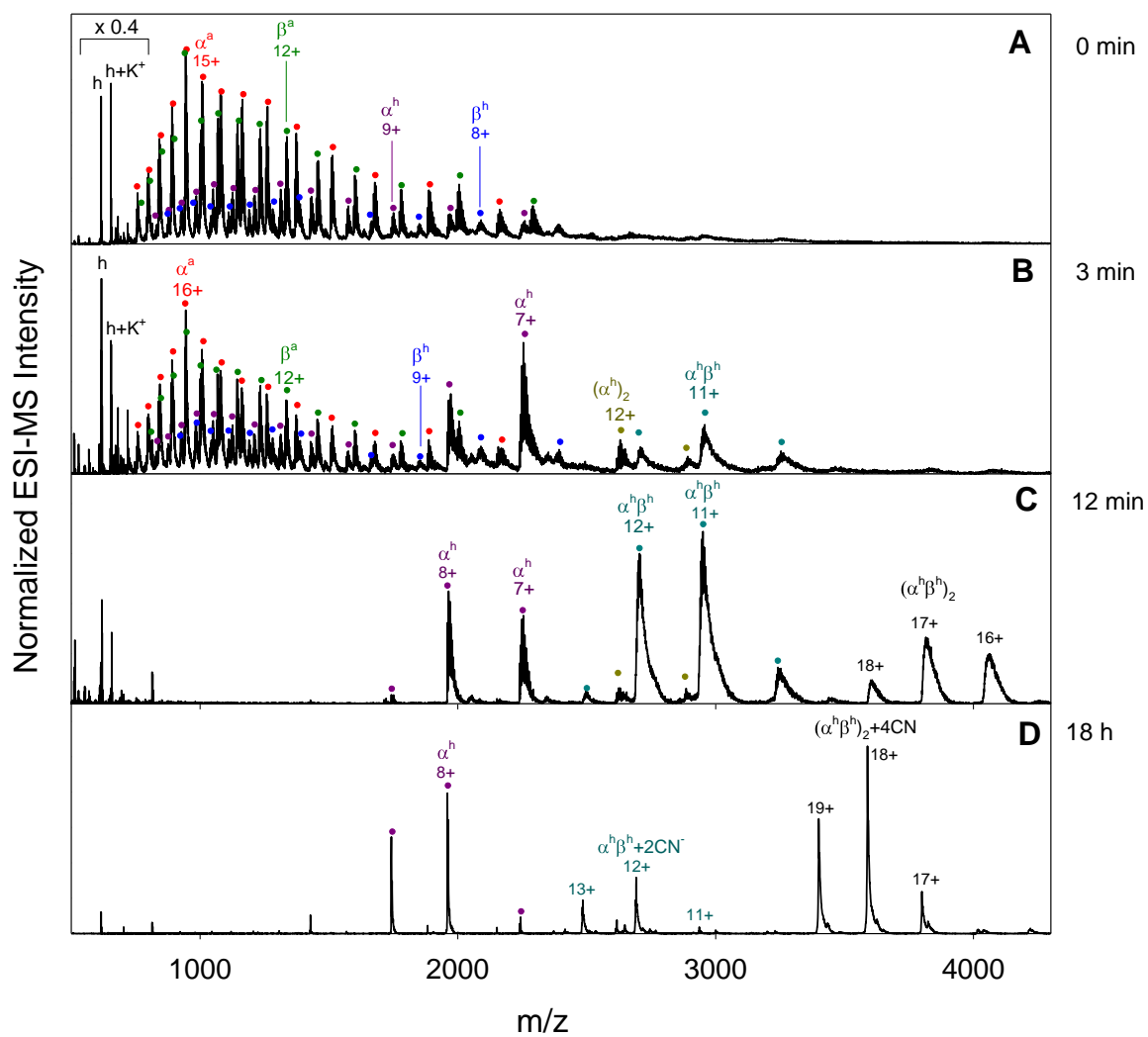
Figure 4-4. Refolding of Hb monitored by ESI-MS under high-yield conditions. (A) $t = 0$, (B) 3 minutes, (C) 12 minutes, (D) 18 hours.

18 h most of the $\alpha^h\beta^h$ has assembled into native Hb tetramers (**Figure 4-4**D). However, a notable contribution of monomeric α^h remains. Thus, a deficiency of freely available β-globin limits the $(\alpha^h\beta^h)_2$ assembly process even under the high-yield conditions of **Figure 4-4**.

4.3.4 Assembly Mechanism Under High-Yield and Low-Yield Conditions

Figure 4-5 allows a direct comparison of the assembly process for the two different scenarios. Temporal ESI-MS intensity profiles were generated from the measured peak areas, integrated over all charge states for any given species.

Under both reaction conditions α^a gets consumed within a few minutes (**Figure 4-5**A, B). Under low yield conditions this rapid α^a disappearance is mirrored by an accumulation of α^h, caused by a shortage of suitable binding partners, i.e., β-globin. This shortage is apparent from the low β^a and β^h intensities in **Figure 4-5**C. α^h accumulation is less pronounced under high-yield conditions (**Figure 4-5**B) due to a more abundant supply of β-globin (**Figure 4-5**D). Low-yield conditions also cause an initial buildup of α-globin that is bound to heme dimers and trimers (α^{2h}, α^{3h}, Figure 5E). Interestingly, these species completely disappear from the reaction mixture at later reaction times. Thus, while α^{2h} and α^{3h} represent off-pathway intermediates, they ultimately equilibrate with other species and get consumed during the reaction. Neither α^{2h} nor α^{3h} becomes significantly populated under high-yield conditions (**Figure 4-5**F). This behavior is in line with the fact that heme retains a soluble monomeric state in the presence of KCN [68,69], whereas partial heme aggregation takes place under low-yield conditions [64]. Heme dimer and trimer binding has previously been observed for myoglobin [71].

Low Yield Conditions — High Yield Conditions

Figure panels A–J: Normalized Signal Intensity versus Time (min), with legends: α^a, α^h (A/B); β^a, β^h (C/D); α^{2h}, α^{3h} (E/F); $(\alpha^h)_2$, $\alpha^h\beta^a$ (G/H); $\alpha^h\beta^h$, $(\alpha^h\beta^h)_2$ (I/J).
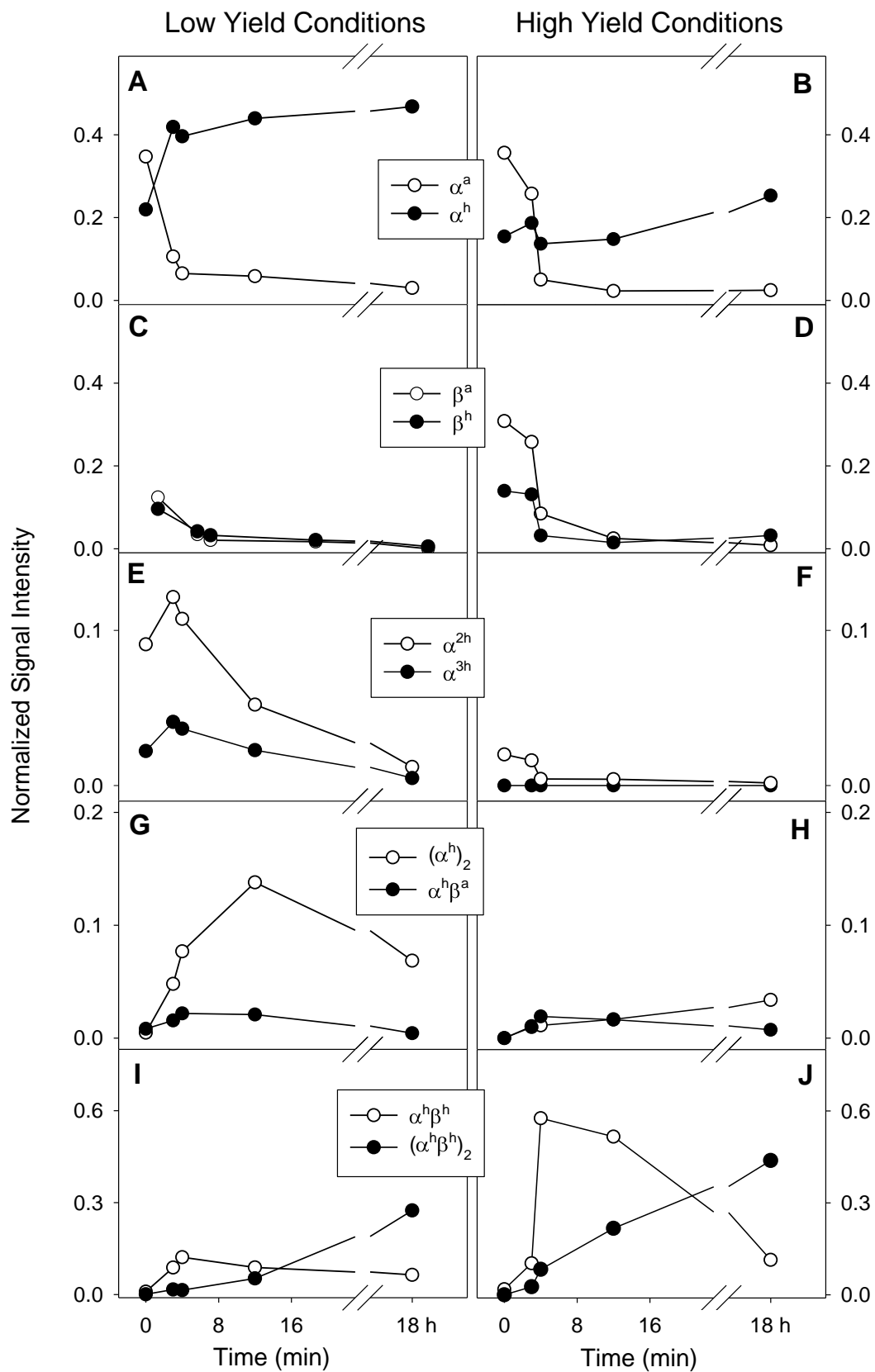
Figure 4-5. Refolding kinetics of Hb monitored by ESI-MS under low-yield conditions (left hand side panels), and under high-yield conditions (panels on the right). These data correspond to signal intensities that were integrated over all charge states for each individual species. Note the differences in intensity axis scaling for some of the panels.

$(\alpha^h)_2$ is another off-pathway intermediate that transiently accumulates under low-yield conditions (**Figure 4-5**G). In earlier work this species has been detected in β-globin-free solutions [28,33]. Thus, it is not surprising that $(\alpha^h)_2$ formation is suppressed in the presence of KCN (**Figure 4-5**H) where a larger supply of β-globin is available.

There is an ongoing discussion in the literature whether the formation of $\alpha^h\beta^h$ proceeds via association of α^h with β^a, followed by heme binding. Such a scenario would involve $\alpha^h\beta^a$ as an *obligatory* intermediate [34,35]. Alternatively, $\alpha^h\beta^h$ could be formed by α^h binding to β^h [57,63]. Our data confirm the presence of $\alpha^h\beta^a$, albeit with very low abundance (< 2%, **Figure 4-5**G, H). Importantly, the abundance of $\alpha^h\beta^h$ reaches much higher values, i.e., 12% (**Figure 4-5**I) and 58% (Figure 5J). The lack of a lag phase between formation of $\alpha^h\beta^h$ and $\alpha^h\beta^a$ suggests that the latter is not an obligatory intermediate under the conditions of this work. Nonetheless, we cannot exclude the possibility that a fraction of $\alpha^h\beta^h$ is indeed formed via heme binding to $\alpha^h\beta^a$, as suggested earlier [34,35]. Thus, our data are compatible with $\alpha^h\beta^a$ as an *optional* intermediate during Hb assembly. However, formation of $\alpha^h\beta^h$ as the result of α^h binding to β^h appears to be the dominant pathway. Regardless of these considerations, formation of $(\alpha^h\beta^h)_2$ from two $\alpha^h\beta^h$ units represents the final step of the Hb assembly mechanism (**Figure 4-5**I, J) [28,33].

We now turn to the question why conducting the reaction at 4 °C with KCN provides a higher refolding yield than 22 °C without KCN. Elevated temperatures generally enhance the Boltzmann population of partially disordered conformers that are prone to aggregation [72]. Thus, it is not unexpected that 4 °C provides conditions that

are more favorable. The second factor responsible for enhancing the refolding yield in our studies is the presence of KCN. As noted above, CN^- leads to the formation of $h(CN)_2$ that is highly resistant to self-association [68,69]. The key problem that limits the refolding yield in our experiments is the aggregation and/or precipitation of β-globin. Our data reveal that KCN helps to maintain β-globin in a soluble state. It is well known that the stability of monomeric apo-globins depends on the presence of heme [27,73]. It is also know that heme is a promiscuous binding partner that can weakly interact with various proteins even under denaturing conditions [67,74,75]. Considering this background information, we propose that residual $h(CN)_2$-protein interactions can stabilize β-globin, thus counteracting the tendency of the protein to precipitate, and promoting its availability as a binding partner during Hb assembly.

4.4 Conclusions

Studies on the folding/assembly of multi-protein complexes are often plagued by the occurrence of nonspecific aggregation phenomena that limit the overall yield [3,16]. The present work offers a unique opportunity to explore the kinetic competition between precipitation and successful assembly of a protein complex. Time-dependent ESI-MS measurements conducted under low-yield and high-yield conditions provide insights into the reasons underlying the different outcomes. Our findings can be summarized using a simple flowchart (**Figure 4-6**). Under "ideal" conditions (depicted in black) semi-denatured α^a and β^a fold into compact α^h and β^h conformers. The holo-monomers bind to form $\alpha^h\beta^h$. Association of heterodimers ultimately results in the native $(\alpha^h\beta^h)_2$ state.
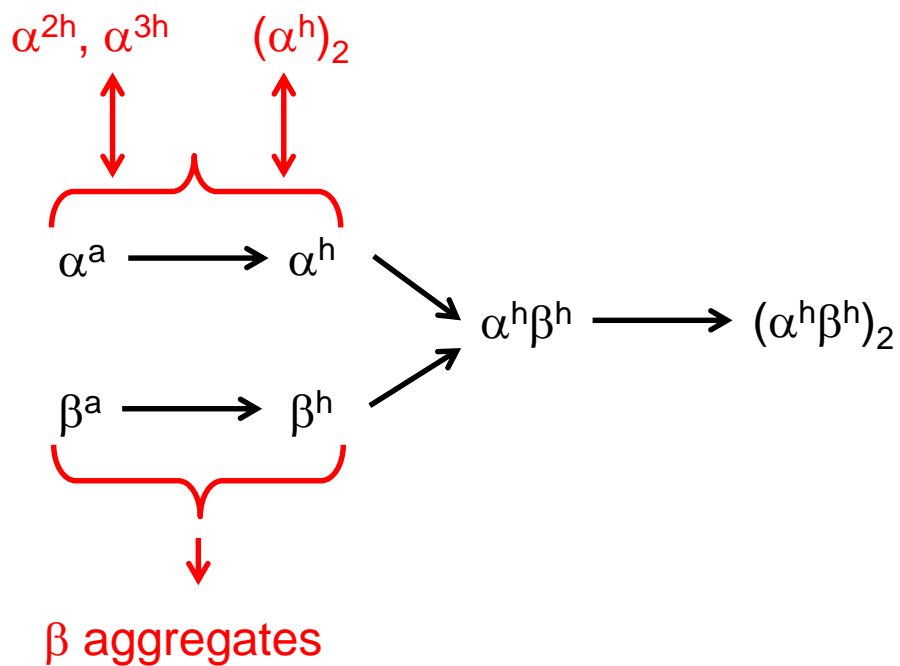
Figure 4-6. Cartoon depiction of the Hb assembly process. Unidirectional steps are represented by single-headed arrows. Double-headed arrows denote reversible events. The main folding/assembly pathway is highlighted in black. Aberrant side reactions are shown in red. Under low-yield conditions these side reactions are more prevalent than under high-yield conditions.

Aberrant side reaction that reduce the refolding yield are highlighted in red. These side reactions are prevalent under low-yield conditions, whereas they are less pronounced under high-yield conditions. Loss of β-globin due to irreversible aggregation represents the main problem. Lowering the temperature helps maintain this subunit in solution. In addition, residual heme-protein interactions appear to be crucial in preventing β-globin aggregation. The preservation of these interactions is promoted by KCN, because cyanide binding counteracts the tendency of heme to self-associate. Related to the findings of this work is the use KCN for high-yield myoglobin reconstitution experiments [68,69]. The formation α-globin off-pathway intermediates depends on the availability of β-globin. Dimerization of α^h is favored if the β-globin supply is limited. In addition, α-globin can bind to small heme aggregates, thus forming α^{2h} and α^{3h}. It is quite possible that sequestering heme in this way further promotes the precipitation-mediated loss of β-globin. In support of this idea, previous work has demonstrated that globin folding can be limited by slow heme dimer dissociation [76].

Overall, this work demonstrates that time-dependent ESI-MS investigations provide detailed insights into the assembly mechanisms of protein complexes, the role of on- and off-pathway intermediates, as well as the kinetic competition between assembly and aggregation. In future studies, the incorporation of ion mobility measurements and on-line hydrogen exchange will be promising avenues to obtain an even deeper understanding of biomolecular self-assembly processes [71,76].

4.5 References

1. Wolynes, P. G.; Eaton, W. A.; Fersht, A. R. Chemical physics of protein folding. *Proc. Natl. Acad. Sci. U. S. A.* **2012,** *109*, 17770-17771.

2. Dill, K. A.; Chan, H. S. From Levinthal to pathways to funnels. *Nat. Struct. Biol.* **1997,** *4*, 10-19.

3. Pastore, A.; Temussi, P. A. The two faces of Janus: functional interactions and protein aggregation. *Curr. Op. Struct. Biol.* **2012,** *22*, 30-37.

4. Clark, P. L. Protein folding in the cell: reshaping the folding funnel. *T. Biochem. Sci.* **2004,** *29*, 527-534.

5. Eichmann, C.; Preissler, S.; Riek, R.; Deuerling, E. Cotranslational structure acquisition of nascent polypeptides monitored by NMR spectroscopy. *Proc. Natl. Acad. Sci. U.S.A.* **2010,** *107*, 9111-9116.

6. Hartl, F. U.; Bracher, A.; Hayer-Hartl, M. Molecular chaperones in protein folding and proteostasis. *Nature* **2011,** *475*, 324-332.

7. Mei, G.; Di Venere, A.; Rosato, N.; Finazzi-Agro, A. The importance of being dimeric. *FEBS J.* **2005,** *272*, 16-27.

8. Rumfeldt, J. A. O.; Galvagnion, C.; Vassall, K. A.; Meiering, E. M. Conformational stability and folding mechanisms of dimeric proteins. *Prog. Biophys. Mol. Biol.* **2008,** *98*, 61-84.

9. Boehr, D. D.; Nussinov, R.; Wright, P. E. The role of dynamic conformational ensembles in biomolecular recognition. *Nat. Chem. Biol.* **2009,** *5*, 789-796.

10.   Wittung-Stafshede, P. Role of Cofactors in Protein Folding. *Acc. Chem. Res.* **2002,** *35*, 201-208.

11.   Kiefhaber, T.; Bachmann, A.; Jensen, K. S. Dynamics and mechanisms of coupled protein folding and binding reactions. *Curr. Op. Struct. Biol.* **2012,** *22*, 21-29.

12.   Seckler, R. Assembly of multi-subunit structures. In *Mechanisms of Protein Folding;* Pain, R. H. Ed.; Oxford University Press: Oxford, 2000; pp. 279-308.

13.   Verkhivker, G. M.; Bouzida, D.; Gehlhaar, D. K.; Rejto, P. A.; Freer, S. T.; Rose, P. W. Simulating disorder-order transition in molecular recognition of unstructured proteins: Where folding meets binding. *Proc. Natl. Acad. Sci. U.S.A.* **2003,** *100*, 5148-5153.

14.   Stocks, B. B.; Rezvanpour, A.; Shaw, G. S.; Konermann, L. Temporal Development of Protein Structure During S100A11 Folding and Dimerization Probed by Oxidative Labeling and Mass Spectrometry. *J. Mol Biol.* **2011,** *409*, 669-679.

15.   Bartlett, A. I.; Radford, S. E. An expanding arsenal of experimental methods yields an explosion of insights into protein folding mechanisms. *Nat. Struct. Mol. Biol.* **2009,** *16*, 582-588.

16.   Mishra, R.; Seckler, R.; Bhat, R. Efficient refolding of aggregation-prone citrate synthase by polyol osmolytes - How well are protein folding and stability aspects coupled? *J. Biol. Chem.* **2005,** *280*, 15553-15560.

17.   Antonini, E.; Brunori, M. *Hemoglobin and Myoglobin in Their Reactions With Ligands*; North-Holland Publishing Company: Amsterdam, London, 1971; Vol. 21.

18. Dickerson, R. E.; Geis, I. *Hemoglobin: Structure, Function, Evolution, and Pathology*; The Benjamin/Cummings Publioshing Company, Inc.: Menlo Park, CA, 1983.

19. Bunn, H. F.; Forget, B. G. *Hemoglobin: Molecular, Genetic and Clinical Aspects*; W.B. Saunders Company: Philadelphia, 1986.

20. Perutz, M. F. Stereochemistry of Cooperative Effects in Haemoglobin. *Nature* **1970,** *228*, 726-739.

21. Aranda IV, R.; Cai, H.; Worley, C. E.; Levin, E. J.; Li, R.; Olson, J. S.; Phillips Jr, G. N.; Richard, M. P. Structural analysis of fish versus mammalian hemoglobins: Effect of the heme pocket enviornment on autooxidation and hemin loss. *Proteins* **2009,** *75*, 217-230.

22. Riggs, A. F. Self-association, cooperativity and supercooperativity of oxygen binding by hemoglobins. *J. Exper. Biol.* **1998,** *201*, 1073-1084.

23. White, S. L. The molecular dissociation of ferrihemoglobin derivatives. *J. Biol. Chem.* **1975,** *250*, 1263-1268.

24. Eaton, W. A.; Henry, E. R.; Hofrichter, J.; Mozzarelli, A. Is cooperative oxygen binding by hemoglobin really understood. *Nat. Struct. Biol.* **1999,** *6*, 351 - 358.

25. Bellelli, A.; Brunori, M. Hemoglobin allostery: Variations on the theme. *Biochim. Biophys. Acta* **2011,** *1807*, 1262-1272.

26. Ishimori, K.; Morishima, I. Study of the specific heme orientation in reconstituted hemoglobins. *Biochemistry* **1988,** *27*, 4747-4753.

27.   Krishna Kumar, K.; Dickson, C. F.; Weiss, M. J.; Mackay, J. P.; Gell, D. A. AHSP (alpha-haemoglobin-stabilizing protein) stabilizes apo-alpha-haemoglobin in a partially folded state. *Biochem. J.* **2010,** *432*, 275-282.

28.   Shaeffer, J. R.; McDonald, M. J.; Bunn, H. F. Assembly of normal and abnormal human hemoglobins. *Trends Biochem. Sci.* **1981,** *6*, 158-161.

29.   Yip, Y. K.; Waks, M.; Beychok, S. Influence of prosthetic groups on protein folding and subunit assembly .1. Conformational differences between separated human alpha-globins and beta-globins. *J. Biol. Chem.* **1972,** *247*, 7237-&.

30.   McDonald, M. J.; Turci, S. M.; Mrabet, N. T.; Himelstein, B. P.; Bunn, H. F. The Kinetics of Assembly of Normal and Variant Human Oxyhemoglobins. *J. Biol. Chem.* **1987,** *262*, 5951-5956.

31.   Adachi, K.; Zhao, Y.; Surrey, S. Effects of heme addition on formation of stable human globin chains and hemoglobin subunit assembly in a cell-free system. *Arch. Biochem. Biophys.* **2003,** *413*, 99-106.

32.   McGovern, P.; Reisberg, P.; Olson, J. S. Aggregation of Deoxyhemoglobin Subunits. *J. Biol. Chem.* **1976,** *251*, 7871-7879.

33.   Kawamura, Y.; Hasumi, H.; Nakamura, S. Kinetic Studies on the Reconstitution of Deoxyhemoglobin from Isolated α and β Chains. *J. Biochem.* **1982,** *92*, 1227-1233.

34.   Vasudevan, G.; McDonald, M. J. Ordered heme binding ensures the assembly of fully functional hemoglobin: a hypothesis. *Curr. Prot. Pept. Sci.* **2002,** *3*, 461-466.

35.   Griffith, W. P.; Kaltashov, I. A. Highly asymmetric interactions between globin chains during hemoglobin assembly revealed by electrospray ionization mass spectrometry. *Biochemistry* **2003,** *42*, 10024 - 10033.

36. Feng, L.; A., G. D.; Zhou, S.; Gu, L.; Kong, Y.; Li, J.; Hu, M.; Yan, N.; Lee, C.; Rich, A. M.; Armstrong, R. S.; Lay, P. A.; Gow, A. J.; Weiss, M. J.; Mackay, J. P.; Shi, Y. Molecular Mechanism of AHSP-Mediated Stabilization of α-Hemoglobin. *Cell* **2004,** *119*, 629-640.

37. Ganem, B.; Henion, J. D. Going gently into flight: analyzing noncovalent interactions by mass spectrometry. *Bioorg. Med. Chem.* **2003,** *11*, 311-314.

38. Loo, J. A. Electrospray Ionization Mass Spectrometry: a Technology for Studying Noncovalent Macromolecular Complexes. *Int. J. Mass Spectrom.* **2000,** *200*, 175-186.

39. Heck, A. J. R. Native mass spectrometry: a bridge between interactomics and structural biology. *Nat. Methods* **2008,** *5*, 927 - 933.

40. Morgner, N.; Robinson, C. V. Linking structural change with functional regulation - insights from mass spectrometry. *Curr. Op. Struct. Biol.* **2012,** *22*, 44-51.

41. Wang, W.; Kitova, E. N.; Klassen, J. S. Influence of solution and gas phase processes on protein-carbohydrate binding affinities determined by nanoelectrospray Fourier transform ion cyclotron resonance mass spectrometry. *Anal. Chem.* **2003,** *75*, 4945-4955.

42. Liu, J.; Konermann, L. Protein-Protein Binding Affinities In Solution Determined by Electrospray Mass Spectrometry. *J. Am. Soc. Mass Spectrom.* **2011,** *22*, 408-417.

43. Cubrilovic, D.; Biela, A.; Sielaff, F.; Steinmetzer, T.; Klebe, G.; Zenobi, R. Quantifying Protein-Ligand Binding Constants using Electrospray Ionization Mass Spectrometry: A Systematic Binding Affinity Study of a Series of Hydrophobically Modified Trypsin Inhibitors. *J. Am. Soc. Mass Spectrom.* **2012,** *23*, 1768-1777.

44. Jørgensen, T. J. D.; Roepstorff, P.; Heck, A. J. R. Direct Determination of Solution Binding Constants for Noncovalent Complexes between Bacterial Cell Wall Peptide Analogues and Vancomycin Group Antibiotics by Electrospray Ionization Mass Spectrometry. *Anal. Chem.* **1998,** *70*, 4427-4432.

45. Konermann, L.; Ahadi, E.; Rodriguez, A. D.; Vahidi, S. Unraveling the Mechanism of Electrospray Ionization. *Anal. Chem.* **2013**.

46. Chowdhury, S. K.; Katta, V.; Chait, B. T. Probing Conformational Changes in Proteins by Mass Spectrometry. *J. Am. Chem. Soc.* **1990,** *112*, 9012-9013.

47. Testa, L.; Brocca, S.; Grandori, R. Charge-Surface Correlation in Electrospray Ionization of Folded and Unfolded Proteins. *Anal. Chem.* **2011,** *83*, 6459-6463.

48. Kaltashov, I. A.; Abzalimov, R. R. Do Ionic Charges in ESI MS Provide Useful Information on Macromolecular Structure? *J. Am. Soc. Mass Spectrom.* **2008,** *19*, 1239-1246.

49. Borysic, A. J. H.; Radford, S. E.; Ashcroft, A. E. Co-populated Conformational Ensembles of b2-Microglobulin Uncovered Quantitatively by Electrospray Ionization Mass Spectrometry. *J. Biol. Chem.* **2004,** *279*, 27069-27077.

50. Grabenauer, M.; Wyttenbach, T.; Sanghera, N.; Slade, S. E.; Pinheiro, T. J.; Scrivens, J. H.; Bowers, M. T. Conformational stability of Syrian hamster prion protein PrP(90-231). *J. Am. Chem. Soc.* **2010,** *132*, 8816-8818.

51. Vis, H.; Heinemann, U.; Dobson, C. M.; Robinson, C. V. Detection of a Monomeric Intermediate Associated with Dimerization of Protein Hu by Mass Spectrometry. *J. Am. Chem. Soc.* **1998,** *120*, 6427-6428.

52.   Kim, M.-Y.; Maier, C. S.; Reed, D. J.; Deinzer, M. L. Conformational changes in chemically modified *Escherichia coli* thioredoxin monitored by H/D exchange and electrospray mass spectrometry. *Protein Sci.* **2002,** *11*, 1320-1329.

53.   Dobo, A.; Kaltashov, I. A. Detection of Multiple Protein Conformational Ensembles in Solution via Deconvolution of Charge-State Distributions in ESI MS. *Anal. Chem.* **2001,** *73*, 4763-4773.

54.   Pan, J. X.; Rintala-Dempsey, A.; Li, Y.; Shaw, G. S.; Konermann, L. Folding Kinetics of the S100A11 Protein Dimer Studied by Time-Resolved Electrospray Mass Spectrometry and Pulsed Hydrogen-Deuterium Exchange. *Biochemistry* **2006,** *45*, 3005-3013.

55.   Fändrich, M.; Tito, M. A.; Leroux, M. R.; Rostom, A. A.; Hartl, F. U.; Dobson, C. M.; Robinson, C. V. Observation of the noncovalent assembly and disassembly pathways of the chaperone complex MtGimC by mass spectrometry. *Proc. Natl. Acad. Sci. U.S.A.* **2000,** *97*, 14151-14155.

56.   Sharon, M.; Witt, S.; Glasmacher, E.; Baumeister, W.; Robinson, C. V. Mass spectrometry reveals the missing links in the assembly pathway of the bacterial 20 S proteasome. *J. Biol. Chem.* **2007,** *282*, 18448-18457.

57.   Boys, B. L.; Konermann, L. Folding and Assembly of Hemoglobin Monitored by Electrospray Mass Spectrometry Using an On-line Dialysis System. *J. Am. Soc. Mass Spectrom.* **2007,** *18*, 8-16.

58.   Smith, A. M.; Jahn, T. R.; Ashcroft, A. E.; Radford, S. E. Direct Observation of Oligomeric Species formed in the Early Stages of Amyloid Formation using Electrospray Ionization Mass Spectrometry. *J. Mol. Biol.* **2006,** *364*, 9-19.

59.   Versluis, C.; Heck, A. J. R. Gas-phase dissociation of hemoglobin. *Int. J. Mass Spectrom.* **2001,** *210/211*, 637-649.

60. Yang, K.; Terrier, P.; Douglas, D. J. Mass Spectra and Ion Collision Cross Sections of Hemoglobin. *J. Am. Soc. Mass Spectrom.* **2011,** *22*, 290-299.

61. Scarff, C. A.; Patel, V. J.; Thalassinos, K.; Scrivens, J. H. Probing Hemoglobin Structure by Means of Traveling-Wave Ion Mobility Mass Spectrometry. *J. Am. Soc. Mass Spectrom.* **2009,** *20*, 625-631.

62. Griffith, W. P.; Kaltashov, I. A. Protein Conformational Heterogeneity as a Binding Catalyst: ESI-MS Study of Hemoglobin H Formation. *Biochemistry* **2007,** *46*, 2020-2026.

63. Boys, B. L.; Kuprowski, M. C.; Konermann, L. Symmetric Behavior of Hemoglobin α- and β- Subunits during Acid-Induced Denaturation Observed by Electrospray Mass Spectrometry. *Biochemistry* **2007,** *46*, 10675-10684.

64. Adams, P. A. The Kinetics of the Recombination Reaction between Apomyoglobin and Alkaline Haematin. *Biochem. J.* **1977,** *163*, 153-158.

65. Crosby, W. H.; Houchin, D. N. Preparing Standard Solutions of Cyanmethemoglobin. *Blood* **1957,** *12*, 1132-1136.

66. Xu, G.; Chance, M. R. Hydroxyl Radical-Mediated Modification of Proteins as Probes for Structural Proteomics. *Chem. Rev.* **2007,** *107*, 3514-3543.

67. Sage, J. T.; Morikis, D.; Champion, P. M. Spectroscopic Studies of Myoglobin at Low pH: Heme Structure and Ligation. *Biochemistry* **1991,** *30*, 1227-1237.

68. Crespin, M. O.; Boys, B. L.; Konermann, L. The reconstitution of unfolded myoglobin with hemin dicyanide is not accelerated by fly casting. *FEBS Lett.* **2005,** *579*, 271-274.

69.   Yee, S.; Peyton, D. H. Proton NMR investigation of the reconstitution of equine myoglobin with hemin dicyanide. *FEBS Lett.* **1991,** *290*, 119-122.

70.   Verkerk, U. H.; Kebarle, P. Ion-Ion and Ion-Molecule Reactions at the Surface of Proteins Produced by Nanospray. Information on the Number of Acidic Residues and Control of the Number of Ionized Acidic and Basic Residues. *J. Am. Soc. Mass Spectrom.* **2005,** *16*, 1325-1341.

71.   Simmons, D. A.; Dunn, S. D.; Konermann, L. Conformational Dynamics of Partially Denatured Myoglobin Studied by Time-Resolved Electrospray Mass Spectrometry With Online Hydrogen-Deuterium Exchange. *Biochemistry* **2003,** *42*, 5896-5905.

72.   Dobson, C. M. Protein folding and misfolding. *Nature* **2003,** *426*, 884-890.

73.   Leutzinger, Y.; Beychok, S. Kinetics and mechanism of heme-induced refolding of human α-globin. *Proc. Natl. Acad. Sci. U.S.A.* **1981,** *78*, 780-784.

74.   Adams, P. A.; Berman, M. C. Kinetics and Mechanism of the Interaction between Human-Serum Albumin and Monomeric Hemin. *Biochem. J.* **1980,** *191*, 95-102.

75.   Robinson, C. R.; Liu, Y.; Thomson, J. A.; Sturtevant, J. M.; Sligar, S. G. Energetics of Heme Binding to Native and Denatured States of Cytochrome b_{562}. *Biochemistry* **1997,** *36*, 16141-16146.

76.   Kuzelova, K.; Mrhalova, M.; Hrkal, Z. Kinetics of heme interaction with heme-binding proteins: The effect of heme aggregation state. *Biochim. Biophys. Acta* **1997,** *1336*, 497 - 501.

Chapter 5-Conclusions and Future Outlook

5.1 Conclusions

Despite the availability of a vast arsenal of biophysical methods, protein structure and functional studies are still facing lots of challenges. Research conducted within this field typically covers protein conformational dynamics, protein-protein interactions, and protein folding. The ultimate goal of work in this area is to decipher the function of intricate biological systems, and to find therapeutic approaches for diseases related to misfolded proteins. To achieve this goal, scientists have to choose the proper tools. X-ray crystallography remains the gold standard for characterizing static protein structures with atomic resolution. However, dynamic information can usually not be obtained in this way. Small-angle X-ray scattering (SAXS) is an alternatice technique that can report on protein shape and dynamics with low resolution. NMR represents another standard tool to characterize protein structure at the atomic level, and also NMR can also provide dynamic information. Unfortunately, NMR suffers from size limitation caused by overlap of resonance peaks. Simple optical spectroscopic methods provide excellent time resolution, but they lack the ability to provide structural details. Importantly, all the methods mentioned above reflect the average behavior of protein samples without distinguishing co-existing sub-populations.

ESI-MS offers the unique opportunity to monitor coexisting protein conformers individually. Different protein conformers and ligand binding states will result in ESI-MS signals with distinct m/z values. Because of these interesting attributes, and considering

its high sensitivity and minimal sample consumption, MS represents a complementary tool to other biophysical methods.

Chapter 2 used ESI-MS in conjunction with HDX and optical spectroscopy for characterizing the solution phase properties of cyt *c* after heat exposure. Previous work demonstrated that heating results in irreversible denaturation for a subpopulation of proteins in the sample, without investigating the physical reasons underlying this effect. We found that the formation of oxidative modifications at elevated temperature plays a key role for the observed behavior. Tryptic digestion followed by MS/MS was used to identify individual oxidation sites. Trp59 and Met80 are among the modified amino acids. In native cyt *c* both of these residues are buried deep within the protein structure, such that covalent modifications will be highly disruptive. ESI-MS analysis after heat exposure results in a bimodal charge-state distribution. Oxidized protein appears predominantly in charge states around 11+, whereas a considerably lower degree of oxidation is observed for the 7+ and 8+ peaks. This finding confirms that different oxidation levels are associated with different solution-phase conformations. HDX measurements for different charge states are complicated by peak distortion arising from oxygen adduction. Nonetheless, comparison with simulated peak shapes clearly shows that the HDX properties are different for high- and low-charge states, confirming that interconversion between unfolded and folded conformers is blocked in solution. In addition to oxidation, partial aggregation upon heat exposure likely contributes to the formation of irreversibly denatured protein.

While it is well known that ESI allows the transfer of multi-protein complexes into the gas phase, it remains unclear whether the measured ion abundance ratios of free and

bound species are suitable for determining solution-phase binding affinities (K_d values). Many types of mass spectrometers employ rf-only quadrupoles as ion guides. Chapter 3 demonstrates that the settings used for these devices are a key factor for ensuring uniform transmission behavior, which is a prerequisite for meaningful affinity measurements. Using bovine β-lactoglobulin and Hb as model systems, it is demonstrated that under carefully adjusted conditions the "direct" ESI-MS approach is capable of providing K_d values that are in good agreement with previously published solution-phase data. Of the several ion sources tested, a regular ESI emitter operated with pressure-driven flow at 1 µL min^{-1} provided the most favorable results. Potential problems in these experiments include conformationally-induced differences in ionization efficiencies, inadvertent collision-induced dissociation, and ESI-induced clustering artifacts. A number of simple tests can be conducted to assess whether or not these factors are prevalent under the conditions used. In addition, the fidelity of the method can be scrutinized by performing measurements over a wide concentration range. Overall, our results support the viability of the direct ESI-MS approach for determining binding affinities of protein–protein complexes in solution.

By using optimized instrument condition characterized in **Chapter 3**, formation of tetrameric Hb is studied in **Chapter 4**. Refolding of tetrameric protein hemoglobin (Hb) was initiated by denaturant removal. All species present at different time points of refolding were carefully assigned based on their *m/z* values. Hb refolding induced by denaturant removal resulted in a low tetramer yield, and the formation of non-canonical aggregates. Enhancing the solubility of the Hb chromophore was found to be a successful

strategy, leading to tetramers as the major species in the ESI mass spectra. The novel aspects of this final chapter are: (i) key intermediates were identified under efficient refolding regime, (ii) non-native interactions were identified under conditions where proteins misfolded.

5.2 Future Outlooks

5.2.1 Conformation and Dynamics of Biopharmaceuticals Studied by ESI-MS

Protein drugs are an important component in of modern medicine [1]. They differ from small molecule drugs in the way they function. Typically therapeutic properties of small molecule drugs are completely determined by their covalent structures. However for protein therapeutics their noncovalent contacts and dynamic motions play a major role. The molecular weight of these protein drugs ranges from several kDa to 1 M. Improperly folded protein drugs can cause aggregation inside the cell, theregy causing undesired side effects [2]. Improper folding of protein therapeutics also decreases their efficiency and it may trigger immune response [3].

Methods that can quickly and accurately determine the safety and stability of protein therapeutics are extremely important for drug design and engineering. ESI-MS is likely to become an important biophysical technique for this purpose that will be widely used in the biopharmaceutical industry. Protein structural studies by ESI-MS have experienced rapid development in recent years. ESI-MS can uniquely distinguish different protein confomers by their charge state distributions [4]. In addition, the combination of labeling techniques and MS provide detailed conformational information by uncovering differences in labeling patterns [5-8]. Some HDX-based MS methods are even capable of revealing protein conformational dynamics with single residue resolution [9,10]. Because of the above progress made in recent years, ESI-MS possesses enormous potential for the characterization of biopharmaceuticals, specifically protein drugs.

5.2.2 Protein Protein Binding Affinities Studied by ESI-MS

Binding affinities of proteins and small ligands have been extensively studied by ESI-MS. However, interactions between subunits of noncovalent protein complexes are less commonly studied by this method. Chapter 3 has established ESI-MS as a tool for probing the affinity of protein interactions, by using proper ion transmission control. In the future it will be interesting to apply the results of Chapter 3 to a range of different systems. Actually, our approach has already been successfully applied to study binding affinities of multi-subunit protein complex systems related to ubiquitin signaling [11].

5.2.3 Hb Formation Studied under the Presence of its Chaperone AHSP

Hemoglobins are highly abundant within our blood as oxygen carriers, and understanding this formation is extremely important. In Chapter 4, Hb formation was studied under different solvent conditions. The results have indicated that the presence of solubilized heme is extremely important for Hb assembly, and at the same time a series of on-pathway and off-pathway intermediates were identified. Kiml et al. have found a chaperone called α-hemoglobin stabilizing protein (AHSP), which specifically interacts with α-globin [12]. At the genome level, there are two α-globin genes to every β-globin gene. As a result, α-globin may be slightly more abundant than β-globins in the cell, thus preventing the formation of Hb H. Hb H $(\beta^h)_4$ does not have normal oxygen binding behavior. However, α-globin itself can also aggregate and form cytotoxic inclusion bodies [13]. AHSP interacts with α-globin to prevent aggregation of this subunit [14]. Studying Hb formation in the presence of AHSP using the approach developed in Chapter 4 would

help us to understand the mechanism through which our body maximize Hb synthesis, and minimizes harmful aggregation formed by either α- or β-subunits.

5.3 References

1. Leader, B.; Baca, Q. J.; Golan, D. E. Protein therapeutics: a summary and pharmacological classification. *Nat Rev Drug Discov* **2008,** *7*, 21-39.

2. Luheshi, L. M.; Dobson, C. M. Bridging the gap: From protein misfolding to protein misfolding diseases. *FEBS Lett.* **2009,** *583*, 2581-2586.

3. Maas, C.; Hermeling, S.; Bouma, B.; Jiskoot, W.; Gebbink, M. F. A role for protein misfolding in immunogenicity of biopharmaceuticals. *Journal of Biological Chemistry* **2007,** *282*, 2229-36.

4. Kaltashov, I. A.; Abzalimov, R. R. Do Ionic Charges in ESI MS Provide Useful Information on Macromolecular Structure? *J. Am. Soc. Mass Spectrom.* **2008,** *19*, 1239-1246.

5. Petrotchenko, E.; Borchers, C. H. Crosslinking Combined with Mass Spectrometry for Structural Proteomics. *Mass Spectrom. Rev.* **2010,** *29*, 862-876.

6. Konermann, L.; Stocks, B. B.; Pan, Y.; Tong, X. Mass Spectrometry Combined with Oxidative Labeling for Exploring Protein Structure and Folding. *Mass Spectrom. Rev.* **2010,** *29*, 651-667.

7. Roeser, J.; Bischoff, R.; Bruins, A. P.; Permentier, H. P. Oxidative protein labeling in mass-spectrometry-based proteomics. *Anal. Bioanal. Chem.* **2010,** *397*, 3441-3455.

8. Konermann, L., Pan, J., Liu, Y.,. Hydrogen Exchange Mass Spectrometry for Studying Protein Structure and Dynamics. *Chem. Soc. Rev.* **2011,** *40*, 1224-1234.

9. Pan, J.; Han, J.; Borchers, C. H.; Konermann, L. Hydrogen/Deuterium Exchange Mass Spectrometry with Top-Down Electron Capture Dissociation for

Characterizing Structural Transitions of a 17 kDa Protein. *J. Am. Chem. Soc.* **2009,** *131*, 12801–12808.

10.   Pan, J.; Han, J.; Borchers, C. H.; Konermann, L. Characterizing Short-Lived Protein Folding Intermediates by Top-Down Hydrogen Exchange Mass Spectrometry. *Anal. Chem.* **2010,** *82*, 8591-8597.

11.   Sokratous, K.; Roach, L. V.; Channing, D.; Strachan, J.; Long, J.; Searle, M. S.; Layfield, R.; Oldham, N. J. Probing Affinity and Ubiquitin Linkage Selectivity of Ubiquitin-Binding Domains Using Mass Spectrometry. *J Am Chem Soc* **2012,** *134*, 6416-6424.

12.   Kihm, A. J.; Kong, Y.; Hong, W.; Russell, J. E.; Rouda, S.; Adachi, K.; Simon, M. C.; Blobel, G. A.; Weiss, M. J. An abundant erythroid protein that stabilizes free alpha-haemoglobin. *Nature* **2002,** *417*, 758-763.

13.   Fessas, P. Inclusions of Hemoglobin in Erythroblasts and Erythrocytes of Thalassemia. *Blood* **1963,** *21*, 21-&.

14.   Luzzatto, L.; Notaro, R. Haemoglobin's chaperone. *Nature* **2002,** *417*, 703-704.

Appendix 1 – Permissions

ELSEVIER LICENSE
TERMS AND CONDITIONS

Dec 17, 2012

This is a License Agreement between Jiangjiang Liu ("You") and Elsevier ("Elsevier") provided by Copyright Clearance Center ("CCC"). The license consists of your order details, the terms and conditions provided by Elsevier, and the payment terms and conditions.

All payments must be made in full to CCC. For payment instructions, please see information listed at the bottom of this form.

Supplier	Elsevier Limited The Boulevard,Langford Lane Kidlington,Oxford,OX5 1GB,UK
Registered Company Number	1982084
Customer name	Jiangjiang Liu
Customer address	Department of Chemistry
	London, ON N6A 5B7
License number	3041451023829
License date	Dec 03, 2012
Licensed content publisher	Elsevier
Licensed content publication	Journal of the American Society for Mass Spectrometry
Licensed content title	Irreversible Thermal Denaturation of Cytochrome$c$Studied by Electrospray Mass Spectrometry
Licensed content author	Jiangjiang Liu,Lars Konermann
Licensed content date	May 2009
Licensed content volume number	20
Licensed content issue number	5
Number of pages	10
Start Page	819
End Page	828
Type of Use	reuse in a thesis/dissertation
Portion	full article
Format	both print and electronic

Are you the author of this Elsevier article?	Yes
Will you be translating?	No
Order reference number	None
Title of your thesis/dissertation	Protein Structures and Interactions Studied by ESI-MS
Expected completion date	Jan 2013
Estimated size (number of pages)	180
Elsevier VAT number	GB 494 6272 12
Permissions price	0.00 USD
VAT/Local Sales Tax	0.0 USD / 0.0 GBP
Total	0.00 USD

Terms and Conditions

INTRODUCTION

1. The publisher for this copyrighted material is Elsevier. By clicking "accept" in connection with completing this licensing transaction, you agree that the following terms and conditions apply to this transaction (along with the Billing and Payment terms and conditions established by Copyright Clearance Center, Inc. ("CCC"), at the time that you opened your Rightslink account and that are available at any time at http://myaccount.copyright.com).

GENERAL TERMS

2. Elsevier hereby grants you permission to reproduce the aforementioned material subject to the terms and conditions indicated.

3. Acknowledgement: If any part of the material to be used (for example, figures) has appeared in our publication with credit or acknowledgement to another source, permission must also be sought from that source. If such permission is not obtained then that material may not be included in your publication/copies. Suitable acknowledgement to the source must be made, either as a footnote or in a reference list at the end of your publication, as follows:

"Reprinted from Publication title, Vol /edition number, Author(s), Title of article / title of chapter, Pages No., Copyright (Year), with permission from Elsevier [OR APPLICABLE SOCIETY COPYRIGHT OWNER]." Also Lancet special credit - "Reprinted from The Lancet, Vol. number, Author(s), Title of article, Pages No., Copyright (Year), with permission from Elsevier."

4. Reproduction of this material is confined to the purpose and/or media for which permission is hereby given.

5. Altering/Modifying Material: Not Permitted. However figures and illustrations may be altered/adapted minimally to serve your work. Any other abbreviations, additions, deletions and/or any other alterations shall be made only with prior written authorization of Elsevier Ltd. (Please contact Elsevier at permissions@elsevier.com)

6. If the permission fee for the requested use of our material is waived in this instance, please be advised that your future requests for Elsevier materials may attract a fee.

7. Reservation of Rights: Publisher reserves all rights not specifically granted in the combination of (i) the license details provided by you and accepted in the course of this

licensing transaction, (ii) these terms and conditions and (iii) CCC's Billing and Payment terms and conditions.

8. License Contingent Upon Payment: While you may exercise the rights licensed immediately upon issuance of the license at the end of the licensing process for the transaction, provided that you have disclosed complete and accurate details of your proposed use, no license is finally effective unless and until full payment is received from you (either by publisher or by CCC) as provided in CCC's Billing and Payment terms and conditions. If full payment is not received on a timely basis, then any license preliminarily granted shall be deemed automatically revoked and shall be void as if never granted. Further, in the event that you breach any of these terms and conditions or any of CCC's Billing and Payment terms and conditions, the license is automatically revoked and shall be void as if never granted. Use of materials as described in a revoked license, as well as any use of the materials beyond the scope of an unrevoked license, may constitute copyright infringement and publisher reserves the right to take any and all action to protect its copyright in the materials.

9. Warranties: Publisher makes no representations or warranties with respect to the licensed material.

10. Indemnity: You hereby indemnify and agree to hold harmless publisher and CCC, and their respective officers, directors, employees and agents, from and against any and all claims arising out of your use of the licensed material other than as specifically authorized pursuant to this license.

11. No Transfer of License: This license is personal to you and may not be sublicensed, assigned, or transferred by you to any other person without publisher's written permission.

12. No Amendment Except in Writing: This license may not be amended except in a writing signed by both parties (or, in the case of publisher, by CCC on publisher's behalf).

13. Objection to Contrary Terms: Publisher hereby objects to any terms contained in any purchase order, acknowledgment, check endorsement or other writing prepared by you, which terms are inconsistent with these terms and conditions or CCC's Billing and Payment terms and conditions. These terms and conditions, together with CCC's Billing and Payment terms and conditions (which are incorporated herein), comprise the entire agreement between you and publisher (and CCC) concerning this licensing transaction. In the event of any conflict between your obligations established by these terms and conditions and those established by CCC's Billing and Payment terms and conditions, these terms and conditions shall control.

14. Revocation: Elsevier or Copyright Clearance Center may deny the permissions described in this License at their sole discretion, for any reason or no reason, with a full refund payable to you. Notice of such denial will be made using the contact information provided by you. Failure to receive such notice will not alter or invalidate the denial. In no event will Elsevier or Copyright Clearance Center be responsible or liable for any costs, expenses or damage incurred by you as a result of a denial of your permission request, other than a refund of the amount(s) paid by you to Elsevier and/or Copyright Clearance Center for denied permissions.

LIMITED LICENSE

The following terms and conditions apply only to specific license types:

15. **Translation**: This permission is granted for non-exclusive world **English** rights only unless your license was granted for translation rights. If you licensed translation rights you may only translate this content into the languages you requested. A professional translator must perform all translations and reproduce the content word for word preserving the integrity of the article. If this license is to re-use 1 or 2 figures then permission is granted for non-exclusive world rights in all languages.

16. **Website**: The following terms and conditions apply to electronic reserve and author websites:

Electronic reserve: If licensed material is to be posted to website, the web site is to be password-protected and made available only to bona fide students registered on a relevant course if:

This license was made in connection with a course, This permission is granted for 1 year only. You may obtain a license for future website posting,

All content posted to the web site must maintain the copyright information line on the bottom of each image,

A hyper-text must be included to the Homepage of the journal from which you are licensing at http://www.sciencedirect.com/science/journal/xxxxx or the Elsevier homepage for books at http://www.elsevier.com , and

Central Storage: This license does not include permission for a scanned version of the material to be stored in a central repository such as that provided by Heron/XanEdu.

17. **Author website** for journals with the following additional clauses:

All content posted to the web site must maintain the copyright information line on the bottom of each image, and the permission granted is limited to the personal version of your paper. You are not allowed to download and post the published electronic version of your article (whether PDF or HTML, proof or final version), nor may you scan the printed edition to create an electronic version. A hyper-text must be included to the Homepage of the journal from which you are licensing at http://www.sciencedirect.com/science/journal/xxxxx . As part of our normal production process, you will receive an e-mail notice when your article appears on Elsevier's online service ScienceDirect (www.sciencedirect.com). That e-mail will include the article's Digital Object Identifier (DOI). This number provides the electronic link to the published article and should be included in the posting of your personal version. We ask that you wait until you receive this e-mail and have the DOI to do any posting.

Central Storage: This license does not include permission for a scanned version of the material to be stored in a central repository such as that provided by Heron/XanEdu.

18. **Author website** for books with the following additional clauses: Authors are permitted to place a brief summary of their work online only. A hyper-text must be included to the Elsevier homepage at http://www.elsevier.com . All content posted to the web site must maintain the copyright information line on the bottom of each image. You are not allowed to download and post the published electronic version of your chapter, nor may you scan the printed edition to create an electronic version.

Central Storage: This license does not include permission for a scanned version of the material to be stored in a central repository such as that provided by Heron/XanEdu.

19. **Website** (regular and for author): A hyper-text must be included to the Homepage of

the journal from which you are licensing at
 http://www.sciencedirect.com/science/journal/xxxxx. or for books to the Elsevier homepage at http://www.elsevier.com

20. **Thesis/Dissertation**: If your license is for use in a thesis/dissertation your thesis may be submitted to your institution in either print or electronic form. Should your thesis be published commercially, please reapply for permission. These requirements include permission for the Library and Archives of Canada to supply single copies, on demand, of the complete thesis and include permission for UMI to supply single copies, on demand, of the complete thesis. Should your thesis be published commercially, please reapply for permission.

21. **Other Conditions**:

v1.6

If you would like to pay for this license now, please remit this license along with your payment made payable to "COPYRIGHT CLEARANCE CENTER" otherwise you will be invoiced within 48 hours of the license date. Payment should be in the form of a check or money order referencing your account number and this invoice number RLNK500909623.
Once you receive your invoice for this order, you may pay your invoice by credit card. Please follow instructions provided at that time.

Make Payment To:
Copyright Clearance Center
Dept 001
P.O. Box 843006
Boston, MA 02284-3006

For suggestions or comments regarding this order, contact RightsLink Customer Support: customercare@copyright.com or +1-877-622-5543 (toll free in the US) or +1-978-646-2777.

Gratis licenses (referencing $0 in the Total field) are free. Please retain this printable license for your reference. No payment is required.

SPRINGER LICENSE
TERMS AND CONDITIONS

Dec 17, 2012

This is a License Agreement between Jiangjiang Liu ("You") and Springer ("Springer") provided by Copyright Clearance Center ("CCC"). The license consists of your order details, the terms and conditions provided by Springer, and the payment terms and conditions.

All payments must be made in full to CCC. For payment instructions, please see information listed at the bottom of this form.

License Number	3041460381276
License date	Dec 03, 2012
Licensed content publisher	Springer
Licensed content publication	Journal of The American Society for Mass Spectrometry
Licensed content title	Protein–Protein Binding Affinities in Solution Determined by Electrospray Mass Spectrometry
Licensed content author	Jiangjiang Liu
Licensed content date	Jan 1, 2011
Volume number	22
Issue number	3
Type of Use	Thesis/Dissertation
Portion	Full text
Number of copies	1
Author of this Springer article	Yes and you are the sole author of the new work
Order reference number	None
Title of your thesis / dissertation	Protein Structure and Interactions Studied by ESI-MS
Expected completion date	Dec 2012
Estimated size(pages)	195
Total	0.00 USD

Terms and Conditions

Introduction

The publisher for this copyrighted material is Springer Science + Business Media. By

clicking "accept" in connection with completing this licensing transaction, you agree that the following terms and conditions apply to this transaction (along with the Billing and Payment terms and conditions established by Copyright Clearance Center, Inc. ("CCC"), at the time that you opened your Rightslink account and that are available at any time at http://myaccount.copyright.com).

Limited License

With reference to your request to reprint in your thesis material on which Springer Science and Business Media control the copyright, permission is granted, free of charge, for the use indicated in your enquiry.

Licenses are for one-time use only with a maximum distribution equal to the number that you identified in the licensing process.

This License includes use in an electronic form, provided its password protected or on the university's intranet or repository, including UMI (according to the definition at the Sherpa website: http://www.sherpa.ac.uk/romeo/). For any other electronic use, please contact Springer at
(permissions.dordrecht@springer.com or permissions.heidelberg@springer.com).

The material can only be used for the purpose of defending your thesis, and with a maximum of 100 extra copies in paper.

Although Springer holds copyright to the material and is entitled to negotiate on rights, this license is only valid, provided permission is also obtained from the (co) author (address is given with the article/chapter) and provided it concerns original material which does not carry references to other sources (if material in question appears with credit to another source, authorization from that source is required as well).

Permission free of charge on this occasion does not prejudice any rights we might have to charge for reproduction of our copyrighted material in the future.

Altering/Modifying Material: Not Permitted

You may not alter or modify the material in any manner. Abbreviations, additions, deletions and/or any other alterations shall be made only with prior written authorization of the author(s) and/or Springer Science + Business Media. (Please contact Springer at (permissions.dordrecht@springer.com or permissions.heidelberg@springer.com)

Reservation of Rights

Springer Science + Business Media reserves all rights not specifically granted in the combination of (i) the license details provided by you and accepted in the course of this licensing transaction, (ii) these terms and conditions and (iii) CCC's Billing and Payment terms and conditions.

Copyright Notice:

Disclaimer

You must include the following copyright and permission notice in connection with any reproduction of the licensed material: "Springer and the original publisher /journal title, volume, year of publication, page, chapter/article title, name(s) of author(s), figure number(s), original copyright notice) is given to the publication in which the material was originally published, by adding; with kind permission from Springer Science and Business Media"

Warranties: None

Example 1: Springer Science + Business Media makes no representations or warranties with respect to the licensed material.

Example 2: Springer Science + Business Media makes no representations or warranties with respect to the licensed material and adopts on its own behalf the limitations and disclaimers established by CCC on its behalf in its Billing and Payment terms and conditions for this licensing transaction.

Indemnity

You hereby indemnify and agree to hold harmless Springer Science + Business Media and CCC, and their respective officers, directors, employees and agents, from and against any and all claims arising out of your use of the licensed material other than as specifically authorized pursuant to this license.

No Transfer of License

This license is personal to you and may not be sublicensed, assigned, or transferred by you to any other person without Springer Science + Business Media's written permission.

No Amendment Except in Writing

This license may not be amended except in a writing signed by both parties (or, in the case of Springer Science + Business Media, by CCC on Springer Science + Business Media's behalf).

Objection to Contrary Terms

Springer Science + Business Media hereby objects to any terms contained in any purchase order, acknowledgment, check endorsement or other writing prepared by you, which terms are inconsistent with these terms and conditions or CCC's Billing and Payment terms and conditions. These terms and conditions, together with CCC's Billing and Payment terms and conditions (which are incorporated herein), comprise the entire agreement between you and Springer Science + Business Media (and CCC) concerning this licensing transaction. In the event of any conflict between your obligations established by these terms and conditions and those established by CCC's Billing and Payment terms and conditions, these terms and conditions shall control.

Jurisdiction

All disputes that may arise in connection with this present License, or the breach thereof, shall be settled exclusively by arbitration, to be held in The Netherlands, in accordance with Dutch law, and to be conducted under the Rules of the 'Netherlands Arbitrage Instituut' (Netherlands Institute of Arbitration).*OR:*

All disputes that may arise in connection with this present License, or the breach thereof, shall be settled exclusively by arbitration, to be held in the Federal Republic of Germany, in accordance with German law.

Other terms and conditions:

v1.3

If you would like to pay for this license now, please remit this license along with your payment made payable to "COPYRIGHT CLEARANCE CENTER"
otherwise you will be invoiced within 48 hours of the license date. Payment should be in the form of a check or money order referencing your account number and this invoice number RLNK500909631.
Once you receive your invoice for this order, you may pay your invoice by credit card. Please follow instructions provided at that time.

Make Payment To:
Copyright Clearance Center

Dept 001
P.O. Box 843006
Boston, MA 02284-3006

For suggestions or comments regarding this order, contact RightsLink Customer Support: customercare@copyright.com or +1-877-622-5543 (toll free in the US) or +1-978-646-2777.

Gratis licenses (referencing $0 in the Total field) are free. Please retain this printable license for your reference. No payment is required.

Appendix 2 – *Curriculum Vitae*

Jiangjiang , Liu

Education:
Undergraduate：
University of Western Ontario
Degree: Honors Bachelor of Chemistry and Major in Biochemistry

Graduate:
University of Western Ontario
Degree: PHD program

Awards and Schorlarships during Graduate program:
-    Western Graduate Research Award
 University of Western Ontario 2007-2012

-    Graduate thesis research award

 University of Western Ontario 2011-2012

Research Experience:

 Graduate Studies, Dr. Lars Konermann Laboratory,
 University of Western Ontario 2007-2012

 Work Experience:
 Teaching Assistant
 University of Western Ontario 2007-2012

 Publications:

1. Liu, J.; Konermann, L. Irreversible Thermal Denaturation of Cytochrome c Studied by Electrospray Mass Spectrometry. *J. Am. Soc. Mass Spectrom.* **2009,** *20*, 819-828.

2. Liu, J.; Konermann, L. Protein-Protein Binding Affinities In Solution Determined by Electrospray Mass Spectrometry. *J. Am. Soc. Mass Spectrom.* **2011,** *22*, 408-417.

3. Sciuto, S. V.; Liu, J.; Konermann, L. An Electrostatic Charge Partitioning Model for the Dissociation of Protein Complexes in the Gas Phase. *J. Am. Soc. Mass Spectrom.* **2011,** *22*, 1679-1689.

4. Howarth, A.; Liu, J.; Konermann, L.; Corrigan, J. F. Probing the Metal Composition of Ternary 12-12'-16 Nanoclusters via Electrospray Ionization Mass Spectrometry. *Z. Anorg. Allg. Chem* **2011,** *637*, 1203-1206.

5. Konermann, L.; Rodriguez, A. D.; Liu, J. On the formation of highly charged gaseous ions from unfolded proteins by electrospray ionization. *Anal Chem* **2012,** *84*, 6798-804.

6. Comeau, A.; Liu, J.; Khadka,C.; Corrigan,J. F.; Konermann, L. Nanocluster Isotope Distributions Measured by Electrospray Time-of-Flight Mass Spectrometry. *Anal. Chem.* submitted (2013).

7. Liu, J.; Konermann, L. Assembly of Hemoglobin from Denatured Monomeric Subunits: Effects of Heme Ligation and Off-Pathway Intermediates Studied by Electrospray Mass Spectrometry. *In preparation*

Conference Proceedings:

Jenna-Jiangjiang Liu and Lars Konermann, **Irreversible Thermal Unfolding of Cytochrome *c* Studied by ESI-MS** , 56th meeting of the American Society of Mass Spectrometry (ASMS), Denver, CO, USA, June 1 – 5, 2008.

Jenna-Jiangjiang Liu and Lars Konermann, **ESI-MS Identifies Protein Oxidation as Major Contributor to Irreversible Thermal Denaturation,** 57th meeting of the American Society of Mass Spectrometry (ASMS), Philadelphia, PA, USA, May 31 – June 5, 2009.

Jenna-Jiangjiang Liu and Lars Konermann, **Comparing Apparent ESI-MS Binding Affinities of Noncovalent Protein Complexes with Solution-Phase Measurements,** 58th meeting of the American Society of Mass Spectrometry (ASMS), Salt Lake City, UT, USA, May 23 – 27, 2010.

Jenna-Jiangjiang Liu and Lars Konermann, **Assembly Mechanism of Hemoglobin Studied by Native   Electrospray Mass Spectrometry,** 59th meeting of the American Society of Mass Spectrometry
(ASMS), Denver, CO, USA, June 5 – 10, 2011.

Jenna-Jiangjiang Liu and Lars Konermann, **Off-Pathway Aggregation during Hemoglobin Folding and   Assembly Studied Using ESI-MS,** 60th meeting of the American Society of Mass Spectrometry
(ASMS), Vancouver, BC, Canada, May 19 – 24, 2012.

Jenna-Jiangjiang Liu and Lars Konermann, **Assembly Mechanism of Hemoglobin Studied by Native   Electrospray Mass Spectrometry,** Biological Molecules in the Gas Phase & in solution, Andover, NH, USA,
July 31 – August 5, 2011.

Lars Konermann, Elias Ahadi, Antony D. Rodriguez, Jiangjiang Liu and Siavash Vahidi, **Unraveling the Mechanism of Electrospray Ionization,** Tandem MS Workshop, Lake Louise, Canada, 2012.